AD-A091 641 CALIFORNIA UNIV LOS ANGELES F/G 11/2
ELECTROCHROMIC GLASSES.(U)
JUL 80 R BRAUNSTEIN DAAG29-76-G-0321
UNCLASSIFIED ARO-14249.14-P NL

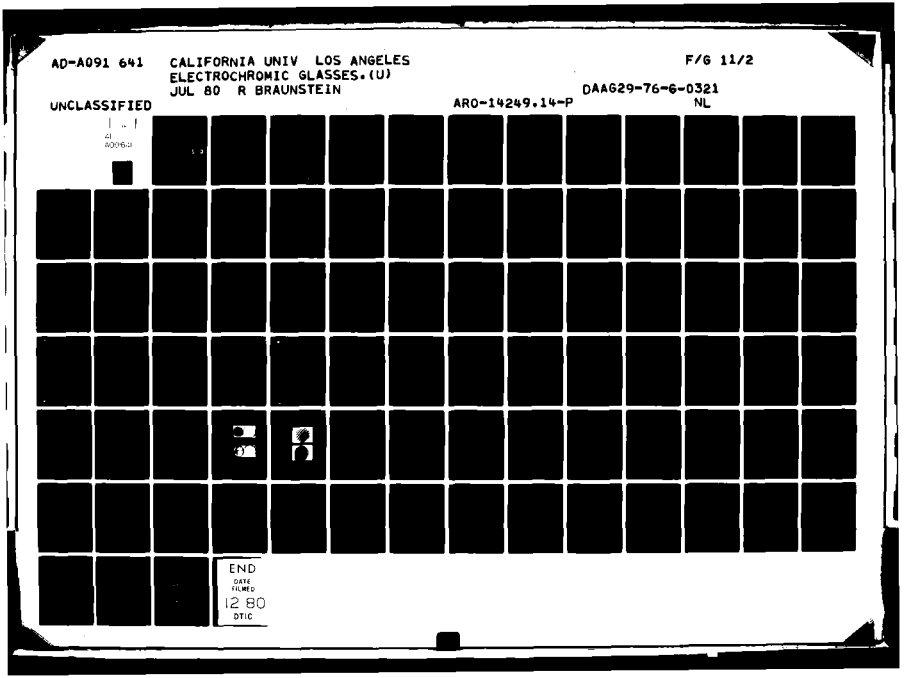

END
DATE FILMED
12 80
DTIC

(12) LEVEL II

ARO 14249.14-P

SECURITY CLASSIFICATION OF THIS PAGE (When Data Entered)

REPORT DOCUMENTATION PAGE

READ INSTRUCTIONS BEFORE COMPLETING FORM

1. REPORT NUMBER: FINAL REPORT
2. GOVT ACCESSION NO.: AD-A091641
3. RECIPIENT'S CATALOG NUMBER:
4. TITLE (and Subtitle): Electrochromic Glasses
5. TYPE OF REPORT & PERIOD COVERED: 9/1/76 - 7/31/80
6. PERFORMING ORG. REPORT NUMBER:
7. AUTHOR(s): Rubin/Braunstein
8. CONTRACT OR GRANT NUMBER(s): DAAG 29-76-G-0321, DAAG 29-79-G-0047
9. PERFORMING ORGANIZATION NAME AND ADDRESS: U.S. Army Research Office, Post Office Box 12211, Research Triangle Park, North Carolina 27709
10. PROGRAM ELEMENT, PROJECT, TASK AREA & WORK UNIT NUMBERS: 31 Jul 80
11. CONTROLLING OFFICE NAME AND ADDRESS: 9 Final 1 Sep 76 - 31 Jul 80
12. REPORT DATE: July 31, 1980 (12) 85
13. NUMBER OF PAGES: 12
14. MONITORING AGENCY NAME & ADDRESS (if different from Controlling Office): ARO 14249.14-P
15. SECURITY CLASS. (of this report):
15a. DECLASSIFICATION/DOWNGRADING SCHEDULE:

16. DISTRIBUTION STATEMENT (of this Report)

Approved for public release; distribution unlimited.

DTIC ELECTE S NOV 12 1980 D B

17. DISTRIBUTION STATEMENT (of the abstract entered in Block 20, if different from Report)

NA

18. SUPPLEMENTARY NOTES

The view, opinions, and/or findings contained in this report are those of the author(s) and should not be construed as an official Department of the Army position, policy, or decision, unless so designated by other documentation.

19. KEY WORDS (Continue on reverse side if necessary and identify by block number)

Electrochromic	Rayleigh-Brillouin Scattering
Photochromic	Fluoride Glasses
Dipole Interactions	Wavelength Modulation
Space Charge	Depolarization Currents

20. ABSTRACT (Continue on reverse side if necessary and identify by block number)

The series of Li_2O-B_2O_3, Na_2O-B_2O_3-WO_3 and TeO_2-WO_3 glasses were prepared which exhibit the phenomena of electrochromic, photochromic and cooperative behaviour of random electric dipoles in an amorphous matrix. The techniques of thermally stimulated depolarization currents were used to measure the relaxation time, dipole moment and activation energy of dipole species in these glasses. Wavelength modulation and Rayleigh-Brillouin scattering techniques were employed to study the optical properties of these glasses.

DD FORM 1 JAN 73 1473

C 12 25C

SECURITY CLASSIFICATION OF THIS PAGE (When Data Entered)

AD A091641

DTIC FILE COPY

8011 03 099

Electrochromic Glasses

Final Report

Rubin Braunstein

July 31, 1980

U. S. Army Research Office

Grant: DAAG 29 76 G 0321; 79G 0047

University of California, Los Angeles

Table of Contents

A. Objectives of Program:

The broad objectives of this research program were to prepare a series of bulk tungstate glasses containing a wide concentration range of WO_6 octahedra that will exhibit electrochromic, photochromic and dipole-dipole interactions in amorphous matrices. These glasses were to serve as protype systems to study electronic and ionic transport in amorphous systems as well as a media to study cooperative behaviour between dipoles in an amorphous system. In the execution of these endeavours instrumentation was to be developed to study the optical properties of these glasses. These include: an optical derivative spectrometer to measure low level absorption; a high contrast ratio tandem Fabry-Perot interferometer to measure Rayleigh-Brillouin scattering in glasses; thermally stimulated depolarization current techniques to study dipole structures in glasses.

The specific areas of research activity pursued were:

Photochromic and Electrochromic Properties of Tungstate Glasses.
Dipole Correlations in TeO_2-WO_3 Glass.

Cooperative Phenomena of Random Electric Dipoles in an Amorphous Matrix.
Space Charge Injection into a Dipolar Glass.
Ultraviolet-Visible Absorption in Highly Transparent Solids by Laser Colorimetry and Wavelength Modulation Spectroscopy.
Evidence for Excitonic Absorption in Metallic $MnAs_{0.88}P_{0.12}$.

Scattering Losses in Single and Polycrystalline Materials.
Rayleigh-Brillouin Scattering in Lithium Borate and Lithium-borate Tungsten Glasses.

Thermally Stimulated Depolarization Currents in $Li_2O(x)\cdot(B_2O_3)(1-x)$ and $Na_2O(x)\cdot(B_2O_3)(1-x)$.

Infrared Transparent Glasses Derived From Fluorides of Zirconium, Thorium and Barium.

The following are the problems studied and the conclusions reached. The reference numbers after each topic are to the publications referenced in the Publication List of reprints which are included in the Appendix.

1. Photochromic and Electrochromic Properties of Tungstate Glasses [2,6].

We have demonstrated that it is possible to prepare a series of bulk transparent glasses containing high concentrations of WO_6 octahedra in various glass forming matrices such as Li_2O-B_2O_3 and Na_2O-B_2O_3 or TeO_2. These glasses exhibit for the first time, electrochromic and photochromic behaviour and have potential for use in solid state display devices. In addition, these glasses serve as prototype systems within which to study small polaron transport, percolation transport, as well as electrochemical potential studies between glass-electrolyte systems.

When electrons and hydrogen ions were simultaneously injected into these glasses, a blue front was found to propagate from the cathode. When the potential across the glass was reversed, the blue coloration bleached. These experiments were performed on bulk glasses using the following configuration: the sample with a gold contact was immersed in an electrolyte of tricloro-acetic acid and methanol containing a platinium counter-electrode. When the gold contact was biased negatively with respect to the platinium electrode with an overpotential of > 2, a blue front diffused from the gold cathode along the surface of the glass. When the bias was reversed, the region adjacent to the gold contact began to bleach and ultimately the entire color front disappeared. The diffusion coefficient for the coloration was $D \sim 3 \times 10^{-6} cm^2 sec^{-1}$.

The photochromic behaviour of these glasses were studied by placing a sample in a solution of trichloro-acetic acid in methanol and illuminating the sample with radiation in the fundamental absorption edge of the glass; upon illumination, the glass developed a blue coloration in transmitted light. Similar results were obtained by using Na and Li electrolytes.

The photochromic and electrochromic behaviour of Li_2O-B_2O_3 glasses can be explained on the basis of the double injection of electrons and protons with the formation of H_xWO_3 within the glass matrix. This glass system can form the basis of display and information storage devices. Although these initial studies were performed with a liquid electrolyte it is clear that the same interaction should be possible by ion injection from a solid electrolyte. The use of fast Li ionic transporting glasses should be a profitable area to explore. The photochromic behaviour allows one to produce photo-images of high resolution with add-on and electric erasure qualities. Device configuration of various types of displays have been delineated in a Patent Disclosure submitted to the granting agency.

2. Dipole Correlations in TeO_2-WO_3 Glass [3].

Glass systems consisting of randomly distributed dipoles of BO_6 soft mode octahedra whose concentration can be controlled in an amorphous matrix suggests the possibililty that such a "doped" electric dipole system could result in correlations between dipoles. If the dipoles are within a "correlation distance", "ferroelectric" or "antiferroelectric" clusters could occur and so exhibit some degree of order in an amorphous matrix with a resulting phase transition at a critical temperature.

A glass consisting of the composition $TeO_2 \cdot 0.23\ WO_3$ was studied by capacitance and thermally stimulated depolarization current (TSDC) techniques from 4.2-300K. Structure was observed in this glass at temperatures where phase transitions are observed in crystalline WO_3. These results indicate that local WO_6-octahedra determine the dielectric constant of this glass and that dipole-dipole correlations contribute to the "ferroelectric-like" character of this amorphous system. The TeO_2-WO_3 glasses can only be prepared with a limited range of WO_3 concentrations. To study the evolution of dipoles from an independent dipole (paraelectric phase) to a dipole-dipole (cooperative behaviour) it was decided to continue these studies on the Li_2O-B_2O_3-WO_3 system where we were able to prepare a continuous variation of WO_3 content in the glass matrix Li_2O-B_2O_3 and so follow the evolution of possible dipole-dipole interaction which are discussed in the following section.

3. Cooperative Phenomena of Random Electric Dipoles in an Amorphous System [4,6].

The techniques of thermally stimulated depolarization currents were used to observe the transition from independent dipole to cooperative behaviour of WO_6 octahedra in the Li_2O-B_2O_3-WO_3 glass system. These measurements allowed us to essentially study the dynamic susceptibility of this dipole system and determine the relaxation time, activation energy and dipole moments of WO_6 in this amorphous system. At concentrations of WO_3 of less than 0.008 mole percent, the system behaved as a paraelectric; however at a critical concentration and temperature, the WO_6 exhibited a transition which behaved as a cooperative phase. This system of random "pseudo-spins" in an amorphous matrix behaves in many ways as the electric analogue of a magnetic spin glass system.

We developed a model for a possible phase transition associated with a random "psuedo-spin" system in an amorphous matrix. Essentially, we adapted the Glauber

formalism for an Ising system of "pseudo-spins" which can be treated in the mean field approximation. In this model, we have allowed for the situation where the spins are in a compensating configuration without the presence of an external electric field. This model exhibits a critical slowing down of the relaxation time at a critical temperature, characteristic of a phase transition. A calculation of the depolarization currents as a function of temperature using this model, exhibits a sharp peak as opposed to the traditional asymmetric glow curve that is normally calculated and observed for independent dipoles.

In this study, depolarization peaks were also observed in the Li_2O-B_2O_3-WO_3 and pure Li_2O-B_2O_3 glasses which exhibit an independent dipole behaviour. The nature of these dipoles was studied in detail and are discussed in the section: Thermally Stimulated Depolarization Currents in $Li_2O(x)\cdot(B_2O_3)(1-x)$ and $Na_2O(x)\cdot(B_2O_3)(1-x)$ glasses.

The observation of these cooperative phenomena in these tungstate glasses which can be controlled by varying the concentration of WO_3, opens up a new class of materials which allow one to study critical phenomena in electric dipole systems. In addition, these glasses suggest various transducer applications. Possible transducer device configurations are described in a Patent Disclosure submitted to the granting agency.

4. Space Charge Injection into a Dipolar Glass [7].

The above studies on the cooperative behaviour were performed using mylar blocking contacts. These studies were extended to the study of two types of contacts, namely ultrasonically soldered indium contacts to the glass as well as the mylar blocking contacts. The use of indium contacts resulted in the injection of large space charge peaks while the use of the blocking contacts completely suppressed these peaks.

A detailed study was made of the effects of injected space charge in the Li_2O-B_2O_3-WO_3 and the Li_2O-B_2O_3 glass systems. In this work a periodic variation in the integrated intensity of the space charge peaks as a function of poling field was observed in the tungstate glasses. A model was developed for this observed periodic variation. The essential features of this model are that at low space charge injection levels, the space charge results in a high field at a Schottky barrier which induces a "ferroelectric-like" behaviour at a critical field. However, at high injection levels, the "cooperative behaviour" of the WO_6 octahedra can be destroyed by the oxidation-reduction reaction of $W^{+5} \rightarrow W^{+6}$.

Consequently, the oscillatory behaviour of the peak depolarization current which is observed as a function of poling field can be interpreted in terms of the migration of "ferro-electric-like" domains into the interior of the glass. Space charge effects in the pure Li_2O-B_2O_3 were also studied without WO_3 no periodic behaviour was observed.

Further studies of the injection of space charge into glass by thermal depolarization techniques can be rewarding as we have observed the amount of space charge injected depends upon the metal contact employed. These studies can yield information about the interface states between metals and glasses.

5. Wavelength Derivative Measurements [1].

We have previously developed wavelength derivative techniques to study the band structure of semiconductors and metals. These measurements are capable of detecting a part in 10^5 of a change in absorption out of a relatively smoothly varying background. Residual impurities in the Li_2O-B_2O_3 and Na_2O-B_2O_3-WO_3 glasses were detected by this technique which can readily detect absorption bands at levels of 0.1 ppm.

Since there is a great technologic interest in synthesizing highly transparent materials, the wavelength derivative technique was utilized for examining such materials. A number of the state of the art prepared highly transparent materials namely: SiO_2, Al_2O_3, NaF, LiF, CaF_2, SrF_4, MgO, and LaF_3 were examined in the ultraviolet-visible regions of the spectrum. It was possible to measure the complete spectral distribution of the absorption at levels of $10^{-5}cm^{-1}$ for the first time. In the past, it was only possible to measure low level absorption by laser colorimetry which yields the absorption coefficient at a few discrete wavelengths. By obtaining the complete spectral distribution of the absorption at levels at 10^{-5}cm it was possible, for the first time, to identify extrinsic impurities in highly transparent solids.

This unique technique can form an important diagnositc tool for materials preparation groups, especially in the area of laser windows and low-loss optical fibers.

6. Evidence for Excitonic Absorption in Metallic $MnAs_{0.88}P_{0.12}$ [5].

Wavelength modulation techniques were used to study the reflection spectra

of the double ferromagnet $MnAs_{0.88}P_{0.12}$ at 300 and 100K for energies between 1.6 and 5.0 eV. The rich structures observed by the derivative techniques allowed us to distinguish between intraband transitions (free electron) and von Hove singularities in the band structure. In addition, the nearly Lorentzian line shape and the strong temperature of some of the bands indicate their excitonic-like origin.

A calculation of the energy levels for extended resonance states in $MnAs_{0.88}P_{0.12}$ indicate the possible existence of triangular resonance states in this material which agree with the experimental observations. The power of wavelength derivative techniques even in the metallic reflection regime, indicates that it may be fruitful to employ these methods to look for excitonic effects in other metallic systems.

7. Rayleigh-Brillouin Scattering in Lithium Borate and Lithium-Boro -Tungstate Glasses.

Since our electrical measurements using thermally stimulated depolarization currents in $(Li_2B_4O_7)(1-x)\cdot(WO_3)(x)$ and $(Na_2B_4O_7)(1-x)\cdot(WO_3)(x)$ glass systems have yielded evidence for cooperation between electric dipoles, we decided to search for critical opalescence and soft-mode behaviour in this "pseudo-spin" glass system.

For this purpose, we assembled a high contrast ratio five-pass Fabry-Perot interferometer. In addition, a tandem Brillouin spectrometer has been assembled for the extended free spectral up to 100 cm^{-1} to examine low frequency modes in these glasses. The systems are under computor control using a CAMAC interface. Aside from studying the inelastic Brillouin and Raman regimes using the interferometers, the electronic system enables us to also study quasi-elastic (Rayleigh) scattering by digital photon-counting and self-beating techniques.

The variation of the transverse and longitudinal acoustic velocities of the glasses $(Li_2O\cdot 4B_2O_3)_{1-x}(WO_3)_x$ were studied at room temperature. This study was necessary before one begins to look for temperature dependent soft modes associated with a possible phase transition of the "pseudo-spin" glasses. Because of the high contrast ratio obtainable with our instrumentation, it was possible to perform 90^o scattering on 1mm thick discs of glass without being overwhelmed by the Rayleigh line.

An abrupt decrease occurs both in the transverse and longitudinal sound velocities of the Li_2O-B_2O_3 glasses by adding x = 0.009 of WO_3 with a subsequent increase to a peak velocity at x = 0.165. The same behaviour is observed with the Na_2O-B_2O_3-WO_3 system. Without WO_3, the system $(Li_2O)(x)\cdot(B_2O_3)(1-x)$ with x=0.05 to 0.25 shows a monatonic increase in the TA and LA modes. It is interesting to note that the abrupt changes in the transverse and longitudinal velocities of the tungstate glasses occur in the same composition range as we observed the abrupt changes in relaxation times by TSDC. This is to be contrasted with the monatonic behaviour of the TA and LA modes observed in glasses without WO_3.

These Rayleigh-Brillouin measurements are now being extended as a function of temperature and in the presence of poling electric fields to look for optical manifestations of "pseudo-spin"glass behaviour.

8. Scattering Losses in Single and Polycrystalline Materials for Infrared Fiber Applications [9].

Concomitant with our Rayleigh-Brillouin measurements on our glasses, measurements were also performed in single and polycrystalline KCℓ to check the operation of our light scattering apparaturs as well as to make a contribution in an adjacent research area.

There is a current technological interest to look for candidate materials which exhibit low optical losses at specific wavelengths for utilization in fiber optics and light guiding applications. Considerations have been given to the ultimate theoretical intrinsic-loss mechanisms and the practical extrinsic losses due to impurities and imperfections in crystalline and glassy materials. The ultimate transparency in materials should like in a valley between the intrinsic electronic absorption edge and the tail of the multi-phonon transitions. In this region, the ultimate losses should be due to Rayleigh and Brillouin scattering. The Brillouin scattering results from light that has been inelastically scattered (Bragg scattering) from acoustical phonons and is an intrinsic property of a given material. The Rayleigh scattering of light results from nonpropagating fluctuations in the dielectric constant. In glasses these fluctuations include: density variations resulting from frozen-in random variations in the dielectric in a disordered solid; concentration fluctuations resulting from local composition variations present in mixtures; entropy fluctuations resulting from temperature variations.

Using our Rayleigh-Brillouin scattering system, we have completed an initial study of scattering from single and polycrystalline materials in cooperation with a group at the Hughes Research Laboratory to probe the mechanisms responsible for light scattering losses in highly transparent materials. Although we have found that polycrystalline materials scatter more strongly than single crystal materials, but have not as yet explicitly associated a particular elastic scattering process which contributes to the total scattering. Grain boundaries, dislocations and the decoration of these structures by impurity-pinning and possible candidates. In addition, our results indicate the even in very pure single crystal KCℓ samples, there is more scattering than predicted for an ideal KCℓ crystal.

9. Infrared Transparent Glasses Derived From Fluorides of Zirconium, Thorium and Barium [8].

Because of our continued interest in glass fabrication techniques in this program, we have maintained a liason with groups at the Hughes Research Laboratories involved in materials synthesis. Although the main thrust of the present grant was concerned with photochromic, electrochromic and the dielectric properties of the tungstate glasses, our developed instrumentation for measuring absorption and scattering and the fabrication of glasses have importance in other areas of glass utilization. In this work, glasses consisting solely of high purity ZnF_4 ThF_4, and BaF_2 have been synthesized using reactive atmosphere processing (RAP) techniques. RAP has previously been applied to the growth of single crystal rare earth fluorides to totally eliminate many solid-solid phase transitions thought to be intrinsic to these compounds. The utilization of RAP processing in the synthesis of glasses is new and has shown that the infrared transparency and the mechanical strength of these halide glasses are greatly improved by eliminating anionic impurities such as OH^- and $\theta^=$ resulting in glasses which are continuously transparent from 0.3 to 7μm and are water insoluable and unusually hard and strong. In addition, these glasses can yield high-fidelity replication surfaces by die casting.

Although the above work was not in the main stream of the glass synthesis of the present program, we have summarized this work since it points the way for innovative production of glasses that can apply to our glass systems. In particular, since our glasses are prepared in air, they contain appreciate OH^- which can influence the optical and electrical measurements of the present work.

10. Thermally Stimulated Depolarization Currents in $Li_2O(x)\cdot(B_2O_3)(1-x)$ and $Na_2O(x)\cdot(B_2O_3)(1-x)$ glasses.

Our previous published measurements on Li_2O-B_2O_3 glasses have revaled a dipole bearing species which is present in pure $Li_2O\cdot 2B_2O_3$. It was of interest to perform similar TSDC measurements on a series of $Li_2O(x)\cdot(B_2O_3)(1-x)$ and $Na_2O(x)\cdot(B_2O_3)(1-x)$ glasses in an attempt to identify the origin of this peak which would allow the use of TSDC as a tool to study glass structures.

Borate glasses are of interest because their structural properties are quite different from silicate glasses and boric oxide is used extensively in borosilicate glasses. An extensive body of literature utilizing nuclear magnetic resonance, infrared and Raman spectra, and other physical properties indicate that the boroxyle group B_2O_3 plays an important role in vitreous alkali borate glasses. As the alkali content is increased there is evidence that the number of boraxyle (3-coordinated B) groups decrease and are replaced with diborates (4-coordinated B) groups. As the alkali content is increased, the number of non-bridging oxides can increase and the Na^+ and Li^+ ions which can reside in the voids near the tetrahedral boron sites are also expected to increase.

A series of glasses of composition: $Li_2O(x)\cdot(B_2O_3)(1-x)$ and $Na_2O(x)\cdot B_2O_3(1-x)$ with x = 0 to 0.33 were investigated using TSDC techniques. The samples were poled at room temperature in E-fields of 10^4V/cm and the samples cooled to 77K and short circuited and subsequently subjected to a linear temperature ramp and the depolarization currents measured. The samples were isolated from the capacitor electrodes by 10 mil thick mylar foils as blocking contacts to prevent the space charge injection effects associated with metal electrodes discussed in this report.

Two TSDC peaks were observed in the $Li_2O(x)\cdot B_2O_3(1-x)$ glasses at -77°C and in the temperature range (26°C to -47°C). The area of these peaks was independent of composition up to x = 0.16 and then abruptly increased by a factor of 30 at x = 0.25. Similar peaks were observed in the $Na_2O(x)\cdot B_2O_3(1-x)$ glasses. It is interesting to note that the abrupt change in peak intensity occurs at x = 0.16 which is the composition where nuclear magnetic resonance, infrared and Raman spectra show a possible charge in the coordination of B. All the "borate anamolies" also occur at this composition in the alkali borate glasses. The interpretations of our TSDC indicate that we have identified dipoles due to diborates and non-bridging oxides. This work is being completed and will be prepared for publication

and indicates that TSDC can be used to study dipolar structural entities in a glass system. We have also observed dipole species in alkali silicate glasses; the development of electrical methods, i.e. TSDC that signal the presence of dipolar structural entities in amorphous systems can form a powerful analytical technique.

B. Publications During Grant Period:

1. "Ultraviolet-Visible Absorption in Highly Transparent Solids by Laser Calorimetry and Wavelength Modulation Spectroscopy," with J.A. Harrington, B.L. Bobbs, M. Braunstein, R.K. Kim, R. Stearns and R. Braunstein, Applied Optics 17, 1541 (1978).

2. "Photochromic and Electrochromic Properties of Tungstate Glasses," R.Braunstein, Solid State Comm. 28, 839 (1978).

3. "Dipole Correlations in TeO_2-WO_3 Glass," R. Braunstein, I. Lefkowitz and J. Snare, Solid State Comm. 28, 843 (1978).

4. "Cooperative Phenomena of Random Electric Dipoles in an Amorphous Matrix," R. Braunstein and K. Bärner, Solid State Comm. 28, 847 (1978).

5. "Evidence for Excitonic Absorption in Metallic $MnAs_{0.88}P_{0.12}$," K. Bärner, R. Stearns and R. Braunstein, Phys. Stat. Sol (b) 95, 483 (1979).

6. "Ferroelectric, Photochromic and Electrochromic Glasses," R. Braunstein and I. Lefkowitz, Ferroelectrics 27, 1225 (1980).

7. "Space Charge Injection Into a Dipolar Glass," Solid State Comm. 33, 941 (1980).

8. "Infrared-Transparent Glasses Derived From the Fluorides of Zirconium, Thorium and Barium," M. Robinson, R.C. Pastor, R.R. Turk, D.P. Devor, M. Braunstein and R. Braunstein, Mat. Res. Bull. 15, 735 (1980).

9. "Scattering Losses in Single and Polycrystalline Infrared Materials for Infrared Fiber Applications," J. A. Harrington, M. Braunstein, B. Bobbs and R. Braunstein, (to appear in Proceedings of Am. Ceramic Society Annual Meetig, April 1980, to be published as Volume on Physics of Optical Fibers, 1980).

C. Participating Scientific Personnel:

Bradley Bobbs	Ph.D. Candidate
Michael Burd	Ph.D. Candidate
Donald Deal	Ph.D. Candidate
M. Entemadi	Ph.D. Candidate
R. K. Kim	Ph.D. Candidate
Robert Martin	Ph.D. Candidate
Paul Robusto	Ph.D. Granted 1978
Ronald Stearns	Ph.D. Candidate
John Stevens	Ph.D. Candidate
Prof. K. Bärner	Sabbatical Visitor (Göttingen University)
Prof. L. Muldauer	Sabbatical Visitor
M. Robinson	Leave of Absence (Hughes Research Laboratory)

Appendix

Reprinted from APPLIED OPTICS, Vol. 17, page 1541, May 15, 1978

Ultraviolet–visible absorption in highly transparent solids by laser calorimetry and wavelength modulation spectroscopy

James A. Harrington, Bradley L. Bobbs, Morris Braunstein, R. K. Kim, R. Stearns, and Rubin Braunstein

The requirements for low-loss optical materials for use on excimer lasers have stimulated the investigation of optical absorption in a variety of highly transparent materials at visible and uv wavelengths. To provide information over a wide spectral range at low absorption levels ($\simeq 10^{-5}$ cm^{-1}), laser calorimetric and wavelength modulation spectroscopic techniques were used. Blending these two methods provided, for the first time, spectral information well below the usual levels of absorption measured in studies of the Urbach tail.

Introduction

In this paper we report on the first use of laser calorimetry in conjunction with wavelength modulation techniques to measure the spectral distribution of absorption at levels of 10^{-5} cm^{-1} in highly transparent solids. Various problems concerning the optical properties of solids have created a need for measuring low levels of absorption in highly transparent solids. In particular, the requirements for high power laser windows and fiber optic systems have led to the development of new techniques of material growth and surface preparation that yield absorption levels on the order of 10^{-5} cm^{-1}. The high power operation of ir, visible, and uv lasers is often limited by the lack of satisfactory materials for laser windows and other optical components.

Measurement of the small residual optical absorption in highly transparent solids most generally involves laser calorimetric techniques[1] for determining the absorption coefficient β at specific laser frequencies of interest. These methods, which have been almost universally applied in the study of low-loss coating and window materials for use as ir laser optical components, have been refined to the point that not only can extremely small absorptions (in KCl at 5.3 μm, for example, where $\beta \simeq 10^{-6}$ cm^{-1}) be measured, but the surface and bulk contributions to the total absorption can also be dynamically separated.[2,3] Laser calorimetry, however, is limited to a small range of laser wavelengths; to determine intrinsic and extrinsic absorption mechanisms and also to identify impurities, measurements should be performed over an extended spectral region.

Wavelength derivative techniques have been used at visible and uv wavelengths for optical studies at levels of one part in 10^5 in the band structure of semiconductors,[4] metals,[5] and band tails.[6] Wavelength modulation techniques yield essentially the energy derivative of the absorption coefficient. The absolute value of the absorption coefficient can be obtained by numerically integrating the observed derivative spectra, the constant of integration being supplied by an independent direct-loss measurement at a few fixed wavelengths. In the work reported here, measurements were performed in spectral regions of high transparency, and the constants of integration were supplied from laser calorimetry measurements at fixed wavelengths. Blending these two methods permits, for the first time, studying spectral features at low levels of absorption. In particular, the spectrum from approximately 500 nm to 250 nm in various transparent ionic solids has revealed structure in the extrinsic Urbach tail region never before observed.

To demonstrate the power and versatility of these techniques, a systematic study was made of optical absorption in a wide variety of materials that potentially could be used as low-loss coatings or windows on excimer lasers. The materials with large bandgaps that have been investigated from approximately 500 nm to 250 nm were alkali halides, alkaline earth fluorides,

J. A. Harrington, B. L. Bobbs, and M. Braunstein are with Hughes Research Laboratories, Malibu, California 90265; the other authors are with University of California, Physics Department, Los Angeles, California 90024.

Received 24 December 1977.
0003-6935/78/0515-1541$0.50/0.

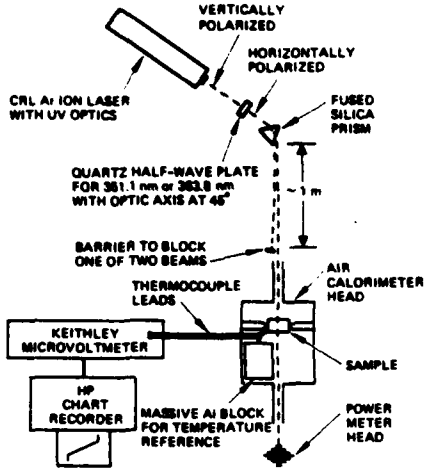

Fig. 1. Ultraviolet–visible calorimeter illustrated in uv mode with external priam for separation of two uv lines and half-wave plate to rotate polarization for maximum single line power.

oxides, and some rare earth fluorides. A comparison of our data and reflectivity/absorption data from the literature in the Urbach tail region suggests, although the spectral regions of the published Urbach tail data and our data do not overlap, that our absorption data are significantly lower than a simple extrapolation of the extrinsic Urbach tail.

Experimental Procedure and Techniques

Laser Calorimetry

Standard laser calorimetric methods[1] were used to measure the small optical absorption coefficients in various single and polycrystalline samples. The experimental arrangement, shown in Fig. 1, consisted of an air calorimeter and a Coherent Radiation Laboratories model CR-12 Ar-ion laser. This laser delivered 2–6 W of single line power at 514.5 nm, 488.0 nm, and 457.9 nm and about 1 W in each uv line at 363.8 nm and 351.1 nm. As illustrated in Fig. 1, the latter two lines were separated using an external prism, and the power was optimized in each line with a quartz half-wave plate that was used to rotate the plane of polarization appropriately. A three-slope method was applied to the calorimetrically obtained temperature–time curves for the calculation of the absorption coefficient β.[1] In two cases, long bar-shaped samples of single crystal KCl and CaF_2 were used to effect the separation of bulk and surface absorption.[2]

Wavelength Modulated Spectrometer

Wavelength modulation to obtain the derivative spectra was accomplished by sweeping the output wavelength across the exit slit by vibrating the output diagonal mirror in a Perkin-Elmer 99G monochromator; the depth of modulation was continuously controlled. Since the background spectra from the source, optics, and detector contribute to the observed derivative signal, a double-beam single-detection system must be used to eliminate the background derivative from the sample derivative. (Such a system is described in Ref. 7.) In the system used (shown schematically in Fig. 2), the modulated beam is directed alternately between the sample and reference channels at 13 Hz, and the wavelength is modulated at 217 Hz. Since a single detector is used, it is necessary to use gating circuits, which permit independent measurement of the sample and reference channels.[8] The depth of modulation with respect to wavelength is measured using the Hg–green line and the known dispersion of the monochromator so that the wavelength-dependent depth of modulation can be calculated throughout the spectrum. To obtain the absorption coefficient, the derivative data (using the measured depth of modulation) are numerically integrated, and the constant of integration is supplied by the absolute absorption coefficient measured at discrete wavelengths by laser calorimetry.

Experimental Results

Calorimetric Measurements

Eleven different materials were measured at visible and uv wavelengths. In some cases, more than one source or different forms of the same material were studied. Figures 3–6 display all the calorimetric data for the various samples studied. In each case, absorption increases with energy. The lowest absorbing crystals are the alkaline earth fluorides, KCl, NaCl, and

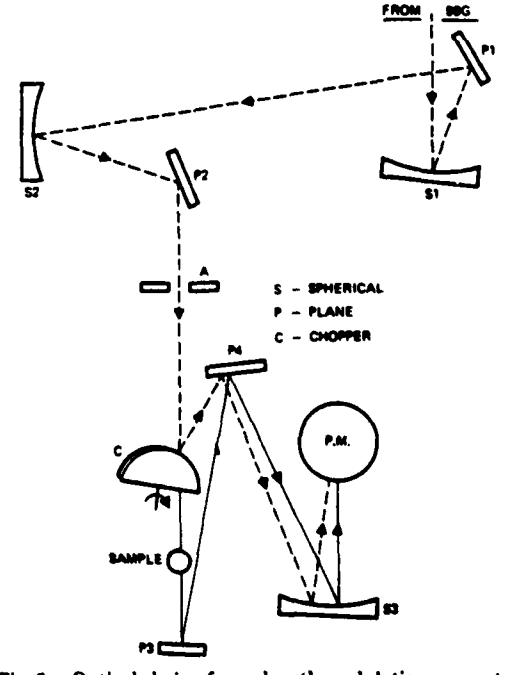

Fig. 2. Optical chain of wavelength modulation apparatus.

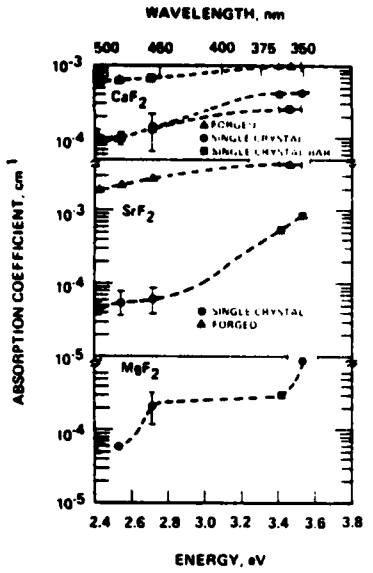

Fig. 3. Calorimetric measurements of uv–visible absorption in various divalent fluorides.

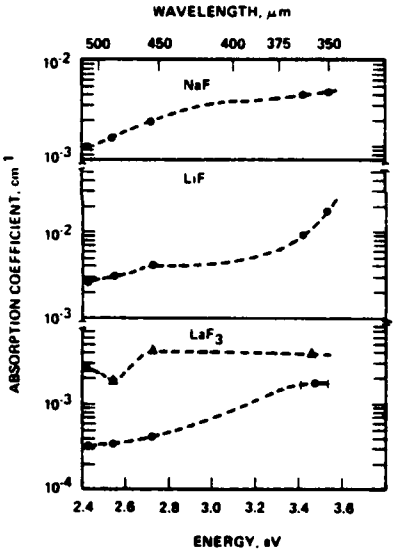

Fig. 4. Calorimetric measurements of uv–visible absorption in NaF, LiF, and LaF_3.

SiO_2 (one sample), where β's in the low 10^{-4}-cm^{-1} region were measured at visible wavelengths. From the two long-bar samples of KCl and CaF_2 studied, it was found that the initial and final slopes of the temperature–time curves were equal, indicating[2] that the low value of absorption found in these samples was entirely bulk absorption. The single crystal KCl grown at Hughes Research Laboratories, for example, had absorption coefficients that were unmeasurable in the blue–green region (see Fig. 5) but were estimated, based on the sensitivity of the calorimeter, to be no greater than 2×10^{-5} cm^{-1}. The highest absorbing materials tended to be some oxides, NaF, and LiF. The latter two samples, obtained from Optovac, Incorporated and Adolf Meller Company, had surprisingly high absorp-

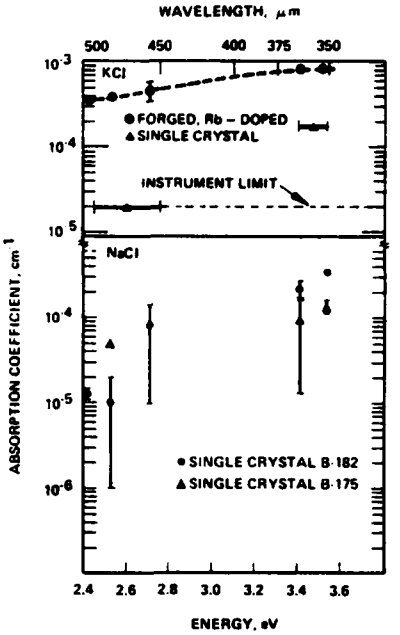

Fig. 5. Calorimetric measurements of uv–visible absorption in KCl and NaCl. These RAP grown materials have yielded the lowest absorptions of any material.

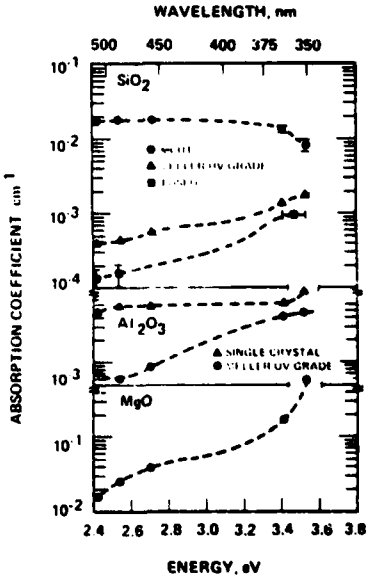

Fig. 6. Calorimetric measurements of uv–visible absorption in various oxides.

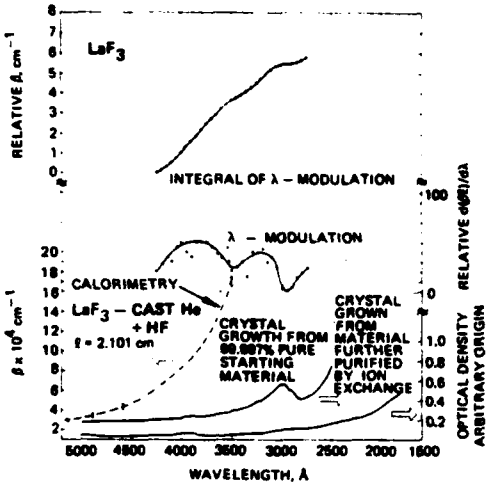

Fig. 7. λ-modulation spectroscopy and calorimetry for LaF_3. Lowest two solid curves, measured on a Cary 14, are given for comparison purposes.

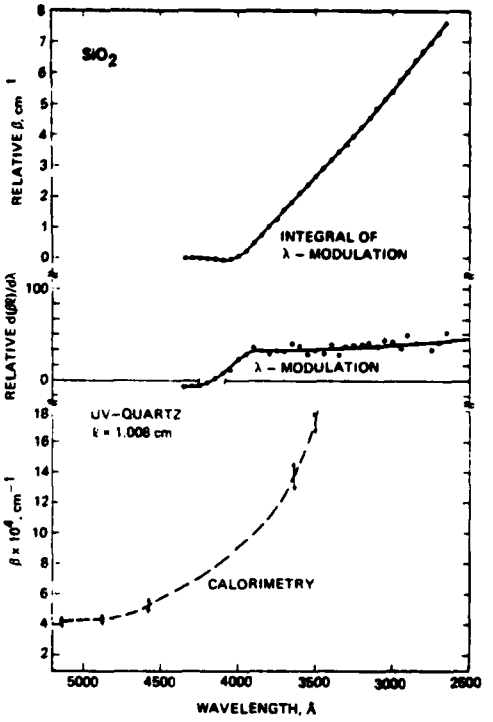

Fig. 9. λ-modulation spectroscopy and calorimetry for SiO_2.

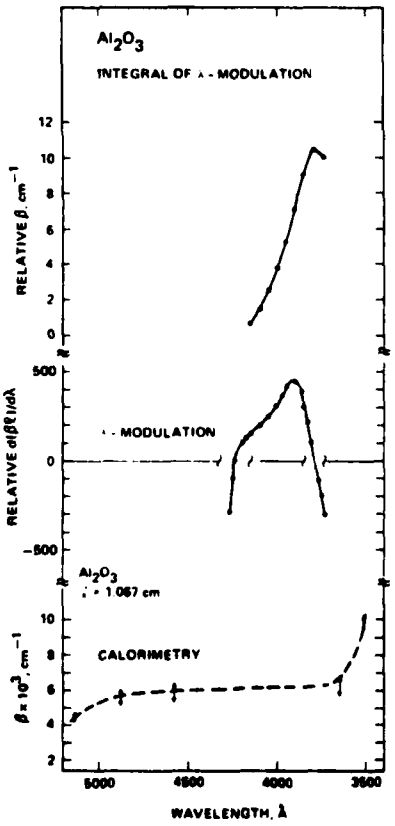

Fig. 8. λ-modulation spectroscopy and calorimetry for Al_2O_3. Note that the peak observed by λ-modulation spectroscopy near 3700 Å is not seen calorimetrically due to the absence of laser lines at this wavelength.

tions, especially considering the large bandgap in these materials. This is probably because these materials are not as pure as the alkaline earth fluorides and other alkali halides, which had been more highly purified because they were to be used in ir laser window applications. In no case, however, did absorption increase with increased exposure to the uv laser radiation, as might occur if color centers were being continuously produced.

Wavelength Modulation Spectroscopy

Absorption coefficients for some of the same samples measured calorimetrically were obtained by wavelength modulation spectroscopy from approximately 450–280 nm. The results of this work for several materials are shown in Figs. 7–11. The raw data are returned as a derivative of the absorptance with respect to wavelength. The depth of modulation employed in these measurements was 8 Å. These spectra are then integrated to yield the relative absorption coefficients, shown as the upper curves in Figs. 7–11. An absolute calibration of these curves is in turn obtained by a comparison with the calorimetric data of Figs. 3–6 (reproduced as the dashed-bottom curves in Figs. 7–11). In general, there is excellent agreement between the calorimetric and λ-modulation data for each host material studied.

The increasing absorption at uv wavelengths is clearly evident in samples of LaF_3, Al_2O_3, and SiO_2. The high

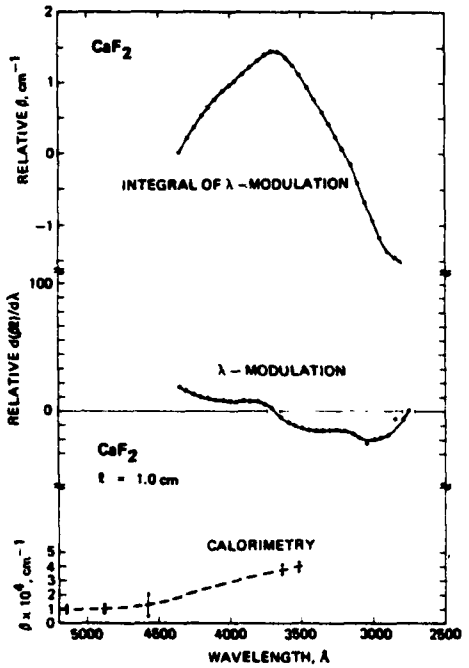

Fig. 10. λ-modulation spectroscopy and calorimetry for CaF_2. Note the decrease in absorption at shorter wavelengths and the peak near 3600 Å presumably due to color centers.

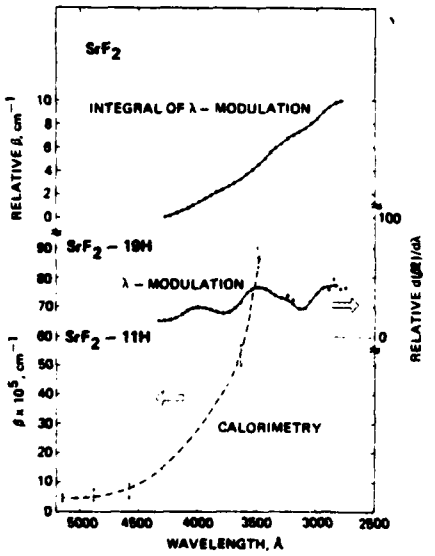

Fig. 11. λ-modulation spectroscopy and calorimetry for SrF_2.

sensitivity of λ-modulation methods in comparison with other forms of spectroscopy is also evident in the spectra of some older LaF_3 material, shown in Fig. 7, measured on a conventional Cary 14 spectrometer. Contrasting the conventional spectroscopic data with the calorimetric and λ-modulation data shows that some structure is visible in the integrated λ-modulated spectrum that is impossible to observe in the Cary 14 data because it is less sensitive than derivative spectroscopy. In Al_2O_3 (see Fig. 8), another complementary feature of λ-modulation spectroscopy can be observed. The peak in the absorption near 380 nm is missed by calorimetry because there are no laser lines at this energy. The 380-nm absorption is probably due to Cr^{3+} ions[9] as wavelength modulation spectroscopy runs on ruby revealed the same structure. By comparison, SiO_2 data in Fig. 9 merely indicate a monotonic increase in absorption with increasing energy. This is in agreement with the calorimeter results (i.e., no sharp absorption bands appear in the spectra).

Calcium fluoride data (see Fig. 10) show a peak in absorption near 370 nm. This is not entirely evident from calorimetry alone, but derivative spectroscopy clearly delineates this band. A likely explanation for this absorption is that it is due to color centers. The absorption in SrF_2, shown in Fig. 11, even though it is at an extremely low level, indicates some structure on an otherwise monotonically increasing absorption with increasing energy.

Comparison with Band Edge Data

The alkaline earth fluorides were singled out for comparison with data in the Urbach tail region taken from existing literature. Figure 12 includes the band edge data of Tomiki and Miyata[10] and our λ-modulation/calorimetric data. Although the two spectral regions do not overlap, the data from this study are significantly lower than any simple extrapolation of the extrinsic Urbach tail data would imply. Presumably, this is because the samples have higher purity, and more sensitive techniques are being used. In general, it is felt that the residual absorption is probably due to electronic transitions in rare earth or transition metal ions[9] or to color centers. Experiments are under way to ex-

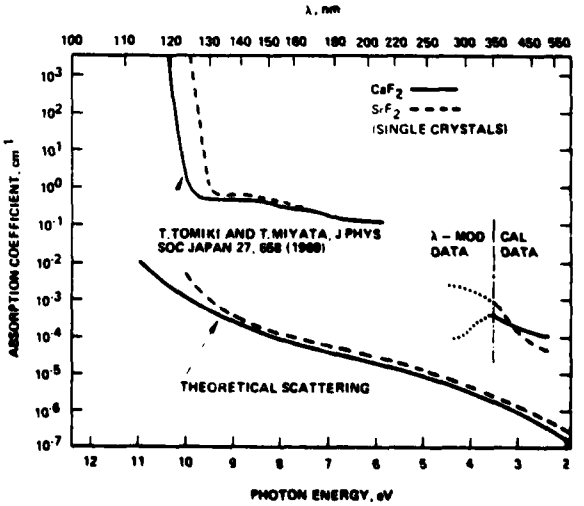

Fig. 12. Ultraviolet–visible absorption in CaF_2 and SrF_2.

tend our measurements to 11 eV so that an accurate comparison can be made. The attenuation due to Brillouin scattering, calculated theoretically, was negligible when compared with the other absorption losses.[11]

Conclusions

Our absorption studies of highly transparent solids for use as low-loss components on uv excimer lasers have led us to conclude that the lowest absorbing materials near 350 nm are the alkaline earth fluorides, NaCl, KCl, and SiO_2. More highly absorbing materials are Al_2O_3, MgO, alkali fluorides, and rare earth fluorides. One reason for this is that the low-absorbing uv materials are also those that have been extensively studied and purified for low loss at ir laser wavelengths. A comparison of our experimental data with extrinsic Urbach tail data indicates less absorption than previously expected.

The authors (at HRL) acknowledge the financial support of Hughes Research Laboratories internal research and development program and (at UCLA) the partial support of the Army Research Office, Durham, North Carolina.

References

1. M. Hass, J. W. Davisson, P. H. Klein, and L. L. Boyer, J. Appl. Phys. **45**, 3959 (1974).
2. H. B. Rosenstock, M. Hass, D. A. Gregory, and J. A. Harrington, Appl. Opt. **16**, 2837 (1977).
3. H. B. Rosenstock, D. A. Gregory, and J. A. Harrington, Appl. Opt. **15**, 2075 (1976).
4. M. Welkowsky and R. Braunstein, Phys. Rev. B **5**, 497 (1972).
5. M. Welkowsky and R. Braunstein, Solid State Commun. **9**, 2139 (1971).
6. H. A. Weakleim, R. Braunstein, and R. Stearns, Solid State Commun. **15**, 5 (1974).
7. M. Welkowsky and R. Braunstein, Rev. Sci. Instrum. **43**, 399 (1972).
8. To be published.
9. D. S. McClure, Solid State Phys. **9**, 399 (1959).
10. T. Tomiki and T. Miyata, J. Phys. Soc. Jpn. **27**, 658 (1969).
11. T. C. Rich and D. A. Pinnow, Appl. Phys. Lett. **20**, 264 (1972).

Solid State Communications, Vol. 28, pp. 839–842.
Pergamon Press Ltd. 1978. Printed in Great Britain.

PHOTOCHROMIC AND ELECTROCHROMIC PROPERTIES OF TUNGSTATE GLASSES*

R. Braunstein

Department of Physics, University of California, Los Angeles, CA 90024, U.S.A.

(*Received* 13 *June* 1978 *by A.A. Maradudin*)

Electrochromic and photochromic behavior have been observed for the first time in the Li_2O–B_2O_3–WO_3 glass system. Double injection of protons and electrons results in the formation of H_xWO_3 in the glass matrix which exhibits a broad absorption band peaking in the vicinity of 1.45–1.65 eV due to electron hopping between W^{+5} and W^{+6} sites. An electron diffusion coefficient of $D_e \sim 3 \times 10^{-6}\,cm^2\,sec^{-1}$ has been measured near the percolation threshold when the volume filling fraction $f > 0.3$ for WO_3 in the glass matrix. The electrochemical potential of these tungstate glasses varies as a function of coloration.

WE HAVE PREPARED a series of bulk transparent glasses containing a wide concentration range of WO_6-octahedra which exhibit, for the first time, electrochromic, photochromic, and ferroelectric-like behavior. Since the WO_6-octahedra play such a central role in the diverse properties of the tungsten bronzes which exhibit the range of properties from ferroelectricity [1], superconductivity [2], and energy storage [3], we were motivated to incorporate various concentrations of the ubiquitous WO_6-unit in various glass forming networks and so form prototype glasses within which electronic and ionic transport and ferroelectric-like behavior could be studied in amorphous systems. In this note, we report the photochromic and electrochromic behavior of the system Li_2O–B_2O_3–WO_3. Elsewhere, the dielectric anomalies of the TeO_2–WO_3 system [4] and cooperative behavior of WO_3 in the Li_2O–B_2O_3–WO_3 system [5] are discussed.

The glasses were prepared from reagent grade oxides in platinum crucibles in air at 800–1100°C. The melts were poured onto a vitreous carbon mold and quenched with a copper disc and then annealed at 300°C for several hours. It was possible to form clear glasses, opalescent glasses, or ceramics depending upon the cooling procedure from the melt. X-ray analysis of the clear glasses showed them to be amorphous. These glasses were impervious to non-aqueous solutions of trichloro acetic acid and could be thermally cycled repeatedly between 4–300 K without cracking or crazing.

The shape of the fundamental absorption edge for amorphous $Li_2B_4O_7$, and $Li_2B_4O_7 \cdot 1WO_3$ are shown in Fig. 1, where it is seen that the absorption edge is shifted towards lower energy with WO_3 present; the samples were 1 mm thick. The photochromic behavior of the tungsten trioxide containing glasses was studied by placing a sample in a solution of trichloro acetic acid in methanol and illuminating the sample with the output of a filtered Hg-arc. When the glass-electrolyte surface was illuminated with radiation in the fundamental absorption edge of the glass, the glass developed a blue coloration in transmitted light. For heavily colored glass, the depth of penetration of the blue layer from the illuminated side of the glass-electrolyte interface was of the order of 10 μm; this depth was measured by sectioning the colored sample and examining the cross sections with a visible microscope. The coloration persisted for days without illumination when the glass remained in contact with the electrolyte, ultimately fading to its original clarity.

The absorption band for two different u.v.-dosages is displayed in Fig. 2 and shows a broad featureless band peaking in the vicinity of 1.45–1.65 eV. Curve (b) shows the band for a higher dosage than curve (a), and it is seen that the band maximum increases in height and shifts to higher energy and broadens for the higher dosage; an estimated total of 10^{18} photons cm^{-2} were incident in the latter case. These bands were measured in transmission with the absorption background due to the uncolored glass and electrolyte subtracted from the raw data. The absorption bands are asymmetrical with apparently greater absorption on the high energy side of the peak; however, this asymmetry could be due, at least in part, to a failure to correct the data for the increase in reflection at the interface caused by an increase in refractive index with energy.

The electrochromic behavior of the glass was studied using the following configuration: the sample with a gold contact and a platinum counter-electrode were immersed in a trichloro acetic acid and methanol

* Work supported by U.S. Army Research Office, Durham, NC, U.S.A.

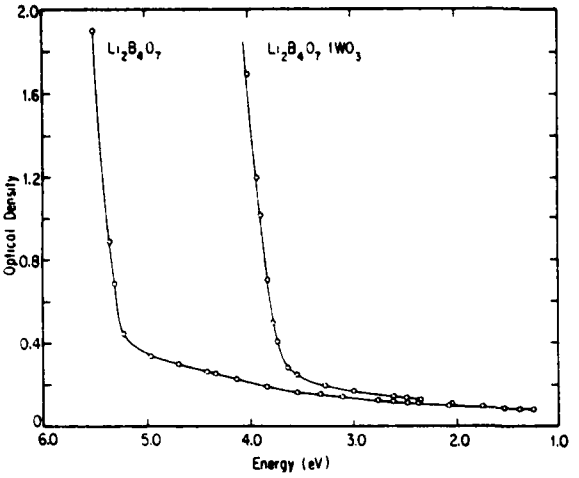

Fig. 1. Optical density of $Li_2B_4O_7$ and $Li_2B_4O_7 \cdot 1WO_3$ glasses. Thickness of samples – 1 mm.

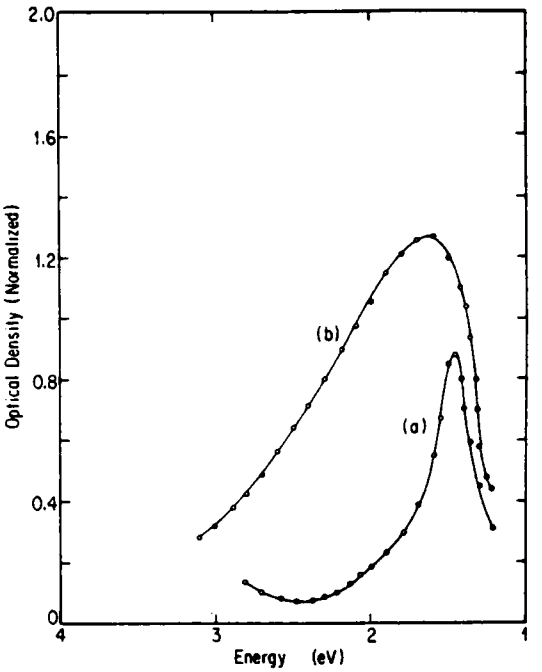

Fig. 2. Optical density of colored $Li_2B_4O_7 \cdot 1WO_3$ layer ~ 10 μm thick for two different u.v.-dosages normalized to the absorption of the uncolored glass and electrolyte; curve (b) has received the larger dosage than curve (a); an estimated total of 10^{18} photons cm^{-2} were incident in the former case.

electrolyte, and the gold contact was masked with an acid-resistant film except for the region immediately in the neighborhood of the gold–glass-electrolyte interface. When the gold contact was biased negatively with respect to the platinum electrode with an over-potential of > 2 V, a blue front diffused from the gold cathode along the surface of the glass. For samples with volume filing fraction of WO_3 $f < 0.3$, no distinct diffusion front was observed but only a network-like percolation. However, for compositions with $f > 0.3$, a distinct diffusion front was observed with diffusion rates increasing with increased WO_3 content. When the bias was reversed, the region adjacent to the gold contact began to bleach and ultimately the entire color front disappeared. The relatively distinct transition to a diffusive regime for high concentrations of WO_3 and the subsequent rapid increase of the diffusion rate indicates a distinct percolation threshold for the transport process responsible for the blue coloration. The diffusion coefficient for the coloration is $D \sim 3 \times 10^{-6}\,cm^2\,sec^{-1}$ at threshold, ($f > 0.3$). We shall see that this is the diffusion coefficient for electrons. The filamentary coloration observed below the diffusion threshold may be due to inhomogeneities of the dispersed WO_3 in the glass.

Electrochromic phenomena in amorphous films of WO_3 have been under active investigation during the last few years for use in display devices [6] as well as the fundamental interest in electronic [7] and ionic transport [3]. The electrochromic behavior has at times been explained as due to defect states in the non-stoichometric films [8]. However, at present it appears as if double injection of protons and electrons forming H_xWO_3 gives a consistent explanation of the coloration of the WO_3 films. The blue color is believed to be due to the electron hopping between W^{+5} and W^{+6} sites [6], although the closely related mechanism of small polaron hopping has also been proposed [9, 10]. A "blue" absorption band occurs when an injected electron is trapped at a W^{+6} site, and optical absorption is due to intervalence band transfer between W^{+5} and W^{+6} sites [6].

The electrochromic activity in WO_3 films has been found to depend upon the physical properties of the film; in fully oxidized films, no electrochromic behavior is observed. Since the coloration rate is known to vary by orders of magnitude depending upon preparation conditions of the film, it is clear that impurities and structural defects can account for these variations in the films. In contrast, the tungstate glasses of this study were prepared in a strongly oxidizing atmosphere, and since they are bulk glasses they do not have the porosity of the films. For a given composition and method of preparation, the diffusion rate of the coloration was found to be approximately the same for several samples.

The photochromic and electrochromic behavior of the Li_2O–B_2O_3–WO_3 glass system can be explained on the basis of the double injection model of electrons and protons with the formation of H_xWO_3 within the glass-matrix similar to the mechanism proposed for pure WO_3 films [7]. The positions of the absorption bands in

the colored glass in Fig. 2 are in the neighborhood of the band observed in colored WO_3 films [6] as well as the absorption band seen in crystals [11]. A glass sample can remain immersed indefinitely in the electrolyte without color change. However, when an electron–hole pair is created by illumination in the fundamental edge of $Li_2B_4O_7 \cdot 1WO_3$ in the presence of the electrolyte, the space charge limited diffusion of the hydrogen ions into the glass is neutralized and H^+ ions can diffuse into the glass with a proton attaching to an oxygen and the electron reducing the tungsten in WO_3 resulting in the formation of a H_xWO_3 molecule in the glass.

In the electrochromic experiments, the color front originates at the cathode and diffuses close to the surface of the glass; the space charge limited diffusion of H^+ from the electrolyte into the glass is neutralized by the injected electrons from the cathode. Electron diffusion seems to control the movement of the colored region since the proton needs only diffuse a short distance into the glass for the geometry employed. The depth of the electrochromic layer is a few microns.

The exact position and shape of the photochromic band can differ in these systems due to the local potential, but the dominant feature seems to be accountable by the intervalence band transition between W^{+6} and W^{+5} ions. Although there is a loss of long range order in these amorphous tungstates, it is reasonable to expect that there is integrity of the WO_6-octahedra with possible slight distortion due to the glass-forming network. Evidence for the integral presence of the WO_6-octahedra unit in these glasses is found from the dipole moments observed in this glass system due to "WO_3" doping [5]. Since not all WO_6-sites are equivalent, one expects the photochromic band to reflect the energy distribution of electrons at various sites. The broadening and shifting to higher energy for larger coloration seen in Fig. 2 requires a detailed knowledge of the electron localization in these glasses for a complete explanation. The oscillator strength of the intervalence transfer between W^{+5} and W^{+6} sites will depend upon the degree of overlap of an electron on neighboring tungsten sites [12].

Since the photochromic and electrochromic process results in the formation of H_xWO_3 in the tungstate glass matrix, one expects the electrochemical potential of the glass to change as a function of coloration. To observe this e.m.f., an electrochemical cell consisting of the configuration:

Au	$Li_2B_4O_7 \cdot xWO_3$	7*N* trichloro acetic acid	Calomel	Au

was assembled so that the gold–glass-electrolyte interface could be illuminated with a u.v.-source. As the coloration proceeded, a change in e.m.f. of the order of 0.3 V was observed. When the glass was allowed to bleach over many days in contact with the electrolyte, the e.m.f. returned to its original value. Studies of the variation of the chemical potential with photocoloration in this tungstate glass system could be rewarding for the study of the free energy of formation of the H_2WO_3 complex in a glass matrix. Measurements of this type have been performed in WO_3 films [13].

In this note, we have reported for the first time on the electrochromic and photochromic processes in the $Li_2O–B_2O_3–WO_3$ glass system. We have observed similar effects in the $Na_2O–B_2O_3–WO_3$ glass system. These and similar tungstate glass systems form convenient amorphous networks to study electronic and ionic transport and electrochemical interactions since it is possible to vary the WO_3 concentration and so control these processes in bulk glasses. Aside from the fundamental interest for electronic and ionic transport in amorphous materials, it is clear that these glass systems can also form the basis for an interesting class of display and information storage devices with better reproducibility than WO_3 films.

Acknowledgements – The author wishes to acknowledge gratefully the technical assistance of Oliver Barrett and Mark Braunstein in the preparation of these glasses and that of R.K. Kim for the aid in some of the optical measurements. Informative discussions with R.S. Crandall are appreciated.

REFERENCES

1. LE BIHAN R. & STELLA C., *J. Phys. Soc. Japan, Suppl.* 28, 377 (1970).
2. LEFKOWITZ I., *Ferroelectrics* 17, 1 (1977).
3. WHITTINGHAM M.S. & HUGGINS R.A., Transport Properties of Inorganic Bronzes, p. 645 in *Fast Ion Transport in Solids, Proc. of the NATO Sponsored Adv. Study Inst. on Fast Ion Transport in Solids, Solid State Batteries and Devices*, Belgirate, Italy, 5–12 Sept. 1972 (Edited by VAN GOOL W.). North-Holland/American Elsevier (1973).
4. BRAUNSTEIN R., LEFKOWITZ I. & SNARE J., *Solid State Commun.* 28, 843 (1978).
5. BRAUNSTEIN R. & BÄRNER K., *Solid State Commun.* 28, 847 (1978).

6. FAUGHNAN B.W., CRANDALL R.S. & HEYMAN P.M., *RCA Review* 36, 177 (1975).
7. FAUGHNAN B.W. & CRANDALL R.S., *Appl. Phys. Lett.* 26, 120 (1975).
8. DEB S.K., *Phil. Mag.* 27, 801 (1973).
9. SCHIRMER O.F., WITTWER V. & BARU G., Abstracts of the Electrochemical Society, Inc., Meeting Oct. 17–22, 1976.
10. HOLLINGER G., MINGH DUC TRAN, & DENEUVILLE A., *Phys. Rev. Lett.* 37, 1564 (1976).
11. DICKENS P.G., QUILLIAN, R.M.P. & WHITTINGHAM M.S., *Mat. Res. Bull.* 3, 941 (1968).
12. HUSH N.S., Intervalence Transfer Absorption, Part 2, Theoretical Considerations of Spectroscopic Data, in *Prog. in Inorganic Chemistry* (Edited by COTTON A.). Vol. 8, p. 319. Interscience, New York (1967).
13. CRANDALL R.S., WOJTOWICZ P.J. & FAUGHNAN B.W., *Solid State Commun.* 18, 1409 (1976).

Solid State Communications, Vol. 28, pp. 843–845.
Pergamon Press Ltd. 1978. Printed in Great Britain.

DIPOLE CORRELATIONS IN TeO_2–WO_3 GLASS*

R. Braunstein

Department of Physics, University of California, Los Angeles, CA 90024, U.S.A.

and

I. Lefkowitz and J. Snare

Department of Physics, University of North Carolina, Chapel Hill, NC, U.S.A.

(*Received* 13 *June* 1978 *by A.A. Maradudin*)

Capacitance and thermally stimulated depolarization current measurements on $TeO_2 \cdot 0.23\,WO_3$ glass from 4.2–300 K reveal structure at temperatures where phase transitions are observed in crystalline WO_3. These results indicate that the local WO_6-octahedra determine the dielectric properties of this glass and that dipole–dipole correlations contribute to the ferroelectric-like character of this amorphous system.

EVIDENCE is presented for dipole–dipole correlations between WO_6-octahedra in a $TeO_2 \cdot 0.23\,WO_3$ glass indicating the ferroelectric-like character of these tungstate glasses. Capacitance versus temperature measurements as well as thermally stimulated depolarization current techniques [1] in the temperature range 4.2–300 K reveal structure at temperature where phase transitions occur in crystalline WO_3. The photochromic and electrochromic properties [2] of bulk transparent glasses containing WO_3 in various glass-forming networks indicate that the WO_6-groups are in octahedral coordination.

Glass systems consisting of randomly distributed electric dipoles of BO_6 soft mode octahedra whose concentration can be controlled in an amorphous matrix suggests the possibility that such a "doped" electric dipole system could result in correlations between dipoles. If the dipoles are within a "correlation distance" ferroelectric or antiferroelectric clustering could occur; such an amorphous system could maintain some degree of order and might exhibit ferroelectric phase transitions at critical temperatures.

Questions relating ferroelectric phenomena to the degree of short-range order in an amorphous system can be particularly instructive since early models relate optic mode instabilities to the balance between short and long-range forces [3, 4]. In fact, there exists some experimental evidence that when a particle size goes below a critical value, ferroelectric phenomena disappear [5] from systems like $BaTiO_3$. However, this issue is beclouded by other considerations involving surface effects in these materials.

* Work supported by U.S. Army Research Office, Durham, NC, U.S.A.

These TeO_2–WO_3 glasses were prepared from reagent grade oxides at 800–950°C in air and the melt cast onto a stainless steel mold and annealed at 300°C for several hours. The samples used in these measurements were one or two millimeters thick, and one and two cm^2 in area. They are transparent and golden in color; X-ray analysis shows them to be amorphous. The glasses are mechanically stable and can be successively temperature cycled between room and liquid helium temperature without cracking or crazing.

The surfaces of the samples were not prepared in any fashion but were utilized as cast. They contain surface blemishes such as small diamond and triangular impressions less than 10 microns on a side to a depth of 75 μm. In these regions some strain birefringence could be observed. The glasses were also examined for field-induced birefringence; none was observed for fields up to approximately 10 kV cm^{-1}. The different areas of the glass were examined to determine whether the presence of the surface imperfections results in a non-uniformity of ϵ the dielectric constant across the sample. To within ± 10% accuracy of the measurements, ϵ was uniform. The contacts for the capacitance measurements were silver paint.

The dielectric constant for WO_3 glasses was determined from three-terminal measurements of capacitance utilizing a General Radio 1615-A capacitance bridge. The capacitances involved were on the order of several picofarads. Both the capacitance C and the dissipative factor $\tan\delta$ were determined as a function of sample temperature. The temperature was controlled by slowly raising and lowering the sample holder in a liquid helium reservoir. The rates of cooling and warming were about 1/2 to 1 K min^{-1}. Measurement of the temperature was

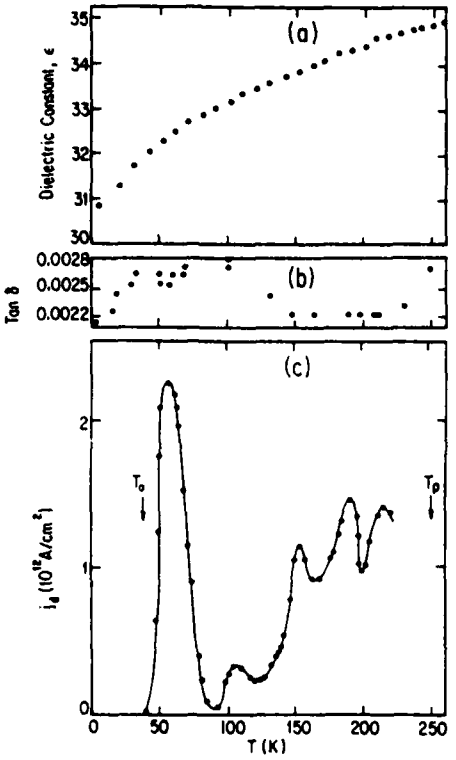

Fig. 1. (a) Dielectric constant as a function of temperature of $TeO_2 \cdot 0.23WO_3$. (b) Loss angle measurement tan δ as a function of temperature in this glass. (c) Thermally stimulated depolarization current peaks in this glass with polarization temperature $T_p = 250$ K, polarization time $t_p = 8.5$ min, linear heating rate $b = 3.4$ K min^{-1}, polarization field $E_p = 7.1$ kV cm^{-1}, and initial temperature $T_0 = 40$ K.

achieved by observation of the voltage across a copper–constantan thermocouple mounted near the sample. The capacitance C_0 of the empty sample holder was essentially independent of temperature. Tan δ of the empty sample holder was less than 0.0005, the smallest value observable with this bridge. The thickness d and the area A of the sample between the contacts were measured. The dielectric constant ϵ of the sample could then be calculated from:

$$\epsilon = 11.3(d/A)(C - C_0),$$

where d and A are in cm and cm^2, respectively, and C and C_0 are in picofarads.

Figure 1a shows the dielectric constant and Fig. 1(b) the tan δ of the WO_3 glass as a function of temperature, from 4.2 to 250 K. The validity of these results was confirmed by repeated measurements. Some thermal hysteresis was observed: the dielectric constant values obtained while the sample was warming from helium temperatures was as much as 3% lower than those observed while cooling from room temperature. This is similar to the thermal hysteresis observed for measurements on single crystal WO_3 [6].

The principal errors involved in determining the dielectric constant arise from the uncertainty in the measured area and thickness of the sample. The thickness is constant only to ± 5% across the surface. The measurement of the area is accurate to ± 5%. The additional error introduced by the capacitance measurements is quite small, on the order of 0.01 pF. The magnitude of the dielectric constant is thus accurate to about 10%. However, relative changes in the dielectric constant with respect to temperature are accurate to within the accuracy of the capacitance and temperature measurements only. Similarly, the accuracy of the measurements of tan δ as a function of temperature is limited only by the accuracy of the tan δ measurements (± 0.0001) and the temperature measurements. For temperatures below 30 K, the accuracy of the temperature measurements from the thermocouple voltage is estimated to be ± 7 K. For temperatures between 40 and 60 K, the accuracy is ± 4 K. For temperatures above 70 K, the accuracy is better than ± 2 K.

No evidence for dispersion was noted; the dielectric constant of the WO_3 glass measured at a frequency of 1.5 kHz was, within experimental accuracy, the same as that measured at a frequency of 1 MHz. No evidence for interfacial polarization has been found. Since this system is part of a weakly uniaxial structure configuration, and since it was not observed even in the single crystal WO_3 case [6], no evidence has been sought for hysteresis loop activity.

The observed changes in capacitance of the WO_3 glass samples can be attributed to three factors. First, there is a geometrical factor involved. Due to thermal expansion as the sample warms, the ratio of the sample's thickness to its area decreases, assuming isotropic and uniform expansion. This would lead to an increase in the observed capacitance, or, equivalently, an apparent increase in the calculated value of the dielectric constant. Secondly, the polarizability of the TeO_2 matrix also contributes to the observed dielectric constant. The third factor, and the one which is of supreme interest to us, is the contribution of the WO_3. It was not possible to arrive directly at a quantity which represents the contribution of TeO_2 and WO_3 to the observed dielectric constant of the glass since it is not possible to form a glass from pure TeO_2 or pure WO_3. In addition, glass compositions were examined only in the range 12–23 mol. WO_3.

Evidence that the WO_6-octahedra are contributing to the large dielectric constant $\epsilon = (30–40)$ of these glasses may be seen from the distinct change in shape at 70 (± 5) K in the capacitance as a function of temperature

in Fig. 1(a). This is presumably related to one of the phase transitions [6] observed in stoichiometric crystalline WO_3 at 40 and 65 K. Additional evidence is the anomalous structure which appears in the tan δ curve, Fig. 1(b), for temperatures below 150 K where there is some evidence of peaks at 40 (± 10) K and at 100 (± 20) K; furthermore the increase in tan δ at temperatures above 220 K occurs where similar structure is observed in crystalline WO_3 [6].

As an ancillary technique to scan for ferroelectric behavior in this glass, a series of thermally stimulated depolarization current [1] measurements were performed in the temperature range 40–300 K. A series of partially overlapping depolarization peaks were found that could be narrowed significantly by reducing the polarization time t_p. Figure 1(c) shows the peaks observed for the indicated poling conditions. Two types of contacts were used between the capacitor plates and the sample, namely ultrasonically soldered indium contacts and blocking contacts of thin mylar. The results were the same with both types of contacts.

The identification of all the peaks in terms of dipole-bearing species is not complete at present; some peaks may be due to impurities or defects characteristic of the glass matrix. However, the fact that some of the peaks occur in the neighborhood of the phase transition [6] temperature observed in crystalline ferroelectric WO_3 indicates that we may be observing different clusters of WO_6-units contributing to the dielectric constant.

The first, and most striking, evidence for the ferroelectric-like character of this glass is the large dielectric constant ~ 30 in contrast to that of standard glasses. The change in slope of the dielectric constant as a function of temperature and the tan δ anomalies which are observed in the neighborhood of similar changes in pure crystalline WO_3 are further evidence for the role played by WO_3. The fact that the thermally stimulated depolarization current peaks due to the dipole-bearing species occur in the neighborhood of the phase transition temperature of crystalline WO_3 emphasizes that the local WO_6-units determine the dielectric properties of crystalline and heavily doped TeO_2-WO_3 glass. The above results are strong evidence that dipole–dipole correlations between WO_6 dipoles are occurring in this glass but are not definitive for solid/solid phase transitions.

Since in this TeO_2–WO_3 glass some of the characteristics of WO_3, which is reported ferroelectric [7, 8] and antiferroelectric [9] in some of the crystalline phases, persist in the glass, further study of the dielectric behavior of WO_3 "doped" glasses with variable concentration could possibly exhibit phase transitions. However, the TeO_2–WO_3 system can only be prepared with a limited range of WO_3 concentrations. It has been possible to prepare bulk glasses of the Li_2O–B_2O_3–WO_3 system with continuous variation of the WO_3 content which shows cooperative behavior between the WO_6 dipoles [10].

Acknowledgements – The authors would like to acknowledge the aid of David Braunstein in the preparation of these glasses and the expertise of Dr. Klaus Bärner in performing the thermally stimulated depolarization current measurements.

REFERENCES

1. BUCCI C., FIESCHI R. & GUIDI G., *Phys. Rev.* 148, 816 (1966).
2. BRAUNSTEIN R., *Solid State Commun.* 28, 839 (1978).
3. ANDERSON P.W., *Fizika Dielektrikov* (Edited by SKANAVI G.I.), Akad. Nauk. SSSR, Moscow (1960).
4. COCKRAN W., *Adv. Phys.* 9, 387 (1960).
5. TOMASHPOLSKI Y.Y., SEVOSTIANOV M.A., PENTAGOVA M.V., SOROKINA L.A. & VENEVSTSEV Y.N., *Ferroelectrics* 7, 257 (1974).
6. LEFKOWITZ I., DOWELL M.B. & SHIELDS M.A., *J. Solid State Chem.* 15, 24 (1975).
7. UEDA R. & ICHINOKAWA T., *Phys. Rev.* 82, 563 (1951).
8. SAWADA S., ANDO R. & NOMURA S., *Phys. Rev.* 82, 952 (1951).
9. KEHL W.L., HAY R.G. & WAHL D., *J. Appl. Phys.* 23, 212 (1952).
10. BRAUNSTEIN R. & BÄRNER K., *Solid State Commun.* 28, 847 (1978).

Solid State Communications, Vol. 28, pp. 847–851.
Pergamon Press Ltd. 1978. Printed in Great Britain.

COOPERATIVE PHENOMENA OF RANDOM ELECTRIC DIPOLES IN AN AMORPHOUS MATRIX

R. Braunstein* and K. Bärner†

Department of Physics, University of California, Los Angeles, CA 90024, U.S.A.

(*Received* 13 *June* 1978 *by A.A. Maradudin*)

A ferroelectric phase transition has been observed for the first time in a series of glasses containing WO_6-octahedra. The techniques of thermally stimulated depolarization currents were used to observe the transition from independent dipole behavior to cooperative behavior in this amorphous system as a function of concentration. These measurements yielded the activation energy $\Delta E = 1.2$ eV, the pre-exponential $\tau_0 = 2 \times 10^{-2}$ sec, and the dipole moment $\bar{p} = 1.3 \times 10^{-15}$ esu cm for WO_3 in $Li_2B_4O_7$. A dipole moment bearing species due to $Li_2B_4O_7$ was observed with $\Delta E \simeq 0.44$ eV and pre-exponential $\tau_0 = 5 \times 10^{-8}$ sec. The depolarization peaks of WO_3 occur in the temperature range 265–275 K depending upon WO_3 concentration and are pressure dependent with an initial slope of 2×10^{-5} K dyne^{-1} cm^2. A model was developed for a possible phase transition associated with a random "pseudo-spin" system in an amorphous matrix.

WE HAVE OBSERVED for the first time an amorphous ferroelectric phase transition in a series of bulk glasses containing WO_6-octahedra *in various glass-forming* networks. These "doped" electric dipole glass systems exhibit dipole correlations if the local dipole moments are within a "correlation distance" of each other. In the ground state, the "pseudo-spins" are in a spin-compensated configuration; however, when an external electric field is applied, a ferroelectric transition is observed at a specific temperature involving the cooperative interaction of the WO_6-octahedra. The phenomena exhibited by these "pseudo-spin" glasses have analogous properties similar to the magnetic spin glasses with the additional feature that the dielectrically active soft modes of the WO_6-groups seem to initiate the long range dipole–dipole coupling. Using the techniques of thermally stimulated depolarization currents [1], it has been possible to observe the transition from an independent dipole behavior to cooperative phenomena of random electric dipoles in an amorphous system.

Ferroelectrics were originally considered one of the accidents of nature since very specific crystal compounds exhibited this type of phase transition. The discovery of the oxygen octahedral ferroelectrics made up of the basic BO_6 building block where B is a metal ion widened the recognition of the class of ferroelectrics [2]. However, the structure-sensitive character of the phenomena of ferroelectricity tended to emphasize the delicate balancing of long and short range forces for the onset of the phase transition. This connection between lattice dynamics and ferroelectricty [3] focused attention on the soft modes to describe the displacive lattice instability which results from a small atomic displacement occurring below a Curie temperature. A more disorderly class of ferroelectrics has also been recognized – namely a dirty displacive ferroelectric [4] in which each unit cell is different from each other yet there is on the average the translational symmetry of the lattice.

Recently, the concept of a ferroelectric glass has been proposed in which the essential ingredient is a dielectrically soft local atomic configuration which remains identifiable though possibly distorted in a glass matrix [5]. Attempts to observe such a ferroelectric glass were made by producing the amorphous modification of a crystalline ferroelectric [6]. In these attempts, large dielectric constant anomalies were observed at temperatures near the Curie temperature of the crystalline ferroelectric. However, at these temperatures, which are close to the devitrification temperatures of the glasses, the possibility that interfacial polarization due to the movement of ions was responsible for these large dielectric constant anomalies was not ruled out.

These evolutionary ideas proceeding from periodic order to disorder concerning the ferroelectric phase transition leads one logically to consider the possibility of ferroelectric behavior in a glass system fashioned from randomly distributed electric dipoles consisting of BO_6 local soft mode octahedra whose concentration can

* Work supported by U.S. Army Research Office, Durham, North Carolina, U.S.A.

† Permanent address: IV Physikalisches Institut der Universität Göttingen, 34 Göttingen, West Germany.

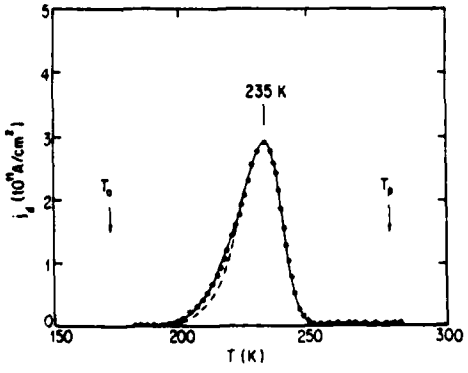

Fig. 1. Thermal depolarization current $j_d(T)$ of a $Li_2B_4O_7$ glass: Polarization temperature $T_p = 281$ K; Initial temperature $T_0 = 172$ K; Polarization time $t_p = 4$ min; Contact pressure $P_0 = 4 \times 10^5$ dyne cm^{-2}; Polarization field $E_p = 5$ kV cm^{-1}; Time constant of exponential cooling: $t_0 = 11.4$ min; Heating rate $b = 4.3$ K min^{-1}; —o— Experiment; — — — Theory.

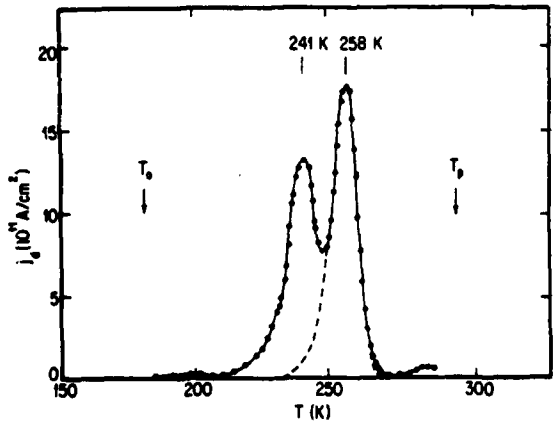

Fig. 2. $j_d(T)$ for a $Li_2B_4O_7 \cdot xWO_3$ glass ($x = 0.005$ mol): $T_p = 294$ K; $E_p = 5.9$ kV cm^{-1}; $P_0 = 4 \times 10^5$ dyne cm^{-2}; $t_p = 4$ min; $b = 3.4$ K min^{-1}; $T_0 = 185$ K; $t_0 = 8$ min; —o— Experiment; — — — Theory.

be controlled in an amorphous glass-forming matrix. Above a critical concentration, these systems might exhibit a paraelectric–ferroelectric electric phase transition at a critical temperature.

We have prepared a series of bulk transparent glasses containing a wide range of concentrations of WO_6-octahedra in various glass-forming networks and studied the photochromic [7], electrochromic [7], and dielectric [8] behavior of these tungstate glasses. These glasses contain WO_3 in various glass forming networks such as Li_2O–B_2O_3, Na_2O–B_2O_3, and TeO_2. Evidence that the tungsten oxide ions are in octahedral coordination and are dispersed in a glass matrix comes from the coloration produced in these glasses [7]. These glasses were prepared from reagent grade oxides at 800–950°C

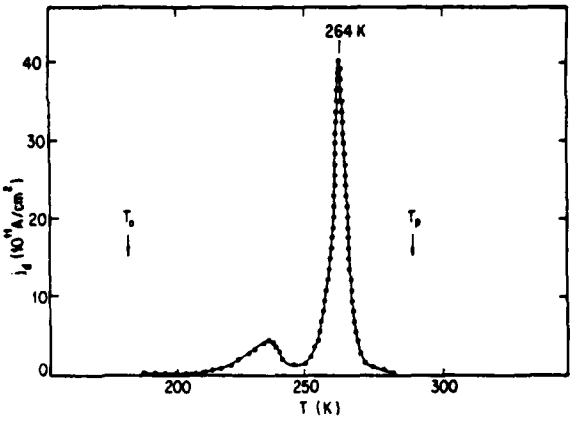

Fig. 3. $j_d(T)$ for a $Li_2B_4O_7 \cdot xWO_3$ glass ($x = 0.08$ mol): $T_p = 290$ K; $E_p = 6.2$ kV cm^{-1}; $P_1 = 4 \times 10^5$ dyne cm^{-2}; $t_p = 6.8$ min; $b = 2.5$ K min^{-1}; $T_0 = 181$ K; $t_0 = 9.6$ min.

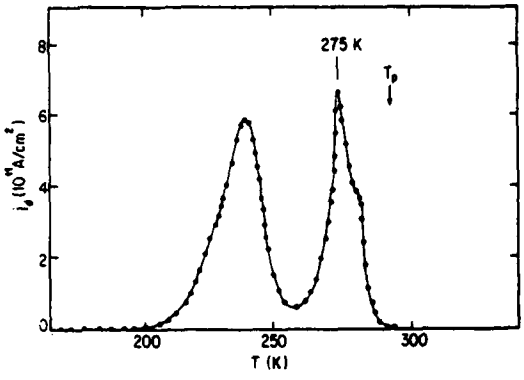

Fig. 4. $j_d(T)$ for a $Li_2B_4O_7 \cdot xWO_3$ glass ($x = 1.0$ mol): $T_p = 292$ K; $E_p = 5.2$ kV cm^{-1}; $P_0 = 4 \times 10^5$ dyne cm^{-2}; $t_p = 2.8$ min; $b = 2.4$ K min^{-1}; $T_0 = 146$ K; $t_0 = 10$ min.

in air and the melt cast into a stainless steel mold and annealed at 300°C for several hours.

We explored the possible ferroelectric character of the Li_2O–B_2O_3–WO_3 glass system using the technique of thermally stimulated depolarization currents [1] in the temperature range 4–300 K. Depolarization peaks were observed which can be identified with the dipole moments of the WO_6-octahedra and with a dipole-bearing species of the Li_2O–B_2O_3 glass network. Figures 1–4 show the depolarization currents observed in a series of glasses containing different concentrations of WO_3 under the indicated poling and depoling conditions. Two types of contacts were made between the capacitor plates and the sample, namely ultrasonically soldered indium contacts and blocking contacts using thin mylar. The results were the same with both types of contacts provided the polarization temperature T_p was below 200 K. When T_p was above 200 K, with the In-contacts, a large space charge peak was observed

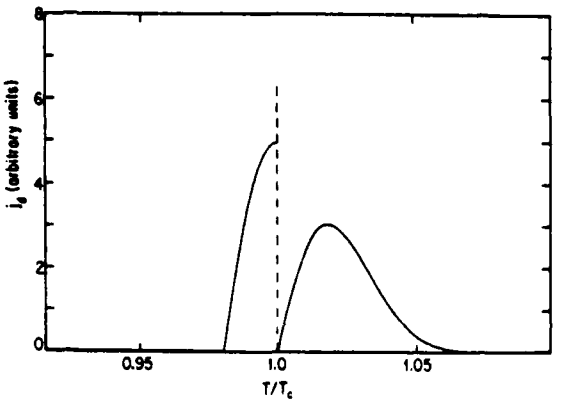

Fig. 5. Thermal depolarization current $j_d(T)$ as calculated for a compensated random electric dipole collective system: $\alpha = 2 \times 10^{-2} K^{-2}$, $T_c = 264$ K, $T_0 = 10$ K (see text for details).

which could be completely suppressed using the mylar blocking contacts. With the blocking contacts, a sharp peak was observed near 265 K and another one at 235 K. The peak at 235 K is associated with the $Li_2B_4O_7$ glass network, since it is present in the $Li_2B_4O_7$ glass without WO_3 (see Fig. 1) and is also present in the WO_3 glasses. The presence of the $Li_2B_4O_7$ glass peak serves as an excellent calibration point to which to relate the behavior of WO_3 in this glass network.

The dramatic behavior of the WO_6-octahedra in this glass system is shown by the magnitude and line shape of of the 265 K peak as a function of concentration. The solid curve in Fig. 1 shows a peak in the depolarization current at 235 K in pure $Li_2B_4O_7$ glass. The dotted curve in this figure is a theoretical fit to the data using an independent dipole model [1] for the dipole-bearing species in this glass. The slight difference between theory and experiment is due only to a slight deviation from linearity in the heating rate as a function of time. This 235 K peak is also observed in all samples of the tungstate glasses $Li_2B_4O_7 \cdot xWO_3$ in Figs. 2, 3, and 4 containing $x = 0.005$, $x = 0.08$, and $x = 1$ mol. WO_3 respectively. It maintains its lineshape and its integrated intensity as is expected for an independent dipole peak. However, the peak in the neighborhood of 265 K undergoes a dramatic change in line shape and peak intensity as a function of WO_3 concentration. In Fig. 2 with 0.005 mol of WO_3 both the $Li_2B_4O_7$ glass peak and the peak which is due to WO_3 can be fitted by an independent dipole model [1]. For the glass peak the activation energy ΔE is 0.44 eV and the pre-exponential $\tau_0 = 5 \times 10^{-8}$ sec, while for the WO_3 peak $\Delta E = 1.2$ eV and $\tau_0 = 2 \times 10^{-22}$ sec. The dipole moment per unit of WO_3 is $\bar{p} = 1.3 \times 10^{-15}$ esu cm; it should be noted that this seems to be the first determination of $\bar{p}$ for WO_3 in a glass matrix. This dipole moment is rather large compared to the typical observed values which are of the order of 10^{-17}–10^{-18} esu cm. At 0.08 mol of WO_3, the WO_3 peak shows a dramatic change in intensity and line shape, while the glass peak remains about the same shape and has the same order of magnitude as it has in pure $Li_2B_4O_7$, as can be seen in Fig. 3. In Fig. 4 with 1 mol of WO_3 the anomalous line shape persists although the peak is significantly lower and also shows a broadening of some structure.

The fact that the thermally stimulated depolarization current peaks due to WO_3 occur close to the temperature at which a phase transition is observed [9] in crystalline WO_3 is again strong evidence that this peak is associated with the dipole-bearing WO_6-octahedra in the glass matrix. The transition from an independent dipole peak to a sharply peaking structure is strongly suggestive that cooperative behavior of the WO_3 is setting in at a critical "coherence" distance. If the system is not electrically poled, no depolarization current is observed as the sample is warmed between 40–300 K, thus excluding a spontaneous polarization when we do not allow for domains in our random system. Therefore without an external electric field, the dipoles of WO_3 are in compensated configurations for all concentrations of WO_3. However, with an external electric field present at low WO_3 concentrations, the system behaves as a paraelectric, while above a critical concentration the dipoles exhibit cooperative behavior. In this cooperative regime, the position of the WO_3 peak is strongly dependent upon pressure; the position of the peak shifts with an initial slope of $\sim 2 \times 10^{-5}$ K dyne^{-1} cm^2, indicating a strong pressure dependence of the interaction constants.

The observations of the behavior of WO_3 in this glass matrix can be explained on the basis that when the WO_3 dipoles are at random sites but within a "coherence length" of each other they undergo a phase transition at a specific temperature. Such a phase transition would have associated with it a critical slowing-down of the relaxation times of "pseudo-spin" clusters as the transition temperature is approached. The thermally stimulated depolarization measurements essentially measure dP/dt, i.e. the time rate of change of the polarization as a function of temperature and this is a measure of the dynamics of the electric susceptibility of the dipole system.

We have developed a model for a possible phase transition associated with a random "pseudo-spin" system in an amorphous matrix. Essentially, we have adopted the Glauber [10] formalism for an Ising system of "pseudo-spins" which will be reduced to a mean field approximation. However, we have allowed for the situation where the spins are in a compensated configuration without the presence of an external electric field.

Consider the Hamiltonian for a deep-double-well-potential:

$$H = \sum_{l}^{N} \sum_{l'}^{N} v_{ll'} S_l S_{l'} - \bar{p} E^z \sum_{l=1}^{N} S_l \tag{1}$$

where the symbols are the ones conventionally defined for a one-dimensional crystalline ferroelectric [11]. In this Hamiltonian E^z is the static "perturbing field" and $\bar{p}$ is the average dipole moment of an individual spin unit. If the system is connected to a heat bath the equation of motion for the configurational average $\langle S_l \rangle$ is

$$\tau_0 \frac{\mathrm{d}}{\mathrm{d}t} \langle S_l \rangle = -\langle S_l \rangle + \langle \tanh \beta E_l \rangle \tag{2}$$

where

$$\frac{1}{\bar{p}} E_l = E^z + \frac{1}{\bar{p}} \sum_{l'=1}^{N} v_{ll'} S_{l'}$$

is the effective field and τ_0 the "single spin" relaxation time. For a random compensated dipolar configuration at $E^z = 0$, $\langle S_l \rangle = \Sigma' S_l p(S_1, \ldots, S_N, t) = 0$ for all temperatures T, i.e. equation (2) is valid but yields no information. For $E^z > 0$, $\langle S_l \rangle \neq 0$ and the probability function $p^z = p\{E^z, S, t\}$ since the Stark-energy $\bar{p}E^z$ competes with the internal energy to give a partial alignment. Writing $p^z = g^z p$ and $\langle S_l g^z \rangle = g(E^z) \langle S_l \rangle$ where p is the probability function at $E^z = 0$ and g^z a weight function, which states that the probability that a state $\{s\}$ of $E^z = 0$ changes into the state $\{s'\}$ of maximal alignment with the external field $E^z > 0$, it follows that

$$\langle S_l \rangle^z = g(E^z) \langle S_l \rangle. \tag{3}$$

For $\langle S_l \rangle^z$ the molecular field approximation can be made:

$$g S_l = \langle S_l \rangle^z = \langle S \rangle^z. \tag{4}$$

This statement corresponds to the assumption that each spin behaves on the average like every other spin and therefore it is valid for a random system in an amorphous matrix. Normally this assumption is stated in terms of the translational invariance of the spin behavior and is considered to apply to crystalline ferroelectrics. Inserting (3), (4) into (2), the equation of motion for an average z-component of the electric dipole moment is

$$\tau_0 \frac{\mathrm{d}}{\mathrm{d}t} \langle S \rangle^z = -\langle S \rangle^z + g(E^z) \tanh \{\beta \bar{p} (E^z + g^{-1} v_0 \langle S \rangle^z)\}. \tag{5}$$

where

$$v_0 = v_0^l = \frac{1}{\bar{p}} \sum_{l'} v_{ll'}.$$

From the competition between the external and the internal fields, it is reasonable to assume:

$$1 - g = \exp(-\bar{p} E^z / \bar{p} v_0).$$

Expanding tanh to cubic terms and the exponential to quadratic terms we obtain:

$$\tau_0 \langle \dot{S} \rangle_z = -\tilde{\epsilon} \langle S \rangle_z - Q \langle S \rangle_z^3 \tag{6}$$

for the decay to equilibrium; where

$$\tilde{\epsilon} = 1 - \frac{T_c}{T}, \qquad T_c = T_{c0} \left[1 - \frac{1}{2} \frac{E^z}{v_0}\right]$$

$$Q = \frac{1}{3} \frac{T_{c0}^2 T_c}{T^3} (v_0 / E^z)^2 \qquad T_{c0} = \bar{p} v_0 k^{-1}.$$

The equation of motion (6) can be solved for

$$T \neq T_c: \quad \langle S \rangle_z = \left\{ \frac{Q}{\tilde{\epsilon}} + \frac{1}{S_{0z}^2} \exp(2\tilde{\epsilon} t / \tau_0) - \frac{Q}{\tilde{\epsilon}} \right\}^{-1/2}$$

and (7)

$$T = T_c: \quad \langle S \rangle_z = \{S_{0z}^{-2} + 2Q\tau_0^{-1} t\}^{-1/2}.$$

We note that this system exhibits a critical slowing down at the transition temperature T_c. Also, one might expect an asymmetry to the rate of slowing-down as the transition temperature is approached from above or below [10].

If the decay functions are approximated by a single relaxation time $\tilde{\tau}$ for $T \neq T_c$, the depolarization currents with a constant heating rate b can be calculated by integrating

$$-j_d = b(\mathrm{d}\langle S \rangle_z / \mathrm{d}T) = -\langle S \rangle_z / \tilde{\tau}.$$

The results for $S_{0z} \neq S_{0z}(T)$, $\tilde{\epsilon} \cdot T_c \simeq T - T_c$, $Q \simeq$ const. are:

$$T > T_c: \qquad j_d = \alpha S_{0z} (T - T_c) \exp\left[-\frac{\alpha (T - T_c)^2}{2}\right]$$

$$T_c - T_0 < T < T_c: \quad j_d = \alpha S_{0z} (T_0 - T_c + T) \times \exp\left[-\frac{\alpha (T - T_c)^2}{2} + \alpha T_0 (T_c - T)\right] \tag{8}$$

$$T_c - T_0 > T: \quad j_d = 0 \quad \text{with} \quad T_0 = Q S_{0z}^2 T_c, \quad \alpha = (b \tau_0 T_c)^{-1}.$$

It should be noted that this depolarization curve is quite different from the asymmetric glow curve that is normally calculated for independent dipoles [1]. Figure 5 shows an example of a calculated depolarization curve as a function of temperature normalized to the transition temperature. The discontinuity at $T/T_c = 1$ is due

to the decrease in the depolarization current resulting from the critical-slowing down of the spin system. This model indicates that one can have a "pseudo-spin" phase transition in a random electric dipole system in an amorphous matrix. No attempt was made to compare seriously the predicted lineshape of this one-dimensional model to the experimental curves above a critical WO_3 concentration. However, it is interesting to note that, similar to the model, Fig. 4 shows some structure in the 275 K WO_3 peak.

We believe that we have observed a phase transition in a "pseudo-spin" glass system containing various concentrations of WO_3 in a glass matrix. The transition temperature in this amorphous system occurs near the transition temperature of crystalline WO_3 [9], indicating that either a local soft mode of the WO_3 octahedra or a local double-well potential is involved. The observation of these cooperative phenomena in this random system which can be controlled by varying the concentration of WO_3 opens up a new class of materials which allows one to study critical phenomena in electric dipole systems. In addition, these amorphous ferroelectrics can provide a class of materials for various transducer applications since they can be prepared in bulk quantities.

Acknowledgements – The authors wish to acknowledge gratefully the technical assistance of Oliver Barrett and Mark Braunstein in the preparation of these glasses. We would like to thank I. Lefkowitz for many helpful discussions.

REFERENCES

1. BUCCI C., FIESCHI R. & GUIDI G., *Phys. Rev.* **148**, 816 (1966).
2. WUL B. & GOLDMAN I.M., *C. R. Acad. Sci URSS* **46**, 139 (1945).
3. COCHRAN M.J., *Adv. Phys.* **9**, 387 (1960).
4. BURNS G., *Phys. Rev.* **B13**, 215 (1976).
5. LINES M.E., *Phys. Rev.* **B15**, 388 (1977).
6. GLASS A.M., LINES M.E., NASSAU K. & SHRIEVER J.W., *Appl. Phys. Lett.* **31**, 249 (1977).
7. BRAUNSTEIN R., *Solid State Commun.* **28**, 839 (1978).
8. BRAUNSTEIN R., LEFKOWITZ I. & SNARE J., *Solid State Commun.* **28**, 843 (1978).
9. LEFKOWITZ I., DOWELL M.B. & SHIELDS M.A., *J. Solid State Chem.* **15**, 24 (1975).
10. GLAUBER R.J., *J. Math. Phys.* **4**, 294 (1963).
11. LINES M.E. & GLASS A.M., *Principles and Applications of Ferroelectris and Related Materials*, p. 45. Clarendon Press, Oxford (1977).

phys. stat. sol. (b) 95, 483 (1979)

Subject classification: 13.5. 1 and 20.1; 22.8

University of California, Los Angeles

Evidence for Excitonic Absorption in Metallic $MnAs_{0.88}P_{0.12}$

By

K. BÄRNER[1]), R. STEARNS[2]), and R. BRAUNSTEIN[2])

The derivative spectra of the reflectivity are measured for the double exchange ferromagnet $MnAs_{0.88}P_{0.12}$ at 309, 100 K and for quantum energies between 1.6 and 5.0 eV. Excitonic absorption is found beyond interband transitions and is tentatively assigned to a triangular resonant state.

Für den Doppelaustauschferromagneten $MnAs_{0.88}P_{0.12}$ wird die reduzierte erste Ableitung der Reflektivität nach der Wellenlänge $1/R(dR/d\lambda)$ bei Quantenenergien zwischen 1.6 und 5.0 eV und bei den Temperaturen 300 und 100 K gemessen. Neben Interbandübergängen kann exzitonische Absorption identifiziert werden. Es wird untersucht, inwieweit letztere Übergängen in die für diese Substanz vorhergesagten triangularen Resonanzzustände zuzuschreiben ist.

1. Introduction

In view of the many ionic valency states of Mn it has been proposed [1] that if a considerable Mn–As–Mn d-electron transfer exists the ionic $Mn^{3+}As^{3-}$ lattice is unstable against valency fluctuations at the cation sites. However, because of the symmetry of the lattice the fluctuations do not occur in a random fashion but are restricted to dd-electron–hole (eh) resonant configurations which arise from orbital degeneracies (Fig. 1a).

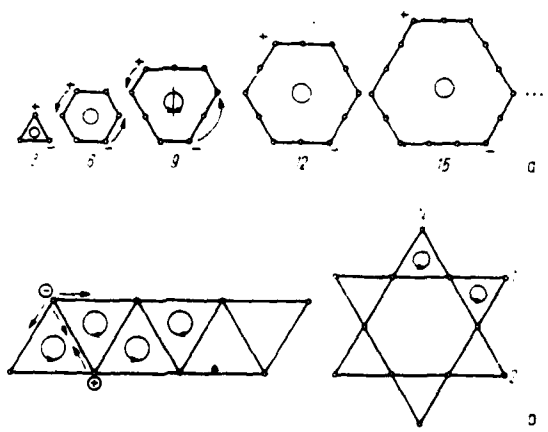

Fig. 1. a) A series of resonant configurations in a hexagonal plane and b) linear propagation of the triangular resonance (for details see text)

[1]) Work supported in part by the Deutsche Forschungsgemeinschaft. Permanent address: IV. Physikalisches Institut der Universität Göttingen, Göttingen, BRD.

[2]) Work supported in part by the U.S. Army Research Office and the Airforce Office of Scientific Research.

Except for defect sites, bound resonant states, as comparable to that of a single benzene-like molecule, cannot occur because of the translational invariance of the lattice. The lowest order resonant configuration of the hexagonal lattice has been suggested to be triangular ($3d^3$–$3d^4$–$3d^5$) [1]; since the corresponding extended resonance involves a translational motion of the eh-pair it does not provide a net charge transport. This is true also for the higher order extended resonances and apparently in conflict with the observed metallic conductivity [2, 3] of the manganese pnictides. However, the eh-pairs can dissociate because of temperature or electric field or could even coexist with correlated one-electron states for all temperatures.

Because of the excitonic character of these many-particle states, in this work an attempt is made to find experimental evidence for their existence in the absorption spectra of the double exchange ferromagnet $MnAs_{0.88}P_{0.12}$ using wavelength modulation spectroscopy.

2. Experimental

The normalized first derivative of the reflectivity $(1/R)\,(dR/d\lambda)$ was obtained as described earlier [4, 5] for a surface $\perp$ [212] of a $MnAs_{0.88}P_{0.12}$ single crystal. Three different surface treatments have been applied in order to detect influences of the condition of the surface on the spectra:

1. 1 μm mechanical polish:
2. 1 μm polish and a short (60 s) etch in bromine-methanol in order to remove chemical surface layers,
3. 1 μm polish and a long (5 min) etch in order to remove all of the surface damage from the mechanical polish.

Treatments 1, 2 showed only minor differences for the spectra at 300 K; the same should be true for all temperatures. Treatment 3 yielded a dramatic sharpening and a considerable shift of the structures with respect to treatments 1, 2 (Fig. 2a, b). However, the main characteristics were conserved indicating that one observes intrinsic effects in all three cases but that there are rather large broadenings and shifts

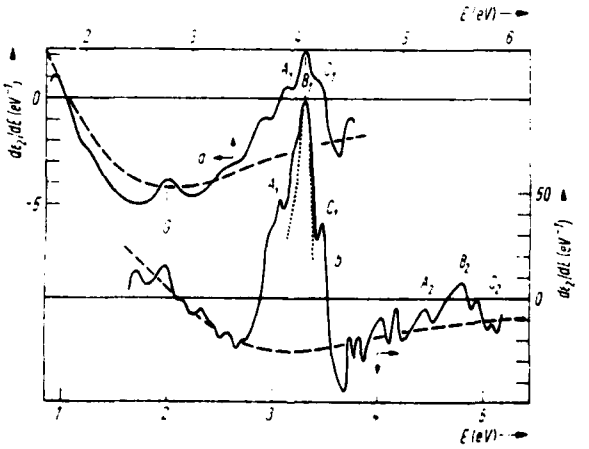

Fig. 2. The first derivative of the imaginary part of the dielectric constant in respect to quantum energy $d\varepsilon_2/dE$ for a surface $\perp$ [212] of a $MnAs_{0.88}P_{0.12}$ single crystal at 300 K. (a), (b) refer to different surface conditions (see text)

of the internal oscillators with lattice distortion. The large value of the shift would cast doubt on the data if it were not for the consistency of all the structures which becomes apparent and for the consistency with the anomalously large sensitivity of the electronic states on lattice parameter variations which has been suggested [1, 6, 7].

While for the 300 K runs the sample was exposed to atmosphere, for the 100 K runs the sample was kept at 10^{-7} Torr in an optical nitrogen cryostat. From optical inspection and consecutive measuring no sign of a layer formation on the sample surface could be detected in both cases. Also, for the 100 K run, formation of adsorption layers on the sample could be ruled out from parallel measurements on compounds with known spectra.

3. Results

The raw data were corrected for the dispersion of the apparatus and R was subjected to a Kramers–Kronig analysis [4]. For the integration constant and extrapolation of R beyond 1.6 and 5.0 eV previous data on the compound $MnAs_{0.85}P_{0.15}$ were used [8].

Note from the different scales used in Fig. 2a, b the sharpening of the structure between surface treatments 1 and 3 amounts to nearly a factor of 20 while the energy shift, as measured between the two absolute maxima is 0.73 eV (!). Although not the primary interest in this work, the large shift will be investigated in a systematic manner (pressure dependence) in the future. Apparently the spectra contain a broad Lorentz-oscillator (dashed line) which does not scale with the structure: it could be related to different surface roughnesses, i.e. correspond to a typical surface excitation. As expected with a removal of lattice damage (Fig. 2, curve b) simultaneously with the sharpening of the structure more details are resolved. Although we cannot be sure of all the new structure by comparison with the broadened spectra, from the sensitivity of the apparatus there is no reason to distrust them. Note, for example, the splitting of the peak which follows the dip after C_1. Also, the small maximum designated G seems to be part of an absorption peak and the triple structure (A_2, B_2, C_2) seems to be a replica of the main structure (A_1, B_1, C_1) at higher quantum energies.

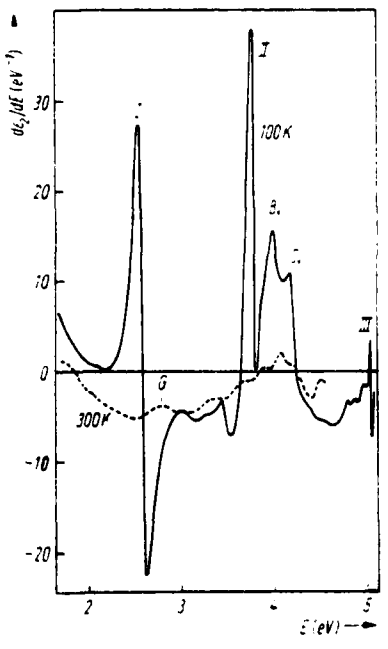

Fig. 3. $d\varepsilon_2/dE$ for $MnAs_{0.88}P_{0.12}$ at 100 K

Fig. 3 shows the spectral dependence of $d\varepsilon_2/dE$ ($E = \hbar\omega$) at 100 K with surface treatment 2; for comparison the corresponding spectrum at 300 K is redrawn (dotted line). Note that the relatively shallow structure between 3.6 and 4.3 eV has sharpened by a factor of 5 while there is only little (≈ 0.1 eV) shift in the peak positions. The most striking

feature is the appearance of the three large structures I, II, III with a nearly Lorentzian shape. Line II sits on an ascending slope and obscures another smaller structure, presumably A_1, as can be concluded from its asymmetry. There might be some doubt as to the reality of the structure III, since it has not the width of I, II and sits at the edge of the experimentally accessible range. However, it is found in the original data, is insensitive to different extrapolation parameters and coincides with the structure A_2 — just as II coincides with A_1 — when the energy shift of 0.73 eV (Fig. 2, curves a, b) is taken seriously. In respect to these large structures the 300 K run appears as a baseline, i.e. I, II, III have vanished at 300 K except for very shallow structures near the sensitivity limits; the structure around G might correspond to I, while for II, III not even a tentative assignment is possible. The positions of all the designated structures are summarized in Table 1.

Table 1

surface treatment	T	I	II	III	A_1	B_1	C_1	A_2	B_2	C_2
2	100 K	2.56	3.78	5.04	—	3.96	4.16	—	—	—
1	300 K	(2.78)	—	—	3.88	4.07	4.18	—	—	—
3	300 K	1.98	—	—	3.06	3.30	3.46	4.45	4.80	4.94*)

*) Shift by +0.73 eV.

4. Discussion

4.1 One-electron excitations

Since for all temperatures T a coexistence of resonant and correlated one-electron states is likely, for the optical absorption $\varepsilon_2(\omega)$ we expect structure due to free carriers, interband absorption and absorption due to many-particle states. The structure between 3.6 and 4.2 eV (Fig. 2, curve a) appears for all T and is consequently attributed to interband one-electron absorption. This is supported by the following details:

1. The structure appears at energies which are near those estimated between Mn^{3+} s- and As^{3-} p-states [8, 9].
2. There is only a minor enhancement and shift of the structure with decreasing temperature.
3. The triple structure (A_1, B_1, C_1) is probably connected with the trigonal symmetry of the anion (As, P) site (neglecting the small orthorhombic distortion of the hexagonal phase).
4. The double-hump shape of the structures A_1 and B_1 suggests lifetime broadened critical points with a precursor due to Coulomb interactions. For the main structure B_1, $d\varepsilon_2/dE > 0$ and the slope is steeper at the high-energy side: this would correspond to an M_1 critical point (Fig. 2: dotted line) [10]. For both A_1 and C_1, $d\varepsilon_2/dE > 0$ and the visible slope is similar to the one or to the other slope of B_1; therefore, they might be M_1 critical points, too. However, they are not sufficiently resolved to allow a definite assignment.
5. The replica A_2, B_2, C_2 indicates interband transitions from the same anion states (p) into higher cation states.

Although some symmetry arguments for allowed dipole transitions in NiAs-type compounds have been given [11] and a few experimental papers give an idea about the quantum energies involved [8, 12], for a detailed comparison a one-electron band

structure calculation would be necessary. This has not been given for these compounds as yet.

Evidence for intraband transitions (free electrons) is ample from the dc-conductivity and the metallic reflectivity at lower quantum energies [8]. However, for $MnAs_{0.88}P_{0.12}$ the Drude tail probably appears at energies below 1.6 eV.

4.2 Excitonic absorption

The width, the nearly Lorentzian shape, and the strong temperature dependence indicate excitonic-like absorption for the structures I, II, III. While the peak II (III) sits on a structure which can be interpreted as a sequence of van Hove singularities and therefore could correspond to a conventional pd (or ps) exciton, this is not possible for peak I. Moreover, the nearly equidistant separation in energy between the centers of I, II, and II, III suggests that peaks I, II, III belong together. If this is correct we have to consider an exciton series which is not hydrogen-like but rather indicates the removal of a three fold degeneracy. Since the double exchange ferromagnetic coupling of $MnAs_{0.88}P_{0.12}$ [13] has been connected with the existence of free triangular resonant states which resemble free excitons [1] it is possible that we have observed absorption connected with excited states of this kind. In an attempt to exclude this possibility or to establish a more close relationship we have calculated the energy levels for a particular resonant configuration.

4.2.1 Energy levels for extended resonant states

As a first step, the energy levels for a particular bound resonance are determined: the standard technique, as has been applied to a pair of cations Mn^{3+}–Mn^{4+} [14, 15], assumes an interaction JSs (J is the intraatomic exchange energy) at the cation sites, an angle θ between the ion spins S_1, S_2, and uses the spinor transformation to evaluate the energy needed for the transfer of an electron while it rotates by θ. With the three cations of a triangle participating, in principle two independent angles θ, Γ could be choosen. As a special case we choose $\theta = \Gamma$ and the electron transfer such that it corresponds to an alternating right-hand (left-hand) rotational half-cycle (Fig. 4a). In this case the ion

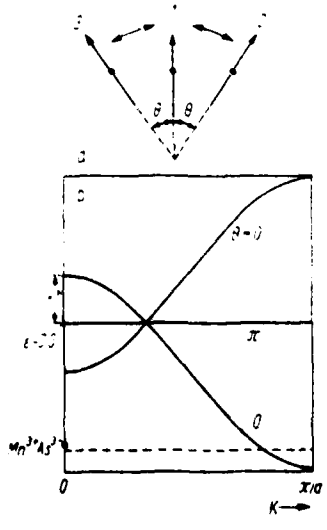

Fig. 4. a) Double exchange transfer of an electron-hole pair on a cation triangle (arrows: cation spins). b) Many-particle bands corresponding to an extended resonant state with double exchange transfer, in respect to the ionic ground state (for details see text)

valences change between $3d^3$–$3d^4(R_2)$, $3d^4$–$3d^5(R_3)$, and $3d^3$–$3d^5(R_1)$. Utilizing only parallel and antiparallel spin states at the cation sites R_1, R_2, R_3 the Hamiltonian matrix is

$$
\begin{array}{c|cccccc}
 & R_1 & R_2 & R_3 & R_1 & R_2 & R_3 \\
 & \uparrow\uparrow & \uparrow\uparrow & \uparrow\uparrow & \uparrow\downarrow & \uparrow\downarrow & \uparrow\downarrow \\
\hline
R_1\uparrow\uparrow & -2J_1S_1 & b_{21}\cos\frac{\theta}{2} & b_{31}\cos\frac{\theta}{2} & 0 & b_{21}\sin\frac{\theta}{2} & b_{31}\sin\frac{\theta}{2} \\
R_2\uparrow\uparrow & b_{21}\cos\frac{\theta}{2} & -J_2S_2 & 0 & -b_{21}\sin\frac{\theta}{2} & 0 & 0 \\
R_3\uparrow\uparrow & b_{31}\cos\frac{\theta}{2} & 0 & -J_3S_3 & -b_{31}\sin\frac{\theta}{2} & 0 & 0 \\
R_1\uparrow\downarrow & 0 & -b_{21}\sin\frac{\theta}{2} & -b_{31}\sin\frac{\theta}{2} & +2J_1S_1 & b_{21}\cos\frac{\theta}{2} & b_{31}\cos\frac{\theta}{2} \\
R_2\uparrow\downarrow & b_{21}\sin\frac{\theta}{2} & 0 & 0 & b_{21}\cos\frac{\theta}{2} & -J_2S_2 & 0 \\
R_3\uparrow\downarrow & b_{31}\sin\frac{\theta}{2} & 0 & 0 & b_{31}\cos\frac{\theta}{2} & 0 & +J_3S_3
\end{array}
,
$$

where b_{21} is the spin-independent transfer integral for a hole hopping from R_1 to R_2 ($3d^3 \rightarrow 3d^4$) simultaneously with an electron from R_1 to R_3 (b_{31}, $3d^4 \rightarrow 3d^5$) and whereby quantum mechanical corrections for S_1, S_2, S_3 are neglected. If we consider only states with energy near $-J_iS_i$ we solve the upper left-hand corner of the determinant and set $J_i \approx J$; $S_i \approx S$ since for high spin states $S_1 = 3/2$, $S_2 = 3/2$, $S_3 = 4/2$.

The solutions are

$$
E_1 = -JS\,, \qquad E_{2,3} \approx -\frac{3}{2}JS \pm (b_{21}^2 + b_{31}^2)^{1/2}\cos\frac{\theta}{2}\,. \tag{1}
$$

E_1 corresponds to the case where one ion spin is antiparallel to the other two, whereupon no electron transfer is possible, while $E_{2,3}$ are the energies for parallel and antiparallel orientation of the electron and hole spin in respect to the three parallel ion spins. Because of the translational invariance of the lattice these states become extended (compare with Fig. 1 b). An estimate for the band energies can be made by calculating the energies for spin-independent transfer and substituting $t^* \cos(\theta/2) = (b_{21}^2 + b_{31}^2)^{1/2} \times \cos(\theta/2)$ for the combined spin-independent transfer integral b_{eh} and $\varepsilon_{eh} - JS$ for the spin-independent excitation energy ε_{eh} of the electron–hole pair.

The states of electron–hole (eh) pairs on spin-independent resonant configurations with $L = 3, 6, 9, \ldots$ atoms (Fig. 1 a, but neighbouring eh-pairs) can be written as Bloch functions constructed from eh-pair excitations at different positions of the ring [16]

$$
\varphi_j = u_1 u_2 \ldots u_{j-1} v_j w_{j+1} \ldots u_L\,, \tag{2}
$$

whereby u_i, v_j, w_j are $3d^4$, $3d^5$, $3d^3$ cation state wave functions. With the use of cyclic boundary conditions the energies involved are

$$
E_k = \varepsilon_{eh} + 2b_{eh}\cos ka\,, \tag{3}
$$

$$
k = \frac{2\pi m}{aL} \qquad \begin{array}{ll} -L < 2m - 1 \leqq L & \text{odd}\,, \\ -L < 2m \leqq L & \text{even}\,. \end{array}
$$

For the propagation of a resonance, say with $L = 3$, in a certain crystal direction, alternating right-hand and left-hand rotations occur in adjoining cells (Fig. 1 b). If one connects N units cyclically one can apply the method of calculation used before once more and obtains

$$E_{k,K} = E_k - 2T_K \cos Ka \approx \varepsilon_{eh} + 2b_{eh} \cos ka + 2b_{eh} \cos Ka\,, \tag{4}$$

$$K = \frac{2\pi M}{aN} \qquad \begin{array}{ll} -N < 2M + 1 \leqq N & \text{odd}\,, \\ -N < 2M \leqq N & \text{even}\,, \end{array}$$

where E_k is the energy of the "bound" resonance and $T_K \approx b_{eh}$ since the eh-pair has to move one unit length a in order to change cells. The particular bound resonant state calculated with spin-dependent transfer involves an alternating left-hand ($k = -2\pi/3a$) and right-hand ($k = -2\pi/3a$) rotation inside one triangle, i.e. it involves a combination of the wave functions of right-hand and left-hand rotating eh-pairs. However, since $E_{k,K}$ is degenerate in respect to $k = \mp 2\pi/3a$ for the band energies we may use

$$E_K = \varepsilon_{eh} - JS \mp 2t^* \cos\frac{\theta}{2}\left(-\frac{1}{2} + \cos Ka\right); \qquad \theta = 0 \text{ or } \pi\,. \tag{5}$$

One obtains three excitonic bands which are equidistant at the center ($K = 0$) and at the boundary ($K = \pi/a$) of the Brillouin zone (Fig. 4 b). If one sets the energy of the ionic lattice $Mn^{3+}As^{3-}$ above the minimal excitonic energy (at $K = \pi/a$) one can have resonant states to exist spontaneously at the zone boundary while there can be an exciton-triplet absorption at $K = 0$.

Although from this result it is suggestive to connect the magnetic coupling and the excitonic absorption of $MnAs_{0.88}P_{0.12}$, further experiments are necessary in order to achieve an unambiguous interpretation of the optical spectra.

Acknowledgements

One of us would like to thank Prof. Dr. H. U. Harten for valuable support and Dr. H. Berg for the preparation of the samples.

References

[1] K. Bärner, phys. stat. sol. (b) **88**, 13 (1978).
[2] H. Berg, K. Bärner, and W. Schröter, Phil. Mag. **31**, 1049 (1975).
[3] K. Bärner, phys. stat. sol. (b) **84**, 385 (1977).
[4] M. Welkowsky and R. Braunstein, Rev. sci. Instrum. **43**, 399 (1972).
[5] D. M. Korn and R. Braunstein, Phys. Rev. B **5**, 4837 (1972).
[6] M. Menyuk, J. A. Kafalas, K. Dwight, and J. B. Goodenough, Phys. Rev. **177**, 942 (1969).
[7] K. Bärner and H. Berg, phys. stat. sol. (a) **49**, 545 (1978).
[8] K. Bärner, R. Braunstein, and E. Chock, phys. stat. sol. (b) **80**, 451 (1977).
[9] G. W. Pratt and R. Colhoe, Phys. Rev. **116**, 281 (1959).
[10] F. Abeles, Ed., Optical Properties of Solids, North-Holland Publ. Co., Amsterdam 1972 (p. 195).
[11] J. M. Tyler and J. L. Fry, Phys. Rev. B **1**, 4604 (1970).
[12] J. W. Allen and J. C. Mikkelsen, Phys. Rev. B **15**, 2955 (1977).
[13] H. Berg and K. Bärner, J. Magnetism Magnetic Mater. **4**, 69 (1977).
[14] P. W. Anderson and H. Hasegawa, Phys. Rev. **100**, 675 (1955).
[15] P. W. Anderson, Magnetism I, Ed. G. T. Rado and H. Suhl, Academic Press, New York 1963.
[16] C. Kittel, Festkörperphysik, Wiley, Frankfurt 1973 (p. 717).

(Received June 5, 1979)

Ferroelectrics, 1980, Vol. 27, pp. 225-230
0015-0193/80/2701-0225$04.50/0

Gordon and Breach, Science Publishers, Inc., 1980
Printed in the United States of America

FERROELECTRIC, PHOTOCHROMIC, AND ELECTROCHROMIC GLASSES*

R. Braunstein
Department of Physics
University of California
Los Angeles, California 90024, U.S.A.

I. Lefkowitz
Department of Physics
University of North Carolina
Chapel Hill, North Carolina, U.S.A.

Bulk transparent glasses containing WO_6-octahedra in various glass forming matrices have been prepared which exhibit ferroelectric-like, electrochromic and photochromic behavior. Cooperative phenomena of random electric dipoles in these systems were studied by the techniques of thermally stimulated depolarization currents. These systems exhibit dipole correlation at a critical concentration in the presence of an external electric field and at a specific temperature. A model was developed for a phase transition associated with such random "pseudo-spins" in an amorphous matrix. The photochromic and electrochromic behavior in these glasses are initiated by the double injection of electrons and ions.

INTRODUCTION

A series of bulk transparent glasses containing WO_6-octahedra which exhibit ferroelectric-like, photochromic, and electrochromic behavior, have been prepared. These glasses contain randomly distributed dipoles whose concentration can be controlled and exhibit a paraelectric-ferroelectric-like phase transition at a critical concentration and temperature; from a theoretical viewpoint, the systems are similar to dilute or amorphous ferromagnets. Such "doped" glasses are in contrast to the vitreous modifications of crystalline ferroelectrics which have been studied theoretically[1] and experimentally.[2] Photochromic and electrochromic behavior are initiated in these glasses by the simultaneous injection of electrons and ions.

EXPERIMENTAL

The glasses containing WO_3 in various glass forming networks of Li_2O-B_2O_3, Na_2O-B_2O_3, and TeO_2 were prepared from reagent grade oxides at 800 C - 950 C in air in platinum crucibles and the melts cast onto vitreous carbon molds and annealed at 300 C; X-ray analyses showed the systems to be amorphous. The glasses are mechanically stable and can be successively cycled between room and liquid helium temperatures without cracking or crazing.

The dielectric constant-ε of $TeO_2 \cdot 0.23\ WO_3$ and $\tan\delta$ were determined between 4.2 and 250 K and are shown in Fig. 1(a) and (b) respectively. In addition, thermally stimulated depolarization current techniques were employed to identify dipole

*Work supported by U. S. Army Research Office, Durham, North Carolina, U.S.A.

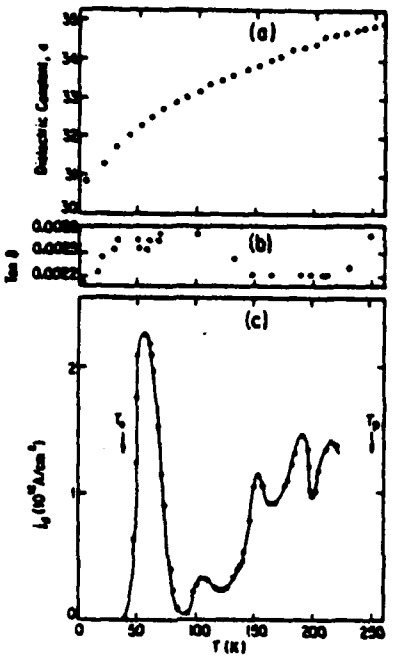

Fig. 1. (a) Dielectric constant as a function of temperature of $TeO_3 \cdot 0.23WO_3$. (b) Loss angle measurement $\tan\delta$ as a function of temperature in this glass. (c) Thermally stimulated depolarization current peaks in this glass with polarization temperature $T_p = 250$ K, polarization time $t_p = 8.5$ min, linear heating rate $b = 3.4$ K min^{-1}, polarization field $E_p = 7.1$ kV cm^{-1} and initial temperature $T_0 = 40$ K.

bearing species; these results are shown in Fig. 1(c). The changes in slope of the dielectric constant and the tanδ anomalies and depolarization current peaks which occur in the neighborhood of phase transitions[3] in crystalline WO_3 indicate that the local WO_6-units contribute to the dielectric properties of the glass. It was not possible to form pure TeO_2 or WO_3 glasses so as to arrive at the relative contribution of the constituents to the observed dielectric constant.

It was possible to prepare bulk glasses of Li_2O-B_2O_3-WO_3 with a continuous variation of WO_3. Depolarization peaks were observed which could be identified with WO_6-dipoles and with a dipole bearing species of the Li_2O-B_2O_3 network. Figures 2 - 5 display the observed peaks in a series of glasses.

The solid curve in Fig. 2 peaking at 235 K in pure $Li_2B_4O_7$ is the observed peak while the dotted curve is a theoretical fit to the data using an independent dipole model.[4] The peak at 258 K in Fig. 3 is due to WO_3 and is also represented by the dotted curve for independent dipoles. From the 235 K glass peak one determines an activation energy $\Delta E = 0.44$ eV and a pre-exponential $\tau_0 = 5\times10^{-8}$ sec, while the WO_3 peak at 258 K yields $\Delta E = 1.2$ eV and $\tau_0 = 2\times10^{-22}$ sec. The dipole moment per unit of WO_3 is $\bar{p} = 1.3\times10^{-15}$ esu cm; it should be noted that this is the first determination of $\bar{p}$ for WO_3 in a glass matrix. This dipole moment is rather large compared to typically observed values which are the order of 10^{-17} - 10^{-18} esu cm.

From Fig. 4 it is seen that at 0.08 moles of WO_3, the tungsten peak shows a dramatic change in intensity and line shape, while the glass peak maintains its shape and has the same order of magnitude as in pure $Li_2B_4O_7$. The fact that the WO_3 peaks occur close to the temperature at which crystalline WO_3 shows a phase transition[3] is again strong evidence that it is associated with WO_6-octahedra in the glass matrix. The strong peaking at this composition is suggestive that cooperative behavior of the WO_6 is occurring at a critical "coherence" distance. If the sample is not poled, no depolarization is observed as the sample is heated between 40 - 300 K; thus a spontaneous polarization is excluded unless domains are present. However, with an external poling field, at low WO_3 concentration, the system behaves as a paraelectric, while above a critical concentration, it appears to exhibit cooperative behavior. In the cooperative regime, the position of the peak is strongly pressure dependent shifting with an initial slope $\sim 2\times10^{-5}$ K dynes^{-1}.

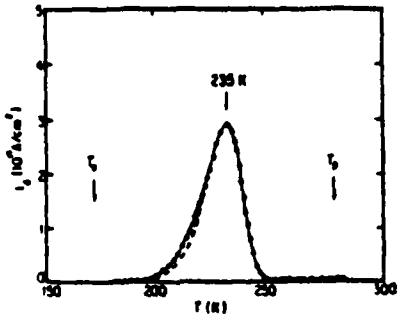

Fig. 2. Thermal depolarization current $I_d(T)$ of a $Li_2B_4O_7$ glass: Polarization temperature $T_p = 281$ K; Initial temperature $T_0 = 172$ K; Polarization time $t_p = 4$ min; Contact pressure $P_0 = 4 \times 10^5$ dyne cm^{-2}; Polarization field $E_p = 5$ kV cm^{-1}; Time constant of exponential cooling: $t_0 = 11.4$ min; Heating rate $b = 4.3$ K min^{-1}; —o— Experiment; — — — Theory.

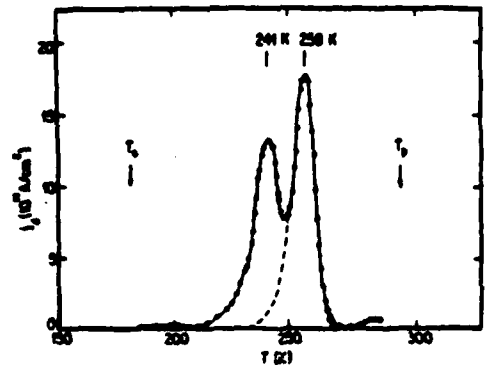

Fig. 3. $I_d(T)$ for a $Li_2B_4O_7 \cdot xWO_3$ glass ($x = 0.005$ mol): $T_p = 294$ K; $E_p = 5.9$ kV cm^{-1}; $P_0 = 4 \times 10^5$ dyne cm^{-2}; $t_p = 4$ min; $b = 3.4$ K min^{-1}; $T_0 = 185$ K; $t_0 = 8$ min; —o— Experiment; — — — Theory.

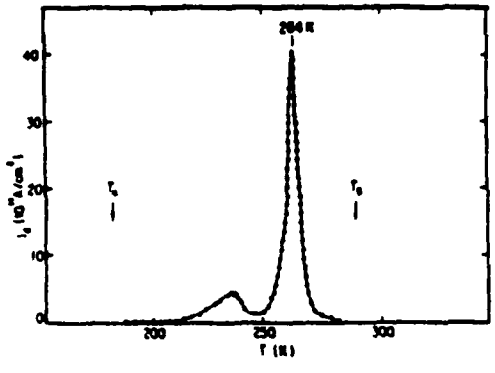

Fig. 4. $I_d(T)$ for a $Li_2B_4O_7 \cdot xWO_3$ glass ($x = 0.08$ mol): $T_p = 290$ K; $E_p = 6.2$ kV cm^{-1}; $P_1 = 4 \times 10^5$ dyne cm^{-2}; $t_p = 6.8$ min; $b = 2.5$ K min^{-1}; $T_0 = 181$ K; $t_0 = 9.6$ min.

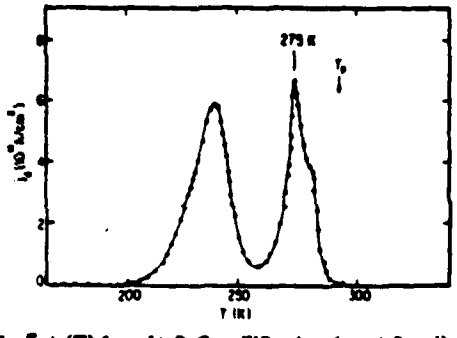

Fig. 5. $I_d(T)$ for a $Li_2B_4O_7 \cdot xWO_3$ glass ($x = 1.0$ mol): $T_p = 292$ K; $E_p = 5.2$ kV cm^{-1}; $P_0 = 4 \times 10^5$ dyne cm^{-2}; $t_p = 2.8$ min; $b = 2.4$ K min^{-1}; $T_0 = 146$ K; $t_0 = 10$ min.

DISCUSSION

The behavior of WO_3 in these glasses is suggestive that the random dipoles undergo a cooperative transition at a critical concentration and a specific temperature. Such a phase transition would have associated with it a critical slowing down of the relaxation times of the "pseudo-spins" as the transition is approached. The thermally stimulated depolarization currents measure dP/dt, i.e., the time rate of change of polarization as a function of temperature and thus is a measure of the dynamics of the electric susceptibility of the random dipole system. A one-dimensional model for a phase transition of a random "pseudo-spin" system has been developed using an Ising model in the mean field approximation and allowing for the situation where the spins are in a compensated configuration without the presence of an external electric field.[5] The depolarization current given by the model is:

$$T > T_c : \qquad j_d = \alpha S_{oz}(T-T_c) \exp\left[\frac{-\alpha(T-T_c)^2}{2}\right]$$

$$T_c-T_o < T < T_c : \qquad j_d = \alpha S_{oz}(T_o-T_c+T) \exp\left[\frac{-\alpha(T-T_c)^2}{2} + \alpha T_o(T_c-T)\right]$$

$$T_c-T_o > T : \qquad j_d = 0$$

with

$$T_o = Q S_{oz}^2 T_c , \qquad \alpha = (b\tau_o T_c)^{-1} , \qquad b = dT/dt ,$$

$$Q = \frac{1}{3} \frac{T_{co}^2 T_c}{T^3} (v_o/E^z)^2 , \qquad T_{co} = \bar{p} v_o k^{-1} ,$$

$$T_c = T_{co}\left[1 - \frac{1}{2}\frac{E^z}{v_o}\right]$$

where S_{oz} and v_o are the symbols conventionally defined for a one-dimensional crystalline ferroelectric.[9]

Figure 6 shows an example of the calculated depolarization current normalized to the transition temperature T_c. The discontinuity at T/T_c is due to the critical slowing down of the "pseudo-spins". No attempt was made to compare seriously the predicted lineshape of this one-dimensional model to the experimental curves above a critical WO_3 concentration. However, it is interesting to note that, similar to the model, Fig. 5 shows some structure in the 275 K WO_3 peak.

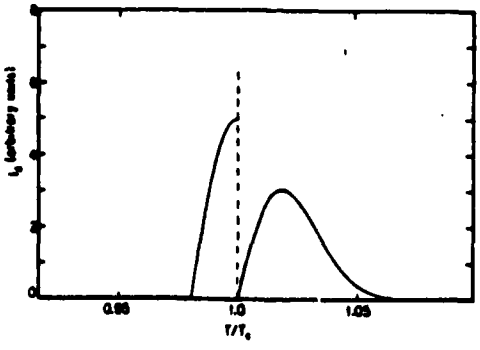

Fig. 6. Thermal depolarization current $j_d(T)$ as calculated for a compensated random electric dipole collective system: $\alpha = 2 \times 10^{-2} K^{-1}$, $T_c = 264$ K, $T_o = 10$ K (see text for details).

The above work on $Li_2B_4O_7 \cdot WO_3$ was performed with blocking contacts of mylar between the capacitor plates. However, when ultrasonically soldered contacts are employed, a large space charge peak occurs near 275 K, two orders of magnitude larger than when blocking contacts are used. Figure 7 and 8 show the maximum peak as a function of externally applied field for two different poling temperatures. While for $T_p = 295$ K the dependence is nearly linear, it shows an unusual oscillatory behavior for $T_p = 238$ K. Since the later poling temperature is below the "pseudo-spin" glass temperature while the former is above T_c, the difference is possibly connected with the dipolar

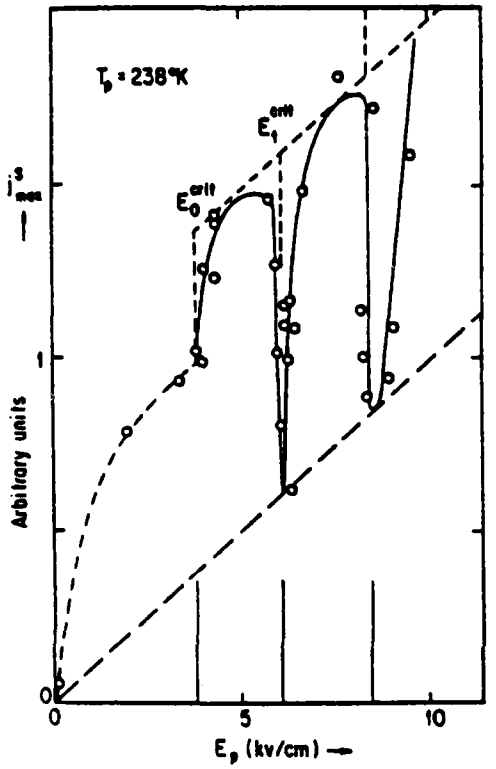

Fig. 7. Maximum space charge depolarization current $j^s_{max}(E_p)$, $(Li_2B_4O_7)_{1-x}(WO_3)_x$ glass [x = 0.01]
T_p = 238 K, b = 3 K/min, t_p = 5 min.

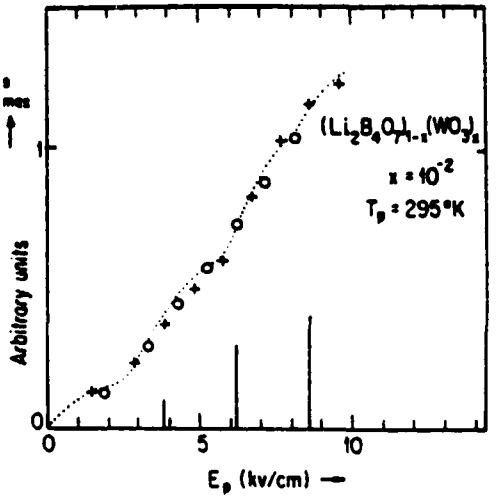

Fig. 8. Maximum space charge depolarization current $j_{max}(E_p)$, $(Li_2B_4O_7)_{1-x}(WO_3)_x$ glass [x = 0.01], T_p = 238 K, b = 3 K/min, t_p = 5 min.

interactions. A model for the effect of injected space charge has been developed.[7] The injected space charge results in a large electric field at the surface and induces a ferroelectric-like behavior at a critical field E_c = 3.8 Kv/cm. As the space charge is located at the dipolar WO_6-sites at higher injection levels, the molecular dipoles and with them the induced ferroelectric-like behavior can be destroyed. This leads to a migration of ferroelectric-like domains into the interior of the sample.

Evidence that the WO_3 ions are in an octahedral coordination and are dispersed in a glass matrix comes from the photochromic and electrochromic[8] behavior of these glasses. When the glass is in contact with a non-aqueous electrolyte, a blue absorption band is produced, peaking at 1.5 eV, when electrons are injected from a contact or the glass is illuminated by band gap light. The band can be explained as due to the production of H_xWO_3 in the glass matrix by the double injection of protons and electrons similar to that which is observed in amorphous WO_3 films.[9]

The observation that the WO_3 peaks occur close to the temperature at which crystalline WO_3 shows a phase transition is suggestive that some features of the data may be due to the presence of microcrystallites. However, X-ray measurements did not indicate the presence of crystalline structures in the glasses.

It is interesting to note that only a small shift in the transition temperature T_c is observed as the concentration is increased from 0.08 mol to 1.0 mol of WO_3. If one uses the virtual crystal approximation for a dilute Ising model to calculate the critical concentration of paraelectric centers at which a ferroelectric transition can occur, one obtains the result that T_c is proportional to concentration.[10] However, this result is only true for systems with long-range interactions where the virtual crystal approximation is a good approximation. For finite range interactions, one expects finite critical concentrations for ordering, and better methods have to be employed to determine this concentration.[11]

CONCLUSION

These tungstate glasses provide prototype systems within which to study cooperative behavior of "pseudo-spins" and electronic and ionic transport. They, in turn, provide a class of materials which suggest possible transducer, display, and information storage devices.

REFERENCES

1. M. E. Lines, Phys. Rev. B, 15, 388 (1976).
2. A. M. Glass, M. E. Lines, K. Nassau, and J. W. Shiever, Appl. Phys. Lett., 31, 249 (1977).
3. I. Lefkowitz, M. B. Dowell, and M. A. Shields, J. Solid State Chem., 15, 24 (1975).
4. C. Bucci, R. Fieschi, and G. Guidi, Phys. Rev., 148, 816 (1966).
5. R. Braunstein and K. Barner, Solid State Comm., 28, 847 (1978).
6. M. E. Lines and A. M. Glass, Principles and Applications of Ferroelectrics and Related Materials (Clarendon Press, Oxford, 1977), p. 15.
7. R. Braunstein and K. Barner (to be published).
8. R. Braunstein, Solid State Comm., 28, 839 (1978).
9. B. W. Faughnan and R. S. Crandall, Appl. Phys. Lett., 26, 120 (1975).
10. B. Žekš, Ferroelectrics, 12, 91 (1976).
11. R. J. Elliott and B. R. Heap, Proc. Roy. Soc., A265, 264 (1962).

Solid State Communications, Vol. 33, pp. 941–946.
Pergamon Press Ltd. 1980. Printed in Great Britain.

SPACE CHARGE INJECTION INTO A DIPOLAR GLASS

R. Braunstein* and K. Bärner†

Department of Physics, University of California, Los Angeles, CA 90024, U.S.A.

(*Received* 15 *October* 1979 *by A.A. Maradudin*)

Space charges can be injected into dipolar $(Li_2B_4O_7)_{1-x}(WO_3)_x$ glasses with the use of indium electrodes. They can be frozen in and are detected by their thermally stimulated depolarization currents. The large electric fields at the surface induce a ferroelectric domain above a critical field $E_0^{crit} = 3.8$ kV cm^{-1}. With increasing injection the induced ferroelectricity is destroyed periodically. This is interpreted in terms of the migration of the ferroelectric domain into the interior of the material.

1. INTRODUCTION

AN ATTEMPT has been made to observed cooperative phenomena of random electric dipoles by applying the techniques of themally stimulated depolarization currents to a series of glasses containing WO_6-octahedra, i.e. $(Li_2B_4O_7)_{1-x}(WO_3)_x$.[1, 2].

In these experiments two types of contacts were employed between the capacitor plates and the glass sample, namely ultrasonically soldered indium contacts and blocking contacts using mylar. The use of indium contacts resulted in the injection of large space charge peaks at temperatures above 200 K which could be completely suppressed by the use of blocking contacts. The results with blocking contacts have been interpreted in terms of a transition between a paraelectric and a spatially pseudo-spin compensated phase [1].

In the present work, we report on the effects of injected space charges on these glass systems. We assume that for low injection levels the high electric fields associated with the space charge layer induce a ferroelectric behavior at a critical field. We assume further that the space charges locate at the dipolar octahedral WO_6 sites so that the spontaneous polarization can be destroyed by recharging all available W in a surface layer (high injection). Consequently, an oscillatory behavior of the peak depolarization current which is observed as a function of poling field can be interpreted in terms of the migration of a ferroelectric domain into the interior of the glass.

*Work supported by the U.S. Army Research Office, Durham, North Carolina, U.S.A.

†Permanent address: IV. Physikalisches Institut der Universität Göttingen, 34 Göttingen, West Germany.

2. EXPERIMENTAL AND RESULTS

2.1. *Depolarization currents*

Thermally stimulated depolarization (TSD) currents in the dipolar glasses are observed using the standard parallel plate capacitor geometry and a constant heating rate, $b = dT/dt$ [1, 2].

Figure 1, curve A, shows a typical glow curve for the WO_3-doped glass, and one for the undoped glass – curve B, when indium contacts are directly attached to the glass surface. Curve A shows one small (1) and one large peak (2). Peak 1 has been ascribed previously to a dipolar species which is characteristic of the $Li_2B_4O_7$-glass matrix [1]. This is confirmed by curve B where this peak (1) is found with a comparable height. A second peak (2) is observed which is considerably smaller as compared to the doped glass, suggesting that the peak 2 is large only when WO_3-units are present. Since peak 2 can be completely suppressed when mylar foil is inserted between the metal electrodes and the glass surface [1] it must also be related to space charge injection. Similarly, when the pure glass ($x = 0$) is used with mylar foils, only peak 1 remains. That the TSD peak 2 may result from an intrinsic conductivity [3] can be ruled out since in that case it should also be observed with the mylar foils. Figures 2(a, b) show the area under the curve 2 as a function of the externally applied field E_0 for the doped glass and for two different poling temperatures T_p. While for $T_p = 295$ K the dependence is near linear, it shows an unusual behavior for $T_p = 238$ K. Since the one poling temperature is above the pseudo-spin glass transition temperature $T_c = 275$ K of the dipolar ensemble [1] and the other poling temperature below T_c the difference is probably connected with the dipole ordering.

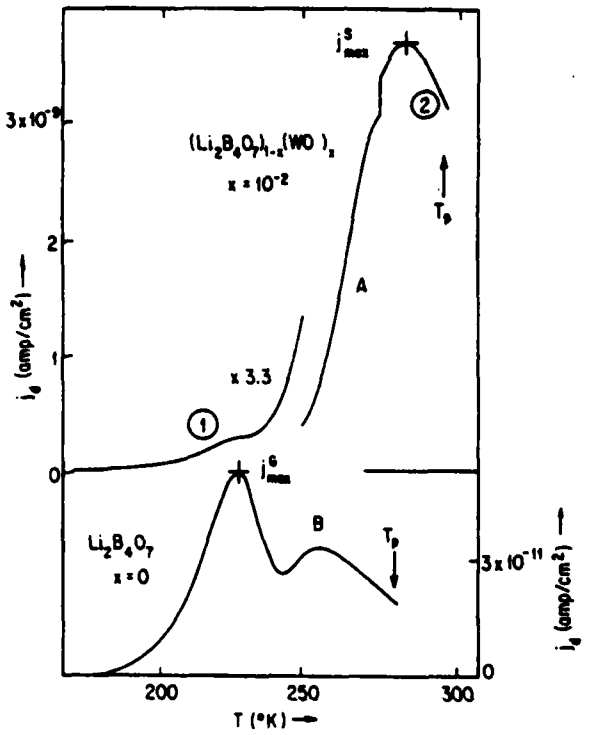

Fig. 1. Depolarization current $j_d(T)$ of a WO_3-doped $Li_2B_4O_7$-glass (curve A) and of the pure glass (curve B) using indium contacts. (A) $E_p = 4.8$ kV cm^{-1} (B) $E_p = 8.0$ kV cm^{-1}. Heating rate $b = 3$ K min^{-1}. Poling time $t_p = 5$ min. Poling temperature $T_p = 295$ K.

2.2. *Calculation of the injected space charge as a function of field*

In what follows an attempt will be made to explain the unusual field dependence of peak 2 assuming that the injected space charge is completely located at the WO_3 dipolar sites. When the charge density N is small compared to the dipole concentration n_0 with increasing charge the electric field at the surface is enhanced and induces a "pseudo-spin" glass to ferroelectric transition at a critical field. This would explain the sudden increase of $j^s_{max}(E_0)$ at $E_0^{crit} = 3.8$ kV cm^{-1}. Subsequent increases of injected charge destroys all of the dipolar species by recharging the tungsten, i.e. $W^{+6} \rightleftarrows W^{+5}$ whereupon the induced ferroelectricity breaks down.

2.2a. *Linear dielectric.* For space charge injection at an interface which is perpendicular to the z-direction, the condition of balance between field and diffusion current is

$$Ne\mu E + eD_0 \frac{dN}{dz} = 0 \qquad (1)$$

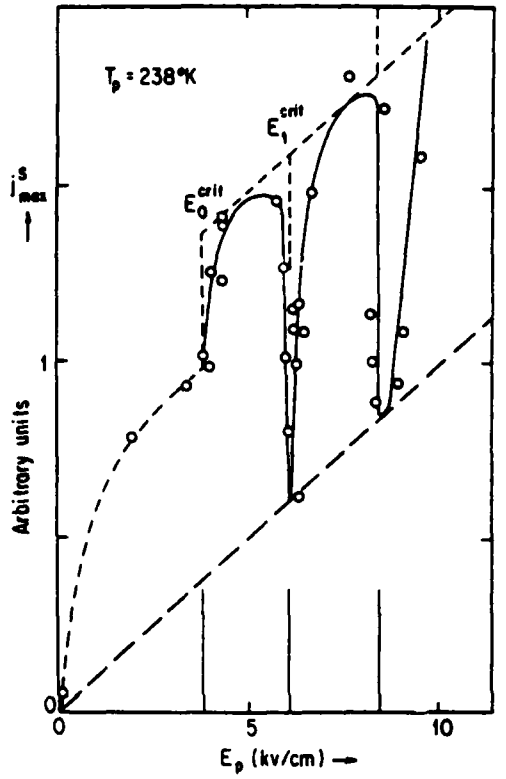

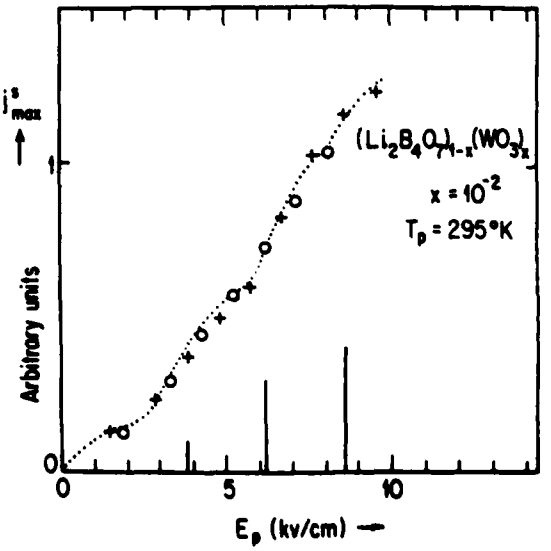

Fig. 2. Field dependence of the maximal space charge depolarization current $j^s_{max}(E_p)$ (compare peak 2, Fig. 1) for a WO_3-dopped$(Li_2B_4O_7)_{1-x}(WO_3)_x$-glass ($x = 10^{-2}$ mol%). (a) $T_p = 238$ K. $b = 3$ K min^{-1}, $t_p = 5$ min. (b) $T_p = 295$ K, $b = 3$ K min^{-1}, $t_p = 5$ min. (0, +: two independent sequences.)

where N = carrier concentration, D_0 = carrier diffusion coefficient, E = electric field and μ = carrier mobility.

Combined with Poisson's equation: $dD/dz = Ne$, and using Einstein's relation [equation (1)] leads to the well known equations for the Schottky barrier [4]:

$$\frac{d(\epsilon\epsilon_0 E)}{dz} = N_0 \exp(-eV/kT), \tag{2}$$

$$V = \frac{2kT}{e} \ln(1 + z/z_0), \tag{3}$$

$$N = N_0 \frac{{z_0}^2}{(z + z_0)^2}. \tag{4}$$

$${z_0}^2 = 2\epsilon\epsilon_0 kT/e^2 N_0, \tag{5}$$

$$E^s = kT/2ez_0, \tag{6}$$

where D = dielectric displacement, V = electric potential, N_0 = carrier concentration at the interface and E^s = electric field at the interface.

Within a band bending model the carrier concentration at the interface N_0 and with it the total space charge $\sigma^s \propto j^s_{max}$ is determined by the externally applied field E_0, the number of surface states and the distribution of their energy levels relative to the electrochemical potential [5, 6].

Empirically, we find a near linear dependence $\sigma^s \propto E_0$ in the paraelectric state [Fig. 2(b), T_p = 295 K] – the shallow dips could indicate some short range order response of the WO_3-dipoles to the injected space charge and will be neglected here. Therefore we can write

$$\sigma^s = \eta\epsilon_0 E_0. \tag{7}$$

When we use ϵ_0 as a factor the proportionality constant η has the dimension of a relative permeability. From the integral of the glow curve [2]

$$\sigma^s = b^{-1} \int_0^\infty j^s(T)dT \tag{8}$$

(Fig. 1, curve 2) η can be estimated: $\eta \simeq 5 \times 10^3$ indicating a large number of localized states on the amorphous surface. When we freeze in the total injected charge in our depolarization experiment with the aid of shallow localized states or a temperature dependent mobility $\mu(T)$ we form an electret and N_0 will be given by the step in the dielectric displacement at the surface ΔD

$$\Delta D = \sigma^s = \int_0^\infty eNdz \tag{9}$$

which remains after the poling field is removed at T_0 analogous to a ferroelectric where $\Delta D = P_0$ (P_0: spontaneous polarization) is conventionally assumed [4]. Then, N_0 is given by:

$$N_0 = \eta^2 \epsilon_0 {E_0}^2/2\epsilon kT_p. \tag{10}$$

With surface condition (9), when both dipole ordering and a space charge electret are present ($T_p < T_c$) we would expect $\sigma \sim E_0$, too. However, in our case, when $T_p < T_c$ [Fig. 2(a)] non-linear contributions seem to be superimposed on the linear rise. This indicates that we will have to consider non-linear effects because of the extreme electric field strengths at the surface connected with the Schottky barrier.

2.2b. *Non-linear dielectric; space charge and dipolar polarization.* In order to account for a possible spontaneous polarization P_0, an accompanying space charge enhancement and the possibility of a breakdown of P, we write the polarization of a two-level dipolar system in analogy to a two-level spin system and use it for a boundary condition at the surface;

$$P^s = P_0 \tanh\left[\frac{\lambda_p P^s}{\epsilon_0 kT_p} + \frac{pE^s}{kT_p}\right], \tag{11a}$$

$$\Delta D = P^s + \epsilon_0 E^s = \sigma \tag{11b}$$

where p = molecular dipole moment of a WO_6-unit and λ = molecular field constant.

We further assume that the space charge distribution is still that of a Schottky barrier [4] and that the aligning field E^s is given by the space charge which would be there without the molecular dipoles, i.e. $E^s = (\eta/\epsilon').(E_0/4)$ using equations (5), (6) and (10) (ϵ': dielectric constant of the uncharged and undoped matrix). This is an approximate treatment since actually one should solve the differential equation (2) for the barrier with the complete polarization term.

Equation (11a) can be solved to give the polarization at the surface P^s as a function of the externally applied field E_0 and with it the portion of the space charge which is due to the dipole alignment $\sigma^p = P^s$ [Fig. 2(a) weakly dashed line, $E_p < E_0^{crit}$]. The field induced spontaneous polarization is simply accounted

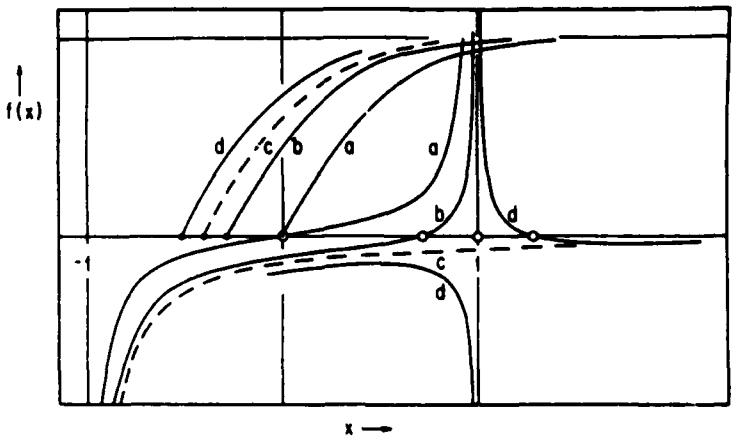

Fig. 3. Graphical solution for polarization at the surface P^s showing instability if $N_0 = n_0$. n_0 dipole concentration, $x = N_0/n_0$ $f(x) = \tanh(bx + cx_0)$; $f(x) = a[(x - x_0)/(1 - x^2)]$; a, b: $x_0 < 1$; c: $x_0 = 1$; d: $x_0 > 1$.

for by setting $\lambda = 0$ and $\lambda = \lambda_0$ for $E_p \lesssim E_0^{crit}$ [Fig. 2(a), weakly dashed line].

Aside from describing the observed total space charge σ, the model also reproduces the instability at E_1^{crit} in the following way. Assume that the polarization at the surface P^s is given by equations (11), (9), (4) and (5), i.e.

$$P^s = (2\epsilon\epsilon_0 kT_p N_0')^{1/2} \tag{12}$$

and that the saturation polarization P_0 is

$$P_0 = n_0 p\left[1 - \frac{N_0}{n_0}\right] \tag{13}$$

where n_0 = molecular density of WO_3-units as required by the recharging assumption. Then, equation (11) can be rewritten in the form

$$\tanh(bx + cE_0) = a\frac{x - \gamma E_0}{1 - x^2} \tag{14}$$

where

$$a = (2\epsilon\epsilon_0 kT_p n_0)^{1/2}/n_0 p, \quad b = 2\epsilon\lambda_0\alpha/a,$$
$$c = \eta p/4\epsilon kT_p, \quad \gamma = \epsilon_0\eta/4n_0 p\epsilon a, \tag{15}$$
$$x = (N_0/n_0)^{1/2}, \alpha = (N_0'/N_0)^{1/2}.$$

When the external field is enhanced there is always a solution (Fig. 3) if the root $x_0 \equiv \gamma E_0$ of $x - x_0/1 - x^2$ is greater or less than 1. For $x_0 = 1$ the function reduces to $-1/(1 + x)$ and there is no solution corresponding to a zero polarization for:

$$E_1^{crit} = \frac{4\epsilon}{\epsilon_0\eta}(2\epsilon\epsilon_0 kT_p n_0)^{1/2}. \tag{16}$$

In Fig. 2(a) this divergency is finite but still in a very narrow ΔE_0 interval around $E_1^{crit} = 6.1\ \mathrm{kV\,cm^{-1}}$.

This and the periodic reoccurrence of this divergency indicate that the spatial variation of the polarization has to be taken into account. It is therefore not surprising that a numerical estimate of E_1^{crit} using equation (16), $n_0 = 6 \times 10^{21}\ \mathrm{mol^{-1}}$ for $x = 10^{-2}$ and $\epsilon \simeq 1 + \chi_{dipoles} + \chi' \simeq 1$ at saturation, yields $E_1^{crit} \simeq 10\ \mathrm{kV\,cm^{-1}}$.

The spatial variation $P(z)$ can be taken into account approximately in the following way: assume that the electric field variation is still given by the derivative of equation (3);

$$E(z) = \frac{kT}{2ez_0}(1 + z/z_0)^{-1}; \tag{17}$$

since the total space charge drops to a linear dependence at E_1^{crit} an estimate for the electric field after the breakdown of the polarization is given by equations (5), (6) and (10), with $N_0 = n_0$ setting

$$E(z^{crit}) = \frac{\eta}{\epsilon}\frac{E_0^{crit}}{4} \text{ and } E(z_0) = \frac{\eta}{\epsilon}\frac{E_1^{crit}}{4} \tag{18}$$

where z^{crit} = width of the breakdown layer, it follows that

$$z^{crit} \simeq \frac{2kT_p\epsilon}{e\eta}\left[\frac{1}{E_0^{crit}} - \frac{1}{2E_1^{crit}}\right]. \tag{19}$$

Taking E_0^{crit} and E_1^{crit} from Fig. 3(a) and $\epsilon \simeq 1 + \chi_{dipoles} + \chi' \gg 1$ because now $\chi_{dipoles} \simeq \chi_i$ and $\chi_i \simeq 4n_0 p\epsilon/\epsilon_0\eta\Delta E_0^{crit}$ (χ_i = initial susceptibility), then: $z^{crit} \simeq 60$ Å.

If we approximate $N(z) = N_0$ in this layer and assume further and consistent with the model that once $N_0 = n_0$ no further space charge can be trapped, no spontaneous polarization will reoccur; however, for $z^{crit} < z < 2z^{crit}$ the charge will continue to

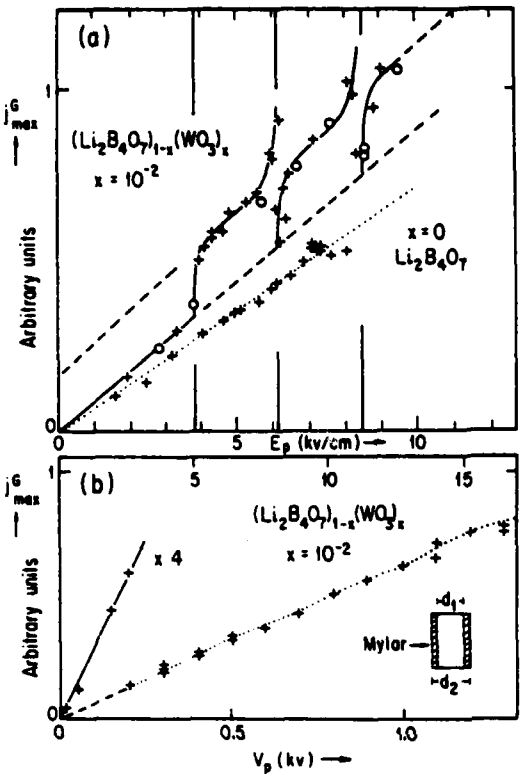

Fig. 4. (a). Field dependence of the maximal depolarization current $j^G_{max}(E_p)$ of the intrinsic glass dipole for WO_3-dopped $Li_2B_4O_7$-glass (upper curve) and for the pure glass (lower curve). (b). $j^G_{max}(E_p)$ for the pure glass using mylar blocking contacts. Lower scale: applied voltage V_p. Upper scale: calculated electric field E_p, assuming a uniform susceptibility. Dimensions: $d_1 = 0.775$ mm, $d_2 = 0.785$ mm, $b = 3$ K min^{-1}, $t_p = 5$ min, $T_p = 238$ K.

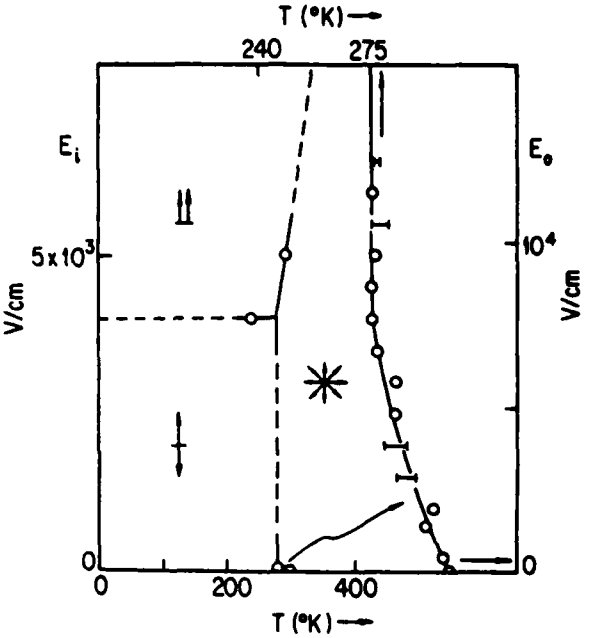

Fig. 5. "Electric" phase diagram for a $(Li_2B_4O_7)_{1-x}(WO_3)_x$-glass ($x = 10^{-2}$ mol.%). E_0 = external electric field. E_i = space charge enhanced electric field. ↔ = paraelectric phase. ↑↑ = ferroelectric phase. ↕ = "pseudo-spin" compenseted phase.

be enhanced and lead to a spontaneous polarization and a subsequent breakdown; apparently, the difference in total charge between the onset of ferroelectricity and the breakdown will always be the same. Because of equations (5), (6) and (10) the same is true for the diffenence in field. This prediction is experimentally verified in Fig. 2(a). Also, the abrupt enhancement of the depolarization current which is sometimes observed (see Fig. 1) indicates the presence of a spontaneous polarization which is destroyed at a Curie-point or when the space charge is thermally disoriented.

When the dipolar glass in in the paraelectric state evidently no ferroelectric polarization can be induced; the shallow dips in $\sigma(E_0)$ for $T_p = 295$ K [Fig. 2(b)] have already been assigned to some short range order response of the dipoles.

However, the most striking evidence for the presence of an internal field is indicated by the periodic variation of the area under the glow curve which is assigned to the intrinsic dipole; since the area is typically 2 orders of magnitude lower that the space charge peak, the intrinsic dipole serves as an indicator of the local electric field which is present under certain poling conditions. From Fig. 4(a) not only the threshold field can be inferred but also the magnitude of the internal field via the intersection with the E_0 axis ($E_i \simeq 10^9$ V m^{-1}, $\lambda_0 \simeq 30$ using $p = 1.3 \times 10^{-15}$ esu cm) [1]. Moreover, the two subsequent breakdowns of the internal fields can be identified again. It is interesting to note that as a precursor of the breakdown the internal field seems to be enhanced; this is probably related to the observation that it is easier to align the dipoles ferroelectrically when their concentration is small [1] – this in turn might be due to a reduction in the coupling constants which lead to the pseudo-spin compensated array.

When no space charge is present in the doped glass or when no dopant is present we do not observe such effects for the intrinsic dipole [Figs.4(a, b)].

2.2c. *Electric phase diagram.* The proposed "field induced" ferroelectricity as contrasted to the pseudospin dipolar array [1] leads one to consider the electric field E as a thermodynamic variable and to construct

an "electric phase diagram" whose boundaries are given by the dependence of the transition temperatures on the field strength $T_c^i(E)$ (Fig. 5). Subsequently, the different regions have to be assigned a particular dipolar order. The experimental points on the paraelectric-"pseudo-spin" glass transition line are obtained from the variation of the dipolar WO_3-peak position with external field when no space charge is present [1]. Although the range of electric field strengths is limited in this case, a decrease of T_c is observed with increasing field which tends to saturate at about 10 kV cm^{-1}; because of the compressed scale it has been redrawn in a different scale in the right hand section of the figure.

The existence of the other phase separation lines can be inferred from the available data; the ferroelectric "pseudo-spin" glass transition occurs at fields which are $\simeq 10^3$ times larger than the externally applied field E_0 from the estimate of η and ϵ. The experimental point on the horizontal line in Fig. 5 is concluded from the existence of E_1^{crit} [Fig. 4(a)]; as substitute of the corresponding equilibrium temperature, T_{max} of the intrinsic dipole has been taken. The experimental point on the paraelectric–ferroelectric transition-line follows if the step in Fig. 1 (curve A) is interpreted as a phase transition temperature at constant electric field.

The dipolar glasses are optically transparent, order electrically near room temperature, and can presumably be prepared in large sheets. Since they also allow for electrical read-in due to the switching phenomena, optical read-out due to the blue W charge transfer band [7] and optical erasure by laser heating they hold a considerable potential for electro-optic memory devices.

REFERENCES

1. R. Braunstein & K. Bärner, *Solid State Commun.* **28**, 847 (1978).
2. C. Bucci, R. Fieschi & G. Guidi, *Phys. Rev.* **148**, 816 (1966).
3. P. Müller, *Phys. Status Solidi. (a)* **23** 165 (1974).
4. M.E. Lines & A.M. Glass, *Principles and Applications of Ferroelectrics and Related Materials*, p. 120. Clarendon Press, Oxford (1977).
5. J.P. McKelvey, *Solid State and Semiconductor Physics*, p. 489. Harper & Row, New York/London.
6. H. Fritsche, *Electronic and Structure Properties of Amorphous Semiconductors* (Edited by P.G. Comber & J. Mort) p. 77. Academic Press, London/New York.
7. R. Braunstein, *Solid State Commun.* **28**, 839 (1978).

Mat. Res. Bull., Vol. 15, pp. 735-742, 1980. Printed in the USA.
0025-5408/80/060735-08$02.00/0

INFRARED-TRANSPARENT GLASSES DERIVED FROM THE FLUORIDES OF ZIRCONIUM, THORIUM, AND BARIUM

M. Robinson, R.C. Pastor, R.R. Turk, D.P. Devor, M. Braunstein
Hughes Research Laboratories, Malibu, California 90265

R. Braunstein
Department of Physics
University of California at Los Angeles, Los Angeles, California 90024

(Received March 24, 1980; Communicated by R. A. Huggins)

ABSTRACT

Glasses consisting solely of high-purity ZrF_4, ThF_4, and BaF_2 have been synthesized using reactive atmosphere processing (RAP) techniques. RAP of the individual components and the molten material with anhydrous HF and CCl_4 is described. The glass molds easily at 312°C and 1920 psi with a high-fidelity replication of the die surface. The glass is water insoluble, unusually hard and strong, and continuously transparent from 0.3 to 7 μm.

Introduction

During the past several years, considerable effort has been directed to the preparation of exceptionally high purity halide materials for a multitude of applications ranging from laser windows to fiber optics. RAP has been successfully developed for crystalline KCl to bring about the reduction in the 10.6-μm absorption coefficient from $\geq 10^{-2}$ cm^{-1} (Ref. 1) to $\leq 10^{-4}$ cm^{-1} (Ref. 2). RAP methods increased the rupture strength by one order of magnitude and greatly reduced surface attack by ambient humidity.

RAP, when applied to the single-crystal growth of rare earth fluorides (3), totally eliminated many solid-solid phase transitions thought to be intrinsic to these compounds. The transitions are triggered by low concentrations of OH^-; minimizing the OH^- level by atmosphere control permitted large single crystals (>1 cm) to be grown from melts of fluorides previously thought to exhibit di-morphism.

Multicomponent fluorozirconate glasses, a relatively new class of materials, were reported first by M. Chanthanasinh (4) in 1976 and later by Poulain et al. in 1977 (5). Both were concerned with the ZrF_4-ThF_4-BaF_2 system; that system is also the subject of this paper. The preparation technique typically used by earlier workers consisted of reacting highly purified components at 800 to 900°C in an argon atmosphere. The starting materials were contained in a hermetically sealed nickel crucible and the glass was formed by pouring the fully reacted melt into a mold residing in a nitrogen-filled glove box. The vitreous

domain for ZrF_4-ThF_4-BaF_2 can be described as an area of a triangle on the ternary diagram bounded by the following points: 63 mole % ZrF_4, 15 mole % ThF_4, and 38 mole % BaF_2. RAP preparations throughout this area readily yield transparent glasses; however, the composition of interest for this paper is 60% ZrF_4, 7% ThF_4, and 33% BaF_2, which is essentially the center of the vitreous domain.

This paper describes the RAP approach to preparing this fluoride glass utilizing open crucibles and controlled atmospheres of anhydrous HF and CCl_4. Physical properties including spectral data are given as well as glass molding techniques.

Experimental

Purification of Materials

ZrF_4 of 99.5% purity was obtained from the Cerac Company. This raw material was treated with dry HF at 400°C and sublimed once at 900°C in a stainless-steel sublimator. The high-purity, colorless, transparent needles were then combined with ThF_4 and BaF_2 to give the desired ratio — 0.60 Zr: 0.07 Th: 0.33 Ba. The ThF_4 was derived from 99.9% ThO_2 (Cerac). The oxide was first reacted with a 49% HF solution, and then the water was evaporated away at about 100°C until a dry powder resulted. Next, this powder was slowly heated and subjected to gaseous HF until melting occurred. The high-purity product was the source of ThF_4 for glass-forming experiments. The BaF_2, from EM Laboratories, was 99.99% pure. It was treated with dry HF to 1000°C prior to use as a starting material for glass preparations.

Each glass forming run consisted of a 93-g batch. Vitreous carbon or platinum crucibles were used in an Astro Industries (graphite resistance) furnace. The furnace was vacuum pumped to 300°C before the start of RAP. The reactive atmosphere was either anhydrous HF diluted to 10 mole % with helium, or gaseous CCl_4 (Mallinkrodt AR) diluted with helium. The mixture was heated to 900°C in 5 hr; the resulting melt was soaked for 5 hr and then cooled abruptly to room temperature. The ingot could then be annealed at 220°C to remove strain.

Glass Molding

Molding was accomplished with a 20-ton PHI hydraulic press with readable pressure to 2.5 psi intervals. A 1/2-in. cylindrical tungsten carbide die was used. The inner faces of the plungers were polished optically flat to 1/2 fringe (sodium spectral line — 5896 Å). The die with sample inside is placed in the press. The temperature is raised to 312°C and increasing pressure is applied until a pressure drop is indicated due to glass flow. Temperature is held constant until the die is filled as indicated by no further pressure drop even as higher pressure is applied. The temperature is then lowered below 300°C, the pressure is released, and the sample is cooled to room temperature.

Results and Discussion

Glass Properties

Early batches of 0.60 ZrF_4:0.07 ThF_4:0.33 BaF_2 glass were prepared exclusively with a RA consisting of HF diluted with helium. Although X-ray powder pattern showed that the specimens were indeed glassy, they appeared to consist of two phases — a primary transparent-colorless phase and a relatively small quantity of an opaque-black phase. Electron microprobe analysis of the samples

indicated that the opaque-black substance contained only one-half the fluorine of the transparent phase. This fluoride-deficient phase formed regardless of whether a platinum or carbon crucible was used, and, surprisingly, its concentration appeared to increase with longer HF soak times.

The formation mechanism of this opaque-black phase is not understood; it would appear to result from the dissociation of ZrF_4.[†] Figure 1 shows the IR transmission curves (Beckman IR 12) of three fluoride glass samples. Curve A is for the glass 0.60 ZrF_4:0.10 ThF_4:0.30 BaF_2. This glass is manufactured in France by La Verre Fluore and, using an inert atmosphere, is prepared with careful attention to the prevention of hydrolysis. The absorption centered at about 2.85 μm may be the result of a trifling amount of OH^- contamination. Curve B results from a HF-prepared glass, 0.60 ZrF_4:0.07 ThF_4:0.33 BaF_2. This specimen appears to have even a higher concentration of OH^- than does A. HF is not an effective reactive atmosphere for these glasses. It can displace OH^- and $O^=$ from simple mixtures of BaF_2 and ThF_4, but, at temperatures above 530°C, ZrO_2 resists conversion to ZrF_4 (i.e., ZrO_2 is thermodynamically favored over ZrF_4 even in the presence of HF). OH^- impurity arises from hydrolysis stemming from water emanating from the interior surfaces of the furnace, and HF of course cannot eliminate this water. The reduced transmission throughput is caused by some precipitated fluoride deficient base. Curve C is 0.60 ZrF_4: 0.07 ThF_4:0.33 BaF_2 glass prepared in a CCl_4 atmosphere. Note that the transmission is continuous. CCl_4 is an extremely effective reactive atmosphere. It reacts with both OH^- in the melt and outgassed water:

$$CCl_{4(gas)} + 2OH^-_{(melt)} \rightleftarrows CO_{2(gas)} + 2HCl_{(gas)} + 2Cl^-_{(melt)}$$

$$CCl_{4(gas)} + 2H_2O_{(gas)} \rightleftarrows CO_{2(gas)} + 4HCl_{(gas)}$$

Moreover, CCl_4 pyrolytically cracks at temperatures above 400°C to give nascent chlorine, which compensates any fluoride deficiency and yields remarkably colorless and transparent ingots.

The absorption coefficients of sapphire, Le Verre Fluore glass, and Hughes fluorozirconate glass are compared as a function of wavelength in Figure 2. The measurements, made with a Cary Model 14R, show the Hughes glass (CCl_4 prepared) to be less absorbing than the Le Verre Fluore, but not nearly as good as sapphire. Fluorozirconate glass prepared in anhydrous HF gives about the same result as Le Verre Fluore glass. The physical properties of the glass 0.60 ZrF_4:0.07 ThF_4:0.33 BaF_2 prepared in CCl_4 are given in Table 1. The glass transition, crystallization, and fusion temperatures were determined for a sample sealed at room temperature in a platinum capsule at a pressure of $<10^{-5}$ Torr. Water insolubility was determined by soaking typical glass samples in tap water for 24 hr at room temperature and observing no weight change.

Molded Glass

Figure 3 shows the fluorozirconate glass (prepared in CCl_4) and the die before and after hot pressing. Pressing was done at 312°C and 1920 psi in air. Note the frosty areas corresponding to flat cut corner bevels on the original blank. Total height reduction was 31.2% — from 0.218 in. to 0.150 in.

[†] Residual gas analysis of crystalline ZrF_4 shows the evolution of fluorine at $T \geq 500°C$, i.e.,(white) $ZrF_4 \rightleftarrows$ (black) $ZrF_2 + F_2$.

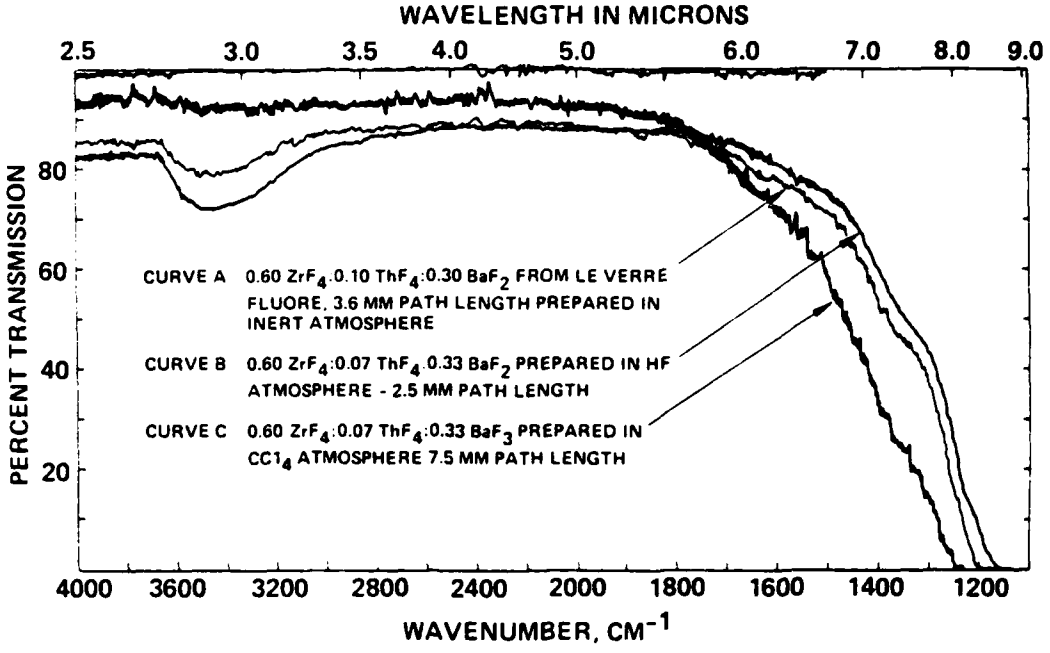

FIG. 1
Transmission spectra of fluorozirconate glasses. Both faces polished to a window finish for all samples.

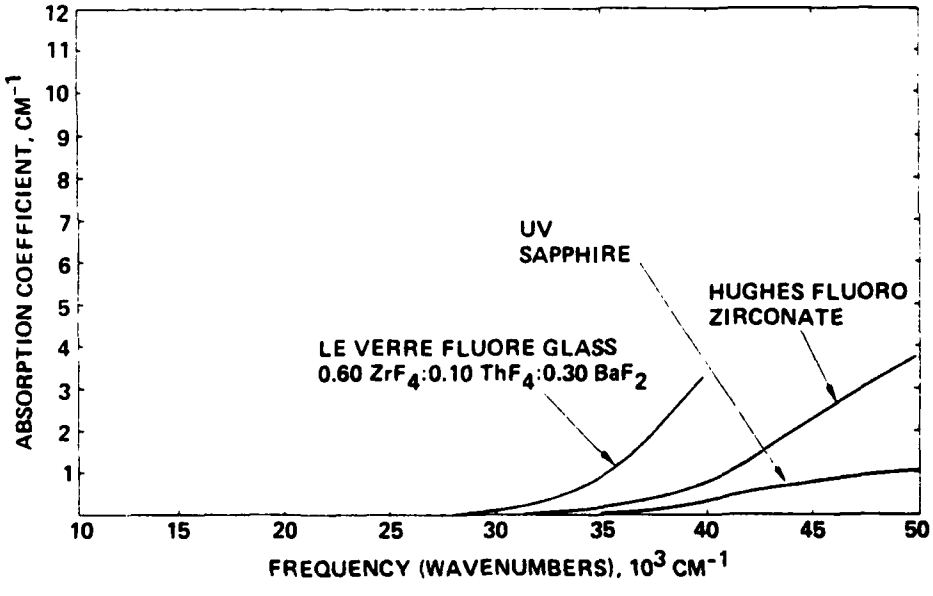

FIG. 2
UV absorption coefficient of uv grade sapphire, Le Verre Fluore and Hughes fluorozirconate glass (prepared in CCl_4 atmosphere).

TABLE 1
Physical Properties of 0.60 ZrF_4:0.07 ThF_4:0.33 BaF_2 Glass
(Prepared in CCl_4 Atmosphere)

Properties	Values
Optical transparency	0.3 μm UV to 7 μm IR[a]
Density	4.8 g/cm^3
Glass transition temperature[d]	295°C
Crystallization temperature[d]	390°C
Fusion temperature[d]	485°C
Refractive index (n_D)	1.53
Knoop hardness[b] ($Kg-mm^{-2}$)	250
Humidity effects	Water insoluble
Heat capacity (C_p) at 45°C[d]	0.511 J/g-°C
Coefficient of linear expansion[d]	
30 to 60°C	4.3×10^{-6}/°C
250 to 270°C	13.8×10^{-6}/°C
Rupture strength[c]	35,300 psi
Absorption coefficient at HF laser wavelength (2.8 μm)	6×10^{-3} cm^{-1}
Absorption coefficient at DF laser wavelength (3.8 μm)	2×10^{-3} cm^{-1}

[a]Prior art fluoride glass shows a strong absorption at 2.85 μm.

[b]Single crystal calcium fluoride (CaF_2) is 155.

[c]Forged CaF_2 is 14,000 psi.

[d]Measured with DuPont thermal analyzer model 1090.

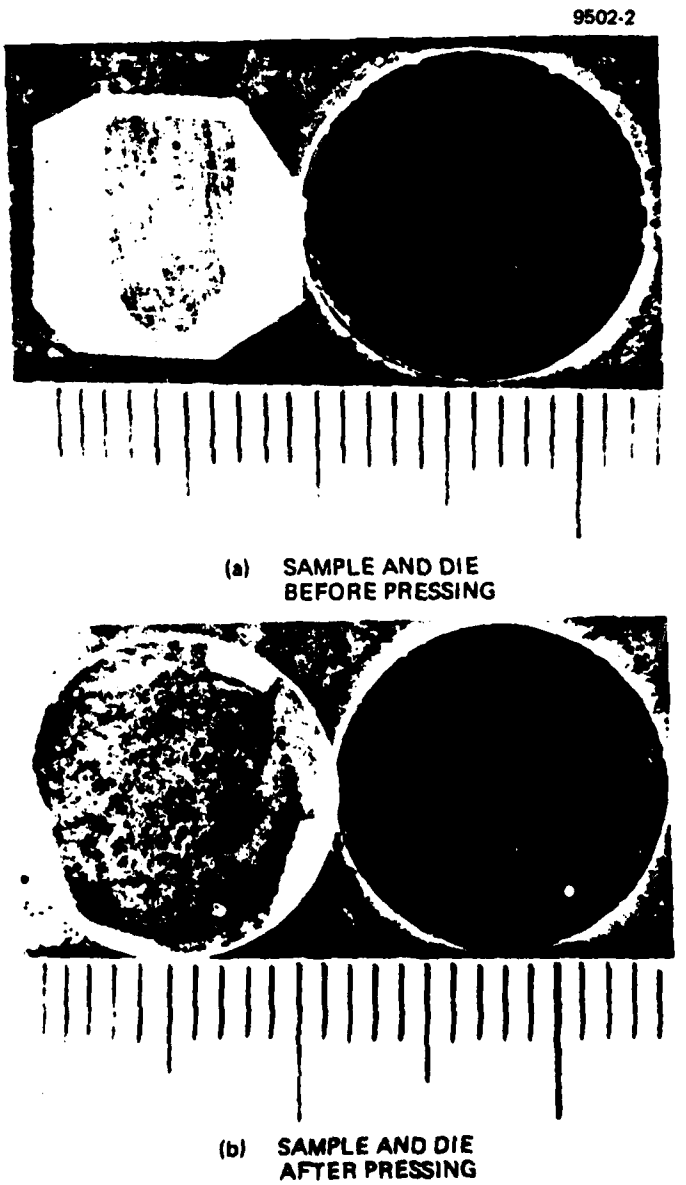

FIG. 3
Hot pressed 0.60 ZrF_4:0.07 ThF_4:0.33 BaF_2 glass (prepared in CCl_4 atmosphere).

9602-4

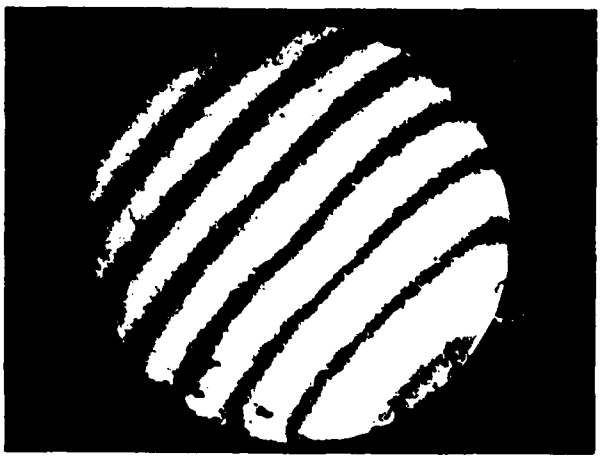

(a) FACE OF DIE PLUNGER

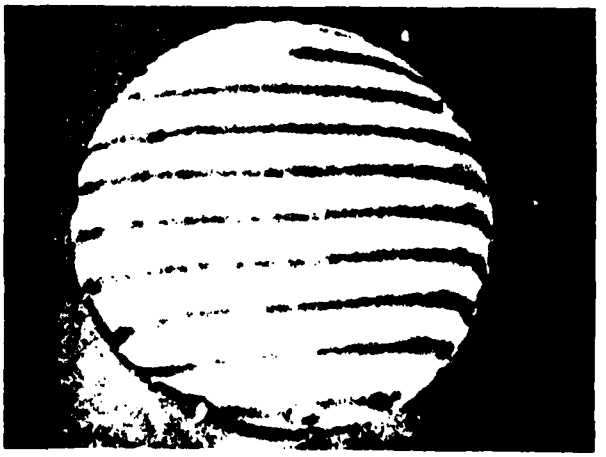

(b) FACE OF PRESSED GLASS

FIG. 4
Hot pressed 0.60 ZrF_4:0.07 ThF_4:0.33 BaF_2 glass (prepared in CCl_4 atmosphere). Both surfaces photographed in sodium light while contacting a 1/20 λ optical reference flat.

Figure 4(a) shows the flatness of the die plunger to be about 1/2 fringe of sodium light (5896 Å/4). Figure 4(b) shows that the molded glass surface closely duplicates the die surface.

Summary

The key to maximizing IR transparency and mechanical strength for these halide glasses lies in eliminating anionic impurities such as OH^- and $O^=$ which enter the condensed phase through hydrolysis during the mixing and melting stages of preparation. The HF scrubbing is not effective in this case. HF will not react with outgassed water emanating from the furnace interior, and, at elevated temperatures, it will not react with ZrO_2 to yield ZrF_4. Moreover, the use of HF appears to promote significant quantities of a black, fluoride-deficient phase. CCl_4, on the other hand, eliminates oxygen-containing species by reacting both with atmospheric water and with oxygen species in the melt.

Furthermore, utilization of CCl_4 for scrubbing compensates fluoride deficiency by adding Cl^- to the F^- vacancies. Fluoride glass prepared with the benefit of CCl_4 RAP is continuously transparent from 0.3 μm to 0.7 μm, is unusually hard and strong, and can be easily molded at moderate temperature and pressure.

Acknowledgments

The authors are grateful for the assistance of the following colleagues: A.C. Pastor and M.B. Klein of this laboratory, who gave considerable time in helpful discussions, J.A. Harrington performed the calorimetric absorptions at HF and DF laser wavelengths, R. Wong-Quen and R. Chew supplied the IR transmission data, and K.T. Miller and A. Timper carried out X-ray determinations on starting materials and final products.

References

1. F. Horrigan, C. Klein, R. Rudko, and D. Wilson, Microwaves 8, 68 (1969).
2. R.C. Pastor and A.C. Pastor, Mat. Res. Bull. 10, 117 (1975).
3. R.C. Pastor and M. Robinson, Mat. Res. Bull. 9, 569 (1974).
4. M. Chanthanasinh, Doctoral Thesis, University of Rennes (France) July (1976).
5. M. Poulain, M. Chanthanasinh, and J. Lucas, Mat. Res. Bull. 12, 151 (1977).

SCATTERING LOSSES IN SINGLE AND POLYCRYSTALLINE MATERIALS FOR INFRARED FIBER APPLICATIONS

J.A. Harrington and M. Braunstein

Hughes Research Laboratories†

Malibu, CA 90265

B. Bobbs* and R. Braunstein

University of California at Los Angeles††

Los Angeles, CA 90024

ABSTRACT

Polycrystalline fiber waveguides, fabricated from infrared transparent solids such as KRS-5 and KCl, have measured losses much greater than conventional silica fibers. One major source of these losses is scattering from grain boundaries present in the polycrystalline fibers. To improve the optical transmission of our infrared waveguides, we have studied the losses due to scattering in single and polycrystalline materials which are suitable for fabrication into infrared transmissive waveguides.

*Hughes Staff Doctoral Fellow.

†This work has been supported by Hughes Aircraft Company internal research and development programs and by RADC, Hanscom AFB, Mass.

††This work has been supported in part by AFOSR and ARO (Durham).

INTRODUCTION

Optical fiber waveguides made from crystalline materials such as KRS-5 (TlBrI), TlBr, AgCl, and KCl have been used for a variety of 10.6-μm, CO_2 laser applications.[1-4] The losses in the current IR fibers, however, are high (lowest loss measured is 300 dB/km at 10.6 μm in KRS-5) and applications in sensor and laser power delivery systems have been limited to short (1- to 2-m) lengths of fiber.[2-4] This measured IR fiber attenuation is considerably higher than that predicted theoretically for these and related IR transparent materials.[2,5] In fact, Gentile et al.[2] and van Uitert and Wemple[5] have shown that these materials have projected losses as low as 10^{-3} dB/km near 5 μm. To develop this ultra-low-loss potential, for such applications as long-distance communication links, requires a careful analysis of the nature of the attenuation mechanisms present in IR transparent waveguides. In this paper, we address the contribution of scattering to the total attenuation in bulk materials that have the potential for being fabricated into highly transparent fibers.

The attenuation mechanisms present in low-loss solids are illustrated in Fig. 1 for fused silica. At the shortest wavelengths, electronic processes (Urbach tail) contribute heavily to the total loss. At the IR wavelengths of interest, however, two mechanisms — scattering and multiphonon absorption — have been identified as the ultimate, limiting loss processes.[2] In Fig. 1, the curves for

scattering (which decreases as λ^{-4} with increasing wavelength) and lattice (multiphonon) absorption (which increases exponentially with increasing wavelength) cross to yield a minimum in the total attenuation. For fused silica, this minimum, which is about 0.25 dB/km at 1.6 μm, has been achieved in kilometer-long fibers.[6] For certain crystalline as well as special glassy solids, minima occur near 5 μm with projected losses well below the intrinsic losses measured in silica (projected losses are given in the next section).

The total attenuation coefficient α_T may be written as the sum

$$\alpha_T = \alpha_S + \alpha_A \quad , \tag{1}$$

where α_S and α_A are the contributions due to scattering and absorption, respectively. Each term in Eq. 1 can be measured independently, thus allowing the individual mechanisms contributing to the overall optical loss in solids to be studied. For example, α_T can be obtained from standard spectroscopic and fiber insertion loss measurements while laser calorimetry has been used very successfully to determine residual absorption α_A in weakly absorbing materials. The scattering terms α_S has not been as well studied. Measurements using integrating spheres for both bulk and fiber materials are generally used to obtain a total integrated scattering (TIS) loss.

These methods, however, have the disadvantage of being unable to distinguish among the various individual scattering mechanisms contributing to TIS. To elucidate the various scattering mechanisms as well as to obtain a value for α_s, we have chosen to study the light scattering spectra of solids. These spectra are composed of elastically (Rayleigh) scattered light that results from various nonpropagating fluctuations in the materials index of refraction and inelastically (Brillouin) scattered light that results from the interaction of light and the thermal motion of ions (sound waves). Although Rayleigh-Brillouin (RB) spectra have been used to measure α_s in glasses,[7] this technique has not been expressly used before to study scattering losses in single- and poly-crystalline materials. In this work, we have measured RB scattering at 90° in bulk single- and poly-crystalline KCl. As discussed in the next section, we expect very little Rayleigh scattering in single-crystal materials; for polycrystalline samples, however, intuition suggests that the residual strain and grain boundaries associated with the hot press-forged, polycrystalline material should lead to larger amounts of scattering. Our preliminary results support this presumption, but we have not yet been able to account for the source of each scattering mechanism contributing to the RB spectra.

GENERAL CONSIDERATIONS

The limiting attenuation mechanisms in transparent solids are scattering and multiphonon absorption. These contributions have

been considered by several investigators in the context of projecting future ultra-low-loss materials for the next generation of fiber waveguides. Van Uitert and Wemple[5] have studied the potential of $ZnCl_2$ (a glass former) while Gentile et al.[2] and Pinnow et al.[1] have concentrated on the crystalline materials. In Fig. 2, we consider the projected transmission for KRS-5 and KCl and compare these predictions to fused silica. The curves in Fig. 2 show the characteristic V shape resulting from the crossing of the scattering (short wavelength) and multiphonon (long wavelength) attenuation mechanisms. The only scattering mechanism assumed in calculating the λ^{-4}-dependent scattering curve for KRS-5 and KCl was Brillouin scattering (α_B - see below). As mentioned above, the V-shaped curve for silica has essentially been traced out experimentally and thus silica fiber losses are now intrinsic. For KCl and KRS-5 (as well as for many other non-oxide ionic solids), however, Fig. 2 shows the extremely low loss potential for these materials near 5 μm.

To determine α_S from RB light scattering experiments requires a careful measurement of the intensity of both the Brillouin- and Rayleigh-scattered light. Brillouin scattering results from light that has been inelastically scattered (Bragg scattering) from acoustical phonons (sound waves). The frequency of the scattered light is Doppler shifted from the frequency of the laser light ω_L by an amount $\pm\Omega$:

$$\Omega = \frac{4\pi n V \sin(\theta/2)}{\lambda_o} \quad ,$$

where n is the index of refraction of the medium, v is the velocity of sound, θ is the scattering angle, and λ_o is the vacuum wavelength of the light. This frequency shift has been well studied in alkali halides.[8] The Rayleigh-scattered light (central maximum at ω_L) is due to scattering of light from nonpropagating fluctuations in the dielectric constant. In glasses, mechanisms which give rise to these fluctuations include: density variations resulting from the frozen-in, random variations in dielectric constant inherent in a disordered solid; concentration fluctuations resulting from the local compositional variations present in mixtures; and entropy fluctuations resulting from temperature variations.[7] Of the three, only entropy fluctuations, which are very weak, would be present in an ideal single crystal.

To obtain α_s, we first evaluate the intensity ratio of the Rayleigh (I_R) to the total Brillouin ($2I_B$) scattered light. This ratio is called, based on its use in light scattering in liquids, the Landau-Placzek ratio R_{LP} and is defined[7] as

$$R_{LP} \equiv \frac{I_R}{2I_B} \quad . \tag{2}$$

Strictly speaking, since I_R and thus R_{LP} are related to specific scattering mechanisms (such as those discussed above for glasses),

measured values of R_{LP} are generally regarded as a property of a given material (e.g., fused SiO_2 has an $R_{LP} \simeq 23$, while $33K_2O\text{-}67SiO_2$ has an $R_{LP} \simeq 10$).[9] In our experiments, we measure I_R without, in general, knowing the specific mechanisms contributing to the Rayleigh component of scattered light. Therefore, we should more appropriately speak of an effective Landau-Placzek ratio with I_R representing the intensity of the central maximum.

The measured R_{LP} is then used to calculate α_S, as described by Pinnow et al.[10] and others,[7,9] from the relationship

$$\alpha_S = \alpha_B(R_{LP} + 1) \quad , \tag{3}$$

where α_B, is the small residual attenuation coefficient due to Brillouin scattering alone. It is given by

$$\alpha_B = \frac{8\pi^3}{3} \frac{1}{\lambda_o^4} (n^8 P_{12}^2)\, k_B\, T B_T \quad , \tag{4}$$

where P_{12} is the photoelastic (Pockels) coefficient, T is the temperature, k_B is Boltzmann's constant, and B_T is the isothermal compressibility. For ideal single crystals, $I_R \simeq 0$, thus $R_{LP} \simeq 0$ and (from Eq. 3) $\alpha_S \simeq \alpha_B$. This leads to the scattering curves in Fig. 2 for KRS-5 and KCl, which were calculated from Eq. 4 alone, while the scattering for fused silica was calculated from Eq. 3 using $R_{LP} = 23$.

An interesting feature of measured R_{LP}s for crystalline solids is their dependence on polarization. For our single-crystal measurements in KCl, a [100] crystal orientation was used for most samples studies. With incoming light along the [100] direction and scattered light along the [010], the polarization of the incident and analyzed scattered light was either vertical (V) or horizontal (H) with respect to the scattering plane. For this geometry, we may determine the intensities of the Brillouin components from the selection rules for the rock salt structure (O_h) and the differential cross section.[11] The intensities I and allowed vibrational modes for the various polarizations (phonon momentum q along [110] direction) are summarized in the matrix given in Table 1a. Using the known photoelastic (P_{12} and P_{44}) and elastic (C_{11}, C_{12}, and C_{44}) constants for KCl,[12] we calculate the matrix elements in Table 1a and give them, normalized to I_{HH} (the weakest intensity), in Table 1b. Table 1b shows that the intensities of the longitudinal modes (frequency equal to 15.8 GHz) in VV polarization are much stronger than those in the other polarizations (transverse mode frequency equal to 7.2 GHz). This means that measured Landau-Placzek ratios may vary greatly depending on crystal orientation and polarization, with the smallest R_{LP} occurring for the VV polarization.

LIGHT SCATTERING MEASUREMENTS

The RB spectra were recorded using as a source an Ar-ion laser (Spectra Physics Model 165) delivering 10 to 300 mW of single-line power and a PZT-scanned Fabry-Perot spectrometer. The experimental set-up is shown in the block diagram in Fig. 3. The spectrometer is a Burleigh Instruments, Inc., actively stabilized Fabry-Perot interferometer with its associated photon counting electronics. Data acquisition is provided by a 512-channel Tracor-Northern multichannel analyzer (MCA). This MCA has proven essential for obtaining good S/N ratios for these crystals (between 2000 and 20,000 scans are generally accumulated for each spectrum).

To improve the contrast of the spectrometer, we added a three-pass attachment to the interferometer. This allowed us to readily detect the Brillouin components in the polycrystalline materials where the Rayleigh scattering is more intense. Fig. 4 shows the results of a 90° scattering measurement on polycrystalline KCl doped with 1.75% RbCl taken with the light passing once (one-pass) or thrice (three-pass) through the interferometer. The improved contrast in the three-pass case is obvious. Note in particular the resolution of the transverse modes in the three-pass case that has been lost in the Rayleigh wing in the one-pass case. Clearly, the three-pass arrangement, which has been used in all our measured data, is necessary to obtain a reliable R_{LP}. The resolution of the triple-pass Fabry-Perot spectrometer was 0.03 cm^{-1} (finesse equal to 50).

RESULTS OF LIGHT SCATTERING EXPERIMENTS

Measurements of scattering losses were made at 488.0 nm in bulk single and polycrystalline KCl. The KCl was reactive atmosphere process (RAP) single-crystal material[13] which was either used in oriented single-crystal (SC) or in hot-press forged, polycrystalline (P) form. The RB scattering data shown in Fig. 5 are for pure, single-crystal KCl oriented as shown in the insert. From the data, we can see the intense stokes (S) and anti-stokes (AS) longitudinal Brillouin components in the VV polarization. The Brillouin components are also seen to become weaker in VH (or HV) and HH polarization, which is in qualitative agreement with the results stated in Table 1 for this scattering geometry. Similar results were obtained for other RAP-grown KCl (SC) although the R_{LP}s were found to vary somewhat from sample to sample.

The data for polycrystalline KCl (average grain size, 10 μm) are shown for two polarizations in Fig. 6. We can see from these data the intense Rayleigh scattering typical of our polycrystalline samples. In this sample, we also note the presence of only longitudinal modes in VV polarization and transverse modes in VH polarization. This leads us to conclude that we have, by chance, illuminated an axis of high symmetry in this sample. Specifically, it would appear from the data that the crystallites are oriented along the [100] direction for this particular experiment. In general, we would expect to observe an admixture of L and T modes

consistent with a random orientation of polycrystalline samples.

Effective Landau-Placzek ratios have been calculated for these two samples from the data in Figs. 5 and 6. These data are summarized in Table 2. For the single-crystal KCl, R_{LP} is lowest for the VV polarization, as discussed above, but the R_{LP}s for other polarizations do not scale with the predicted Brillouin intensities (see Table 1). This is due to the polarization dependence of the Rayleigh-scattered light. Our measurements of I_R indicate that the Rayleigh scattered light is, as expected, most intense for the VV polarization. For this polarization, I_R is approximately 8 to 10 times stronger than when measured under HV, VH, or HH conditions. More detailed studies of the depolarization ratio might give insight into the nature of the static defect contribution to elastic scattering. In general, the values for R_{LP} obtained for polycrystalline KCl(P) are higher than those for KCl(SC) (see Table 2). Again, the VV polarization for this unoriented poly sample yields the lowest R_{LP} and the HH case yields the highest R_{LP} (this trend was also seen in another KCl(P) sample).

Table 2 also gives the values of α_S calculated from Eqs. 3 and 4, which, for KCl at 488.0 nm, reduce to,

$$\alpha_S = 1.5 \times 10^{-6} \, (R_{LP} + 1) \text{ cm}^{-1} \quad .$$

These attenuation coefficients due to scattering may be compared to the absorption coefficients obtained for KCl by laser calorimetric measurements at 488.0 nm by Harrington et al.[14] They found $\alpha_A \tilde{=} 3 \times 10^{-4}$ cm^{-1} for KCl(P) and $\alpha_A < 2 \times 10^{-5}$ cm^{-1} for KCl(SC). We see, therefore, that the total attenuation $\alpha_T (= \alpha_A + \alpha_S)$ is largely due to scattering.

The nature of the Rayleigh scattering in our crystalline samples is not completely understood. The results indicate substantial elastic scattering beyond that predicted above theoretically from entropy fluctuations. One may consider this excess parasitic scattering as arising from mechanical and chemical defects in the crystal. Although all the KCl has been RAP purified, we cannot rule out different amounts of chemical impurities in each sample. It is also evident that residual strain is present in both single and polycrystalline samples (observed as birefringence in crossed polarizers). This strain, which one would intuitively expect to be greater in the hot-forged polycrystalline materials, can lead to substantial elastic scattering. In particular, one would suspect grain boundaries as a potentially strong source of Rayleigh scattering because impurities, voids, and high strain would be more prevalent in these areas.

In our polycrystalline samples, it was not possible to examine the scattering from a single grain boundary because the average grain size (10 μm) was much smaller than the scattering volume

(cylindrical volume, 350 μm long by 30 μm in diameter). Brody et al.,[15] however, were able to study elastic scattering from a single grain boundary in polycrystalline calcium fluoride (Irtran-3). In their measurements, the grain size (150 μm) was larger than the scattering volume and they found essentially no difference in the intensity of light scattered from within a crystallite to that scattered from a volume containing a grain boundary. One might conclude from their results that grain boundaries do not contribute to elastic scattering; however, to assess the effect of grain boundaries properly, one must study high-purity material with a low Rayleigh background. Our future experiments will look more closely at the effect as well as the importance of residual strain on the Rayleigh scattered light.

SUMMARY

Our RB scattering studies on bulk KCl have been an initial attempt to probe the mechanisms responsible for scattering losses in highly transparent materials. We have found that polycrystalline materials scatter more strongly than do single-crystal materials, but we have not as yet been able to explicitly associate a particular elastic scattering process with a finite contribution to the total scattering. Our results, however, do indicate that, even in these very pure KCl samples, there is more scattering than predicted for the ideal KCl crystals and thus future fiber waveguides from these low-loss materials may be limited

more by scattering than absorption losses. Consequently, it is important to study scattering in poly- and single-crystal materials to understand the origin of the Rayleigh scattering and thereby to determine methods of minimizing this contribution to the attenuation.

REFERENCES

1. D.A. Pinnow, A.L. Gentile, A.G. Standlee, A.J. Timper, and L.M. Hobrock, "Polycrystalline Fiber Optical Waveguides for Infrared Transmission," Appl. Phys. Lett., Vol. 33, pp. 28-29, 1978.
2. A.L. Gentile, M. Braunstein, D.A. Pinnow, J.A. Harrington, D.M. Henderson, L.M. Hobrock, J. Myer, R.C. Pastor, and R.R. Turk, "Infrared Fiber Optical Materials," in Fiber Optics: Advances in Research and Development, ed. by B. Bendow and S.S. Mitra, pp. 105-118, Plenum Publishing, N.Y., 1977.
3. D. Chen, R. Skogman, G.E. Bernal, and C. Butter, "Fabrication of Silver Halide Fibers by Extrusion," ibid, pp. 119-122.
4. J.A. Harrington, "Infrared Fiber Optics for CO_2 Laser Applications," in CO_2 Laser Devices and Applications, Proceedings of SPIE Technical Symposium East, Vol. 227, Fall, 1980.
5. L.G. Van Uitert and S.H. Wemple, "$ZnCl_2$ Glass: A Potential Ultralow-Loss Optical Fiber Material," Appl. Phys. Lett., Vol. 33, pp. 57-59, 1978.

6. S. Kobayashi, N. Shibata, S. Shibata, and T. Izawa, "Characteristics of Optical Fibers in Infrared Wavelength Region," Rev. of Elect. Comm. Lab. (Japan), Vol. 26, pp. 453-468, 1978.

7. For a review see J. Schroeder, "Light Scattering of Glass," in Treatise on Materials Science and Technology, Vol. 12 Glass 1: Interaction With Electromagnetic Radiation, pp. 157-222, Academic Press, 1977.

8. G.B. Benedek and K. Fritsch, "Brillouin Scattering in Cubic Crystals," Phys. Rev., Vol. 149, pp. 647-662, 1966.

9. J. Schroeder, R. Mohr, P.B. Macedo, and C.J. Montrose, "Rayleigh and Brillouin Scattering in K_2O-SiO_2 Glasses," J. Amer. Cer. Soc., Vol. 56, pp. 510-514, 1973.

10. T.C. Rich and D.A. Pinnow, "Total Optical Attenuation in Bulk Fused Silica," Appl. Phys. Lett., Vol. 20, pp. 264-266, 1972.

11. W. Hayes and R. Loudon, "Scattering of Light by Crystals, pp. 327-353, J. Wiley & Sons, 1978.

12. Landolt-Bornstein Numerical Data and Functional Relationships in Science and Technology, New Series, ed. by K.H. Hellwege and A.M. Hellwege, Vol. II, pp. 25, 29, 510, and 513, Springer-Verlag, 1979.

13. R.C. Pastor and A.C. Pastor, "Crystal Growth in a Reactive Atmosphere," Mat. Res. Bull., Vol. 10, pp. 117-124, 1975.

14. J.A. Harrington, B.L. Bobbs, M. Braunstein, R. Kim, R. Stearns, and R. Braunstein, "Ultraviolet-Visible Absorption in Highly Transparent Solids by Laser Calorimetry and Wavelength Modulation Spectroscopy," Appl. Opt., Vol. 17, pp. 1541-1546, 1978.

15. E. Brody, C. Roychoudhuri, and M. Hercher, "Brillouin Spectra of CaF_2 Microcrystals Using a Stable 3-Pass Fabry-Perot Interferometer," Appl. Phys. Lett., Vol. 23, pp. 543-545, 1973.

TABLE I

Intensities of Brillouin Components for a Rocksalt Crystal

(a)

Mode	IVV	IVH = IHV	IHH
(110) L	$\frac{4P_{12}^2}{C_{11} + C_{12} + C_{44}}$	0	$\frac{4P_{44}^2}{C_{11} + C_{12} + C_{44}}$
(1$\bar{1}$0) T	0	0	0
(001) T	0	$\frac{P_{44}^2}{2C_{44}}$	0

(b)

Mode	IVV	IVH	IHH
(110) L	133	0	1
(1$\bar{1}$0) T	0	0	0
(001) T	0	4.8	0

TABLE II

Effective R_{LP} and Calculated Values of α_S

Structure	Polarization	R_{LP}	α_S (cm^{-1})
Single	VV	26.2	4.1×10^{-5}
Crystal	VH	38.5	5.9×10
(SC)	HV	44.9	6.9×10^{-5}
	HH	276.4	4.2×10^{-4}
Polycrystalline	VV	496	7.5×10^{-4}
(P)	VH	830	1.2×10^{-3}
	HV	1598	2.4×10^{-3}
	HH	>5000	$>7.5 \times 10^{-3}$

FIGURE CAPTIONS

Fig. 1 - Schematic representation of optical attenuation mechanisms in solids.

Fig. 2 - Projected losses for some IR transparent materials. Short wavelengths are bounded by $1/\lambda^4$-scattering and long wavelengths by multiphonon absorption.

Fig. 3 - Block diagram of scanning Fabry-Perot interferometer for measuring RB spectra.

Fig. 4 - Improved contrast in RB spectra of poly KCl + 1.75% RbCl through the use of 3-pass attachment on Fabry-Perot interferometer. The spectra were all recorded using the 3-pass configuration.

Fig. 5 - Scattering spectra for single-crystal KCl for three different polarizations. Landau-Placzek ratios are given in Table 2 for these data.

Fig. 6 - Scattering spectra for polycrystalline KCl (average grain size is 10 μm). Landau-Placzek ratios are given in Table 2 for these data.

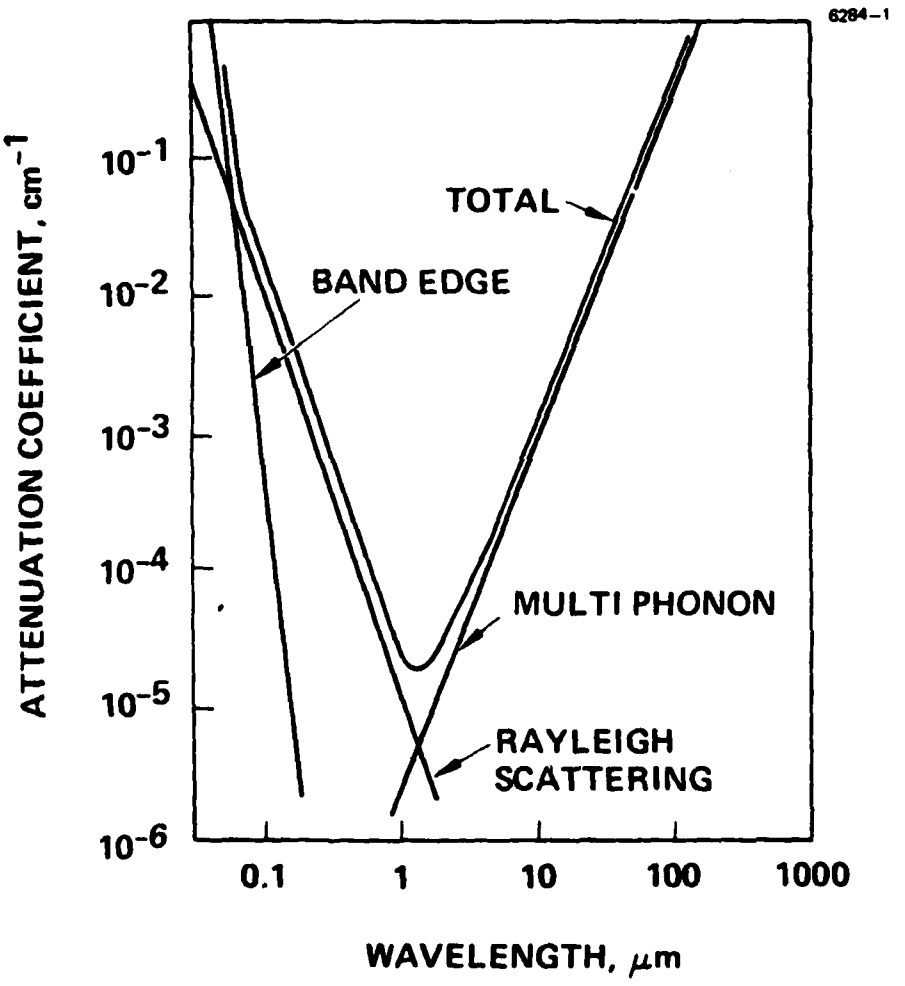
6284-1
ATTENUATION COEFFICIENT, cm^{-1}
10^{-1}
10^{-2}
10^{-3}
10^{-4}
10^{-5}
10^{-6}
TOTAL
BAND EDGE
MULTI PHONON
RAYLEIGH SCATTERING
0.1
1
10
100
1000
WAVELENGTH, μm

Figure 1.

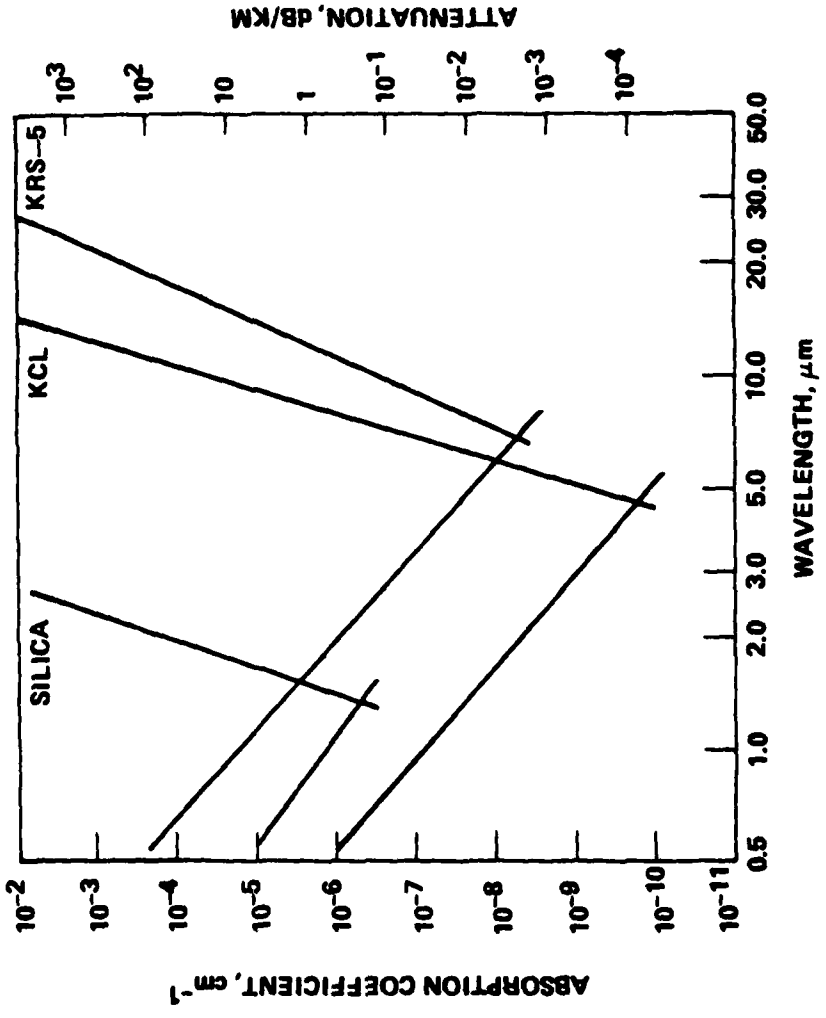
ATTENUATION, dB/KM
10^{3}
10^{2}
10
1
10^{-1}
10^{-2}
10^{-3}
10^{-4}
KRS–5
KCL
SILICA
0.5
1.0
2.0
3.0
5.0
10.0
20.0
30.0
50.0
WAVELENGTH, μm
10^{-2}
10^{-3}
10^{-4}
10^{-5}
10^{-6}
10^{-7}
10^{-8}
10^{-9}
10^{-10}
10^{-11}
ABSORPTION COEFFICIENT, cm^{-1}

Figure 2.

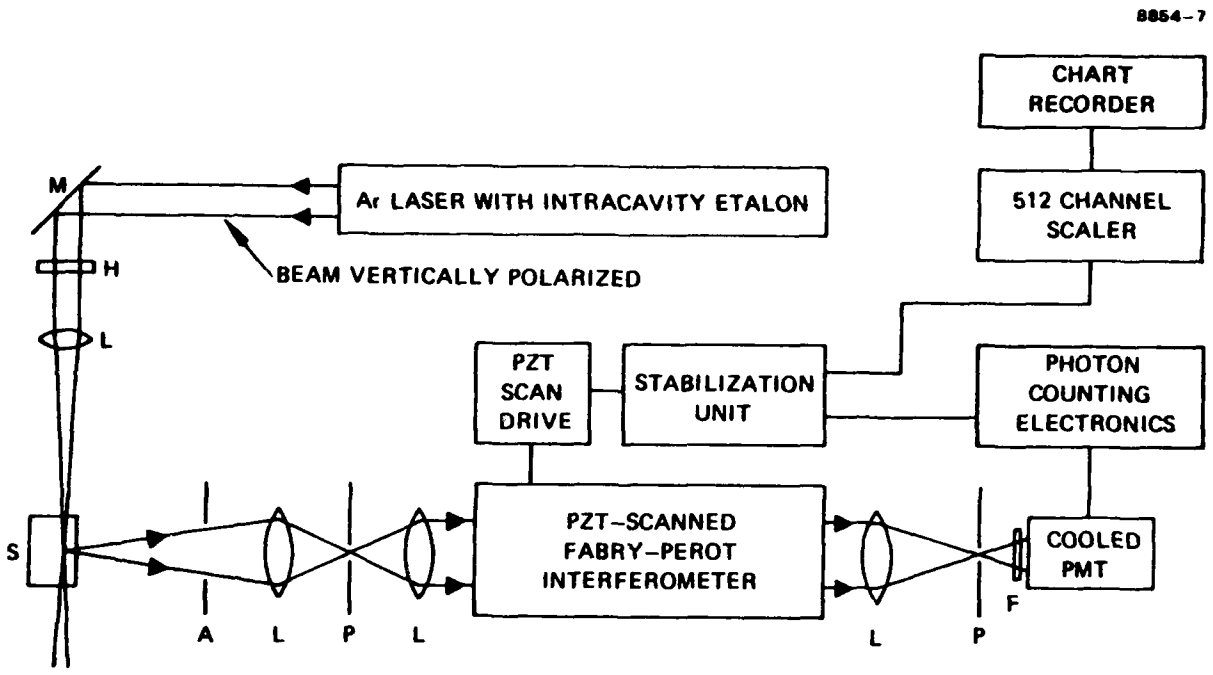

Figure 3.

M : PLANE MIRROR
H : HALFWAVE PLATE TO ROTATE POLARIZATION IF DESIRED
L : LENSES TO FOCUS AND COLLIMATE LIGHT
S : TRANSPARENT SAMPLE
A : APERTURE TO LIMIT RANGE OF SCATTERING ANGLES DETECTED
P : PINHOLES TO BLOCK OFF-AXIS LIGHT
F : NARROWBAND (30 Å) FILTER TO BLOCK FLUORESCENCE, RAMAN SCATTERING AND BACKGROUND RADIATION

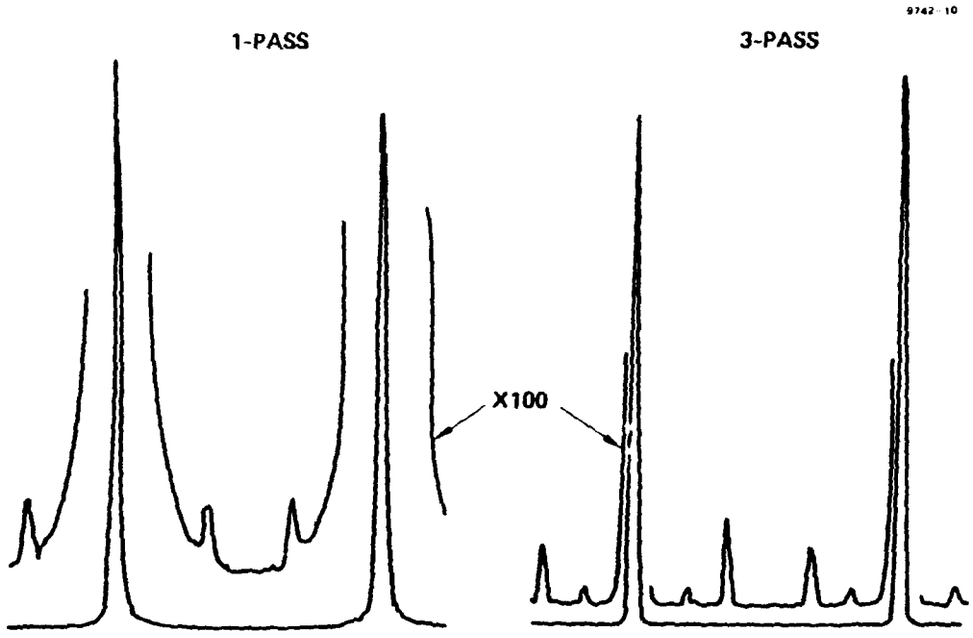

Figure 4.

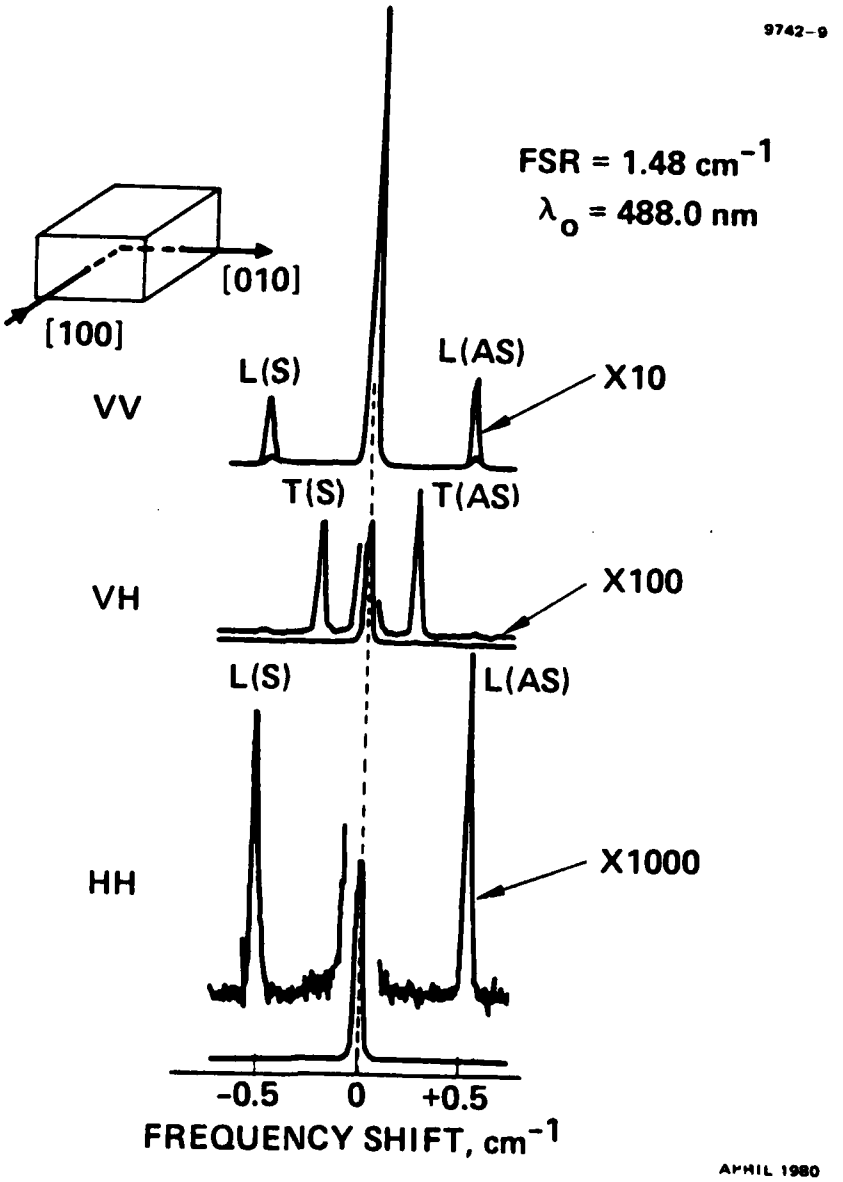
9742-9
FSR = 1.48 cm^{-1}
λ_o = 488.0 nm
[010]
[100]
L(S)
L(AS)
X10
VV
T(S)
T(AS)
VH
X100
L(S)
L(AS)
HH
X1000
-0.5
0
+0.5
FREQUENCY SHIFT, cm^{-1}
APRIL 1980

Figure 5.

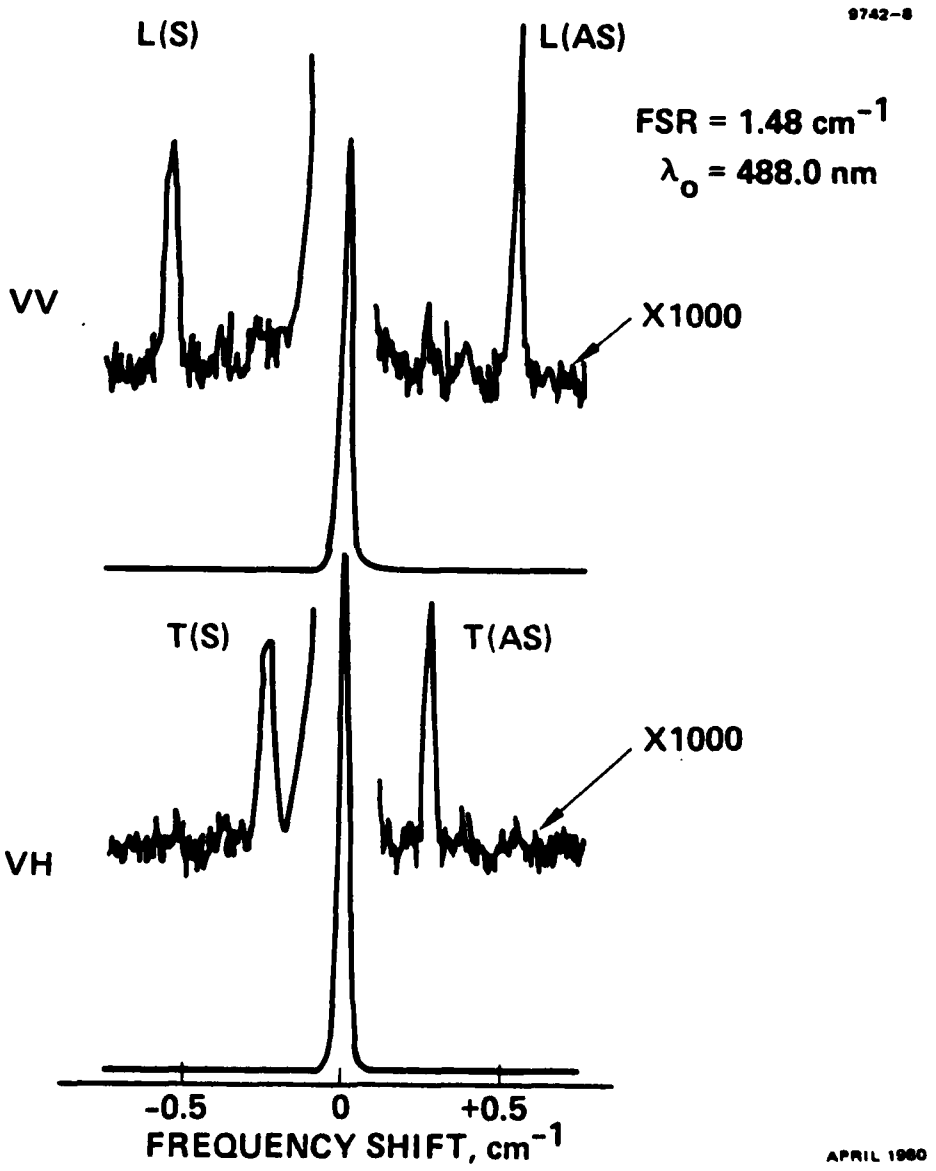
9742-8
L(S)
L(AS)
FSR = 1.48 cm^{-1}
λ_o = 488.0 nm
VV
X1000
T(S)
T(AS)
X1000
VH
-0.5
0
+0.5
FREQUENCY SHIFT, cm^{-1}
APRIL 1980

Figure 6.

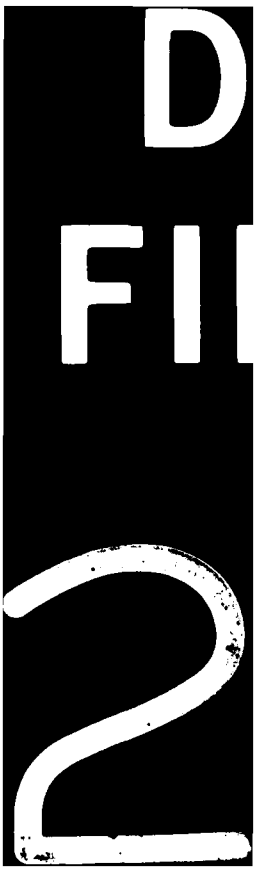
D
FI
2